Copy

RM SL54H05

NACA

RESEARCH MEMORANDUM

for the

Bureau of Aeronautics, Department of the Navy

ADDITIONAL RESULTS ON THE STATIC LONGITUDINAL AND LATERAL STABILITY CHARACTERISTICS OF A 0.05-SCALE MODEL OF THE CONVAIR F2Y-1 AIRPLANE AT HIGH SUBSONIC SPEEDS

TED NO. NACA DE 383

By Kenneth P. Spreeman and Albert G. Few, Jr.

Langley Aeronautical Laboratory
Langley Field, Va.

NATIONAL ADVISORY COMMITTEE
FOR AERONAUTICS

WASHINGTON

AUG 10 1954

NATIONAL ADVISORY COMMITTEE FOR AERONAUTICS

RESEARCH MEMORANDUM

for the

Bureau of Aeronautics, Department of the Navy

ADDITIONAL RESULTS ON THE STATIC LONGITUDINAL AND LATERAL STABILITY CHARACTERISTICS OF A 0.05-SCALE MODEL OF THE CONVAIR F2Y-1 AIRPLANE AT HIGH SUBSONIC SPEEDS

TED NO. NACA DE 383

By Kenneth P. Spreeman and Albert G. Few, Jr.

SUMMARY

Additional results on the static longitudinal and lateral stability characteristics of a 0.05-scale model of the Convair F2Y-1 water-based fighter airplane were obtained in the Langley high-speed 7- by 10-foot tunnel over a Mach number range of 0.50 to 0.92. The maximum angle-of-attack range (obtained at the lower Mach numbers) was from -2° to 25°. The sideslip-angle range investigated was from -4° to 12°. The investigation included effects of various arrangements of wing fences, leading-edge chord-extensions, and leading-edge notches. Various fuselage fences, spoilers, and a dive brake also were investigated.

From overall considerations of lift, drag, and pitching moments, it appears that there were two modifications somewhat superior to any of the others investigated: One was a configuration that employed a full-chord fence and a partial-chord fence located at 0.63 semispan and 0.55 semispan, respectively. The second was a leading-edge chord-extension that extended from 0.68 semispan to 0.85 semispan in combination with a leading-edge notch located at 0.68 semispan.

With ±10° aileron, the estimated wing-tip helix angle was reduced from 0.125 at a Mach number of 0.50 to 0.088 at a Mach number of 0.92, with corresponding rates of roll of 4.0 and 5.2 radians per second. The upper aft fuselage dive brake, when deflected 30° and 60°, reduced the rudder effectiveness about 10 to 20 percent and about 35 to 50 percent, respectively.

INTRODUCTION

A preliminary investigation at high subsonic speeds of the longitudinal and lateral stability characteristics of a 0.05-scale model of the Convair F2Y-1 water-based fighter airplane was conducted by the National Advisory Committee for Aeronautics and has been reported in reference 1.

At the request of the Bureau of Aeronautics, Department of the Navy, the NACA has conducted an additional series of tests at high subsonic speeds of the static longitudinal and lateral stability characteristics of this model. The principal purpose of this investigation was to establish a wing or fuselage fix that would eliminate or at least delay the longitudinal instability encountered at high subsonic speeds and high angles of attack by this model. The investigation included the effects of various arrangements of wing fences, leading-edge chord-extensions, and leading-edge notches. Various fuselage fences, spoilers, and dive brakes were also tested.

The tests were conducted in the Langley high-speed 7- by 10-foot tunnel over a Mach number range of 0.50 to 0.92, with corresponding Reynolds numbers, based on the wing mean aerodynamic chord, from 3.3×10^6 to 4.3×10^6.

COEFFICIENTS AND SYMBOLS

The stability system of axes used for the presentation of the data, together with an indication of the positive directions of forces, moments, and angles, is shown in figure 1. All moments are referred to the 30-percent-chord point of the mean aerodynamic chord.

C_L lift coefficient, $\frac{\text{Lift}}{qS}$

C_D drag coefficient, $\frac{\text{Drag}}{qS}$

C_m pitching-moment coefficient, $\frac{\text{Pitching moment}}{qS\bar{c}}$

C_l rolling-moment coefficient, $\frac{\text{Rolling moment}}{qSb}$

C_n yawing-moment coefficient, $\frac{\text{Yawing moment}}{qSb}$

C_Y lateral-force coefficient, $\frac{\text{Lateral force}}{qS}$

q dynamic pressure, $\rho V^2/2$, lb/sq ft

S wing area, 1.42 sq ft

$\bar{c}$ mean aerodynamic chord of wing, $\frac{2}{S}\int_0^{b/2} c^2 dy$, 1.069 ft

c local wing chord, parallel to plane of symmetry, ft

b wing span, 1.76 ft

ρ air density, slugs/cu ft

V free-stream velocity, ft/sec

M Mach number

R Reynolds number of wing based on $\bar{c}$

α angle of attack of fuselage reference line, deg

β angle of sideslip, deg

δ control surface deflection, deg

pb/2V wing-tip helix angle, radians

p rolling velocity, radians/sec

$C_{l_p} = \frac{\partial C_l}{\partial \frac{pb}{2V}}$, per radian

L/D lift-drag ratio

Subscripts:

b base of model fuselage

e elevon

r rudder

max maximum

min minimum

MODEL DESIGNATIONS

B fuselage

C canopy

V fin

W wing; W also used with following subscripts:

- F_1 fence 1
- F_3 fence 3
- F_4 fence 4
- F_5 fence 5
- F_6 fence 6
- F_7 fence 7
- N_1 notch 1
- N_2 notch 2

MODEL AND APPARATUS

A drawing of the 0.05-scale model of the Convair F2Y-1 airplane employed in this investigation is presented in figure 2. Details of the various fences, chord-extensions, notches, and spoilers employed on the model are shown in figures 3 to 7. Included in figure 7 is a sketch of the fuselage fairing at the aft end of the model. Figure 8 shows the faired duct inlet plugs employed on the model. Details of the upper aft fuselage dive brake are shown in figure 9. Photographs of the model are shown in figure 10.

[redacted]

The model was tested on the sting-type support system shown in figure 10(c). With this system, the model was remotely operated through ranges of either angle of attack or sideslip. A strain-gage balance mounted inside the fuselage was used to measure the forces and moments on the model.

TESTS AND CORRECTIONS

The investigation was made in the Langley high-speed 7- by 10-foot tunnel over a Mach number range from 0.50 to 0.92 at angles of attack ranging from about -2° to 25° and through a sideslip range from -4° to 12°.

The blockage, jet-boundary, buoyancy, and base pressure corrections are the same as those discussed in reference 1. Values of base-pressure-drag coefficient C_{D_b} for average test conditions are presented in figure 11. The corrected model drag data were obtained by adding the base-pressure-drag coefficient to the drag coefficient determined from the strain-gage measurements.

The variation of mean Reynolds number with Mach number for the model of this investigation is presented in figure 12.

RESULTS AND DISCUSSION

The bulk of the data obtained in this investigation is presented in figures 13 to 35; an index of the figures is given in table I. Additional data that are not presented in figures 13 to 35 are tabulated in tables II to VII. Data presented as configuration 1A in figures 13 and 14 were taken from figure 8 in reference 1 to facilitate evaluation of the flexibility of the elevator restraining members. Data presented for configuration 1B (basic model, no fixes of any nature) in figures 15, 17, and 20 were also taken from figure 8 in reference 1. Note that fences 1 and 3 are the same as fences 1 and 3 of reference 1; fence 2 of reference 1 was not used in this investigation. The slopes presented in figure 35 have been averaged over a lift-coefficient range of about 0 to 0.4. In order to expedite the publication of these data, only a brief analysis is included herein.

Lift

The lift characteristics of the model were not greatly altered by any change in wing fences, leading-edge chord-extensions, and notches, except that in the higher lift range the fixes generally resulted in somewhat more linear characteristics. (See parts (a) of figs. 15, 17, and 20.) The lift-curve slopes of configurations 10 and 20 presented in figure 35 are fairly representative of all configurations. The reductions in $\partial C_L/\partial \alpha$ (about 10 to 15 percent) for the trimmed condition are in reasonably good agreement with values obtained in reference 1 for configuration 1A.

Drag

Any alteration to the basic model (configuration 1B, parts (b) of figs. 15, 17, and 20) usually increased the minimum drag coefficient except for configuration 21, wherein the jet inlets were plugged with a smooth fairing - which resulted in reductions of $C_{D_{min}}$ of about 0.003 to 0.004. (See fig. 20(b).) In the medium lift-coefficient range, however, addition of fences, leading-edge chord-extensions, or notches usually gave some reductions in drag. The leading-edge chord-extension alone (configuration 4, fig. 15) appeared to be the most effective modification in this respect.

Compared with the basic model (configuration 1B, fig. 35) the drag due to lift $\partial C_D/\partial {C_L}^2$ was reduced about 10 to 20 percent by fences 1 plus 3 (configuration 10) and the leading-edge chord-extension plus notch 1 (configuration 20). In the trimmed condition, $\partial C_D/\partial {C_L}^2$ was increased about 15 to 45 percent relative to the condition for $\delta_e = 0^\circ$.

Lift-Drag Ratios

The addition of fences 1 and 3 (configuration 10) or the leading-edge chord-extension and notch 1 (configuration 20) resulted in a very slight increase in $(L/D)_{max}$ over that of the basic model (configuration 1B). (See fig. 35.) Trimming the model at the assumed center-of-gravity location ($0.30\bar{c}$) generally reduced the lift-drag ratios about 10 to 20 percent. (See figs. 34 and 35.) These values check very closely those obtained with configuration 1A in reference 1, indicating that trimming the model would result in a loss of about 10 to 20 percent in lift-drag ratios for any of the configurations tested.

Pitching Moment

As previously pointed out in reference 1, for the basic model (configuration 1B, parts (c) and (d) of fig. 15), regions of longitudinal instability were found to exist at a lift coefficient of about 0.40 throughout the Mach number range investigated. All the combinations of wing fences, leading-edge chord-extensions, and notches delayed the instability to considerably higher lift coefficients and angles of attack (usually to values of C_L of 0.6 to 0.8 or angles of attack of 14° to 16°; see parts (c) and (d) of figs. 15, 17, and 20). However, the departures from linearity in the medium lift and angle-of-attack range still are probably undesirable on the basis of pitching-motion considerations. (See ref. 2 for a detailed discussion of the pitch-up problem.) Inverting the model appeared to give small improvements in the pitch characteristics at the lower Mach numbers but at a Mach number of 0.92 the characteristics of the model appeared to be slightly worse when inverted than when in the normal position. (See parts (c) and (d) of fig. 15.) The addition of the fuselage fences and spoilers gave little change in the pitching-moment characteristics of the model. (See fig. 26(b).)

Fences 1 and 3, and the leading-edge chord-extension plus notch 1 (configurations 10 and 20, respectively), provided a slight forward shift in the aerodynamic-center location (about 1 to 2 percent at Mach numbers of 0.85 and 0.92). (See fig. 35.)

From overall considerations of lift, drag, and pitching moments, it appears that configurations 10 and 20 were the most desirable; consequently, all analysis and summary figures are based on these two configurations.

Elevator Effectiveness

The results obtained for various elevator settings (parts (d) of figs. 22 and 23) indicate that the elevator effectiveness for small settings and the lower Mach numbers held up well throughout the lift-coefficient range; however, at a Mach number of 0.92 some appreciable losses were incurred at the higher lift coefficients. At zero lift, small elevator deflections gave gradual increases with Mach number in the effectiveness parameter $\left(\frac{\partial C_m}{\partial \delta_e}\right)_{C_L=0}$, (from about -0.0052 at $M = 0.50$ to -0.006 at $M = 0.90$). (See fig. 32.) These values are in good agreement with those obtained in reference 1 for configuration 1A.

In assessing the elevator effectiveness it should be noted that some flexibility in the elevator restraining members did exist. However, comparisons with a heavier dummy gage and with the elevator securely locked by soldering the elevon actuators to the actuator fairings indicated that the effects of flexibility were small. (See parts (c) and (d) of figs. 13 and 14.) A slight variation in the elevator setting introduced by changes in the elevator restraining members may account for the small shift in the pitching moments at zero lift and in the lift coefficients at zero angle of attack.

Aileron Effectiveness

The results of deflecting the ailerons to ±5° and ±10° are presented in figure 29. From these data and using values of C_{l_p} from reference 3 for a 60° delta wing-body combination, the wing-tip helix angle and rate of roll were calculated for trim conditions at an altitude of 10,000 feet and a wing loading of 32 pounds per square foot. The results of these calculations, presented in figure 33, indicate that with ±10° aileron the wing-tip helix angle was reduced from 0.125 at a Mach number of 0.50 to 0.088 at a Mach number of 0.92, with corresponding rates of roll of 4.0 and 5.2 radians per second.

Effect of Dive Brake on Rudder Effectiveness

Results for a rudder deflection of 10°, with upper aft fuselage dive-brake deflections of 30° and 60°, are presented in figure 30. From these data and data published in reference 1 without dive brakes, it appears that the 30° setting reduced the rudder effectiveness about 10 to 20 percent; whereas the 60° setting reduced this parameter about 35 to 50 percent.

[redacted]

Additional tests to determine the static longitudinal and lateral stability characteristics of various wing and fuselage modifications on a 0.05-scale model of the Convair F2Y-1 water-based fighter airplane at high subsonic speeds indicate the following conclusions:

1. The lift characteristics of the model were not greatly altered by any change in wing fences, leading-edge chord-extensions, and notches.

2. From overall considerations of drag and pitching moments, it appears that there were two modifications somewhat superior to any of the others investigated: first, a configuration that employed a full-chord fence and a partial-chord fence located at 0.63 semispan and 0.55 semispan, respectively; and, second, a leading-edge chord-extension that extended from 0.68 semispan to 0.85 semispan in combination with a leading-edge notch located at 0.68 semispan.

[redacted]

3. With ±10° aileron, the estimated wing-tip helix angle was reduced from 0.125 at a Mach number of 0.50 to 0.088 at a Mach number of 0.92, with corresponding rates of roll of 4.0 and 5.2 radians per second.

4. The upper aft fuselage dive brake, when deflected 30° and 60°, reduced the rudder effectiveness about 10 to 20 percent and about 35 to 50 percent, respectively.

Langley Aeronautical Laboratory,
National Advisory Committee for Aeronautics,
Langley Field, Va., July 21, 1954.

Kenneth P. Spreemann
Kenneth P. Spreemann
Aeronautical Research Scientist

Albert G. Few, Jr.
Albert G. Few, Jr.
Aeronautical Research Scientist

Approved: Thomas A. Harris
Thomas A. Harris
Chief of Stability Research Division

ecc

REFERENCES

1. Spreemann, Kenneth P., and Few, Albert G., Jr.: Preliminary Investigation of the Static Longitudinal and Lateral Stability Characteristics of a 0.05-Scale Model of the Convair F2Y-1 Airplane at High Subsonic Speeds - TED No. NACA DE 383. NACA RM SL54A12, Bur. Aero., 1954.

2. Campbell, George S., and Weil, Joseph: The Interpretation of Nonlinear Pitching Moments in Relation to the Pitch-Up Problem. NACA RM L53I02, 1953.

3. Wiggins, James W.: Wind-Tunnel Investigation at High Subsonic Speeds To Determine the Rolling Derivatives of Two Wing-Fuselage Combinations Having Triangular Wings, Including a Semiempirical Method of Estimating the Rolling Derivatives. NACA RM L53L18a, 1954.

TABLE I.- INDEX OF FIGURES PRESENTING DATA

Figure	Configuration	Fences	Chord-extension	Notch	Dive brake	δ_e, deg		δ_r, deg	Actuator and fairing	Remarks	Tabulated data
						Right	Left				
13	1A	1 at 0.63b/2	None	None	None	0	0	0	On	Original elevon strain gage	
	2	1 at 0.63b/2	None	None	None	0	0	0	On	Dummy elevon strain gage	
	3	1 at 0.63b/2	None	None	None	0	0	0	On	Dummy elevon strain gage plus lock	
14	1A	1 at 0.63b/2	None	None	None	-5	-5	0	On	Original elevon strain gage	
	2	1 at 0.63b/2	None	None	None	-5	-5	0	On	Dummy elevon strain gage	
	3	1 at 0.63b/2	None	None	None	-5	-5	0	On	Dummy elevon strain gage plus lock	
15	1B	None	None	None	None	0	0	0	On		
	4	None	0.60b/2 to 0.77b/2	None	None	0	0	0	On		
	5	None	0.60b/2 to 0.77b/2	None	None	0	0	0	On	Actuator fairing on lower wing surface	
	6	None	0.60b/2 to 0.77b/2	None	None	0	0	0	On	Inverted model	
16	7	1 at 0.63b/2, 3 at 0.25b/2	None	None	None	0	0	0	On		M = 0.50 (table II)
	8	1 at 0.63b/2, 3 at 0.35b/2	None	None	None	0	0	0	On		M = 0.50 and 0.92 (table II)
	9	1 at 0.63b/2, 3 at 0.45b/2	None	None	None	0	0	0	On		
	10	1 at 0.63b/2, 3 at 0.55b/2	None	None	None	0	0	0	On		
17	1B	None	None	None	None	0	0	0	On		
	10	1 at 0.63b/2, 3 at 0.55b/2	None	None	None	0	0	0	On		
18	11	4 at 0.58b/2	None	None	None	0	0	0	Off		
	12	4 at 0.63b/2	None	None	None	0	0	0	Off		
	13	4 at 0.68b/2	None	None	None	0	0	0	Off		
	14	5 at 0.68b/2	None	None	None	0	0	0	Off		
19	15	4 at 0.68b/2	None	None	None	0	0	0	On		C_L, C_D, M = 0.50 and 0.92 (table III)
	16	3 at 0.55b/2	None	None	None	0	0	0	On		C_L and C_D (table III)
	17	1 at 0.63b/2, 6 at 0.45b/2	None	None	None	0	0	0	On		C_L and C_D (table III)
	18	1 at 0.63b/2, 7 at 0.55b/2	None	None	None	0	0	0	On		C_L and C_D (table III)
20	1B	None	None	None	None	0	0	0	On		
	19	None	None	1 at 0.68b/2	None	0	0	0	On		
	20	None	0.68b/2 to 0.85b/2	1 at 0.68b/2	None	0	0	0	On		
	21	None	0.68b/2 to 0.85b/2	1 at 0.68b/2	None	0	0	0	On	Inlets plugged with smooth fairing	
21	22	None	0.68b/2 to 0.85b/2	1	None	0	0	0	Off	Notch 1 at 0.68b/2	
	23	None	0.68b/2 to 0.85b/2	1 plus 2	None	0	0	0	Off	Notch 1 at 0.68b/2, notch 2 at 0.17b/2	
22	10	1 at 0.63b/2, 3 at 0.55b/2	None	None	None	-5	-5	0	On		
	10	1 at 0.63b/2, 3 at 0.55b/2	None	None	None	-10	-10	0	On		
23	20	None	0.68b/2 to 0.85b/2	1 at 0.68b/2	None	0	0	0	On		
	20	None	0.68b/2 to 0.85b/2	1 at 0.68b/2	None	-2	-2	0	On		
	20	None	0.68b/2 to 0.85b/2	1 at 0.68b/2	None	-5	-5	0	On		
	20	None	0.68b/2 to 0.85b/2	1 at 0.68b/2	None	-10	-10	0	On		
24	20	None	0.68b/2 to 0.85b/2	1	None	0	0	0	On	Notch 1 at 0.68b/2	
	22	None	0.68b/2 to 0.85b/2	1	None	0	0	0	Off	Notch 1 at 0.68b/2	
	24	None	0.68b/2 to 0.85b/2	1	30°	0	0	0	On	Notch 1 at 0.68b/2	
	25	None	0.68b/2 to 0.85b/2	1	30°	0	0	0	Off	Notch 1 at 0.68b/2	
	26	None	0.68b/2 to 0.85b/2	1 plus 2	30°	0	0	0	Off	Notch 1 at 0.68b/2, notch 2 at 0.17b/2	M = 0.92 (table IV)

TABLE I.- INDEX OF FIGURES PRESENTING DATA - Concluded

Figure	Configuration	Fences	Chord-extension	Notch	Dive brake	δ_e, deg		δ_r, deg	Actuator and fairing	Remarks	Tabulated data
						Right	Left				
25	20	None	0.68b/2 to 0.85b/2	1 at 0.68b/2	0°	0	0	0	On		
	24	None	0.68b/2 to 0.85b/2	1 at 0.68b/2	30°	0	0	0	On		
	27	None	0.68b/2 to 0.85b/2	1 at 0.68b/2	60°	0	0	0	On		
26	20	None	0.68b/2 to 0.85b/2	1 at 0.68b/2	None	0	0	0	On		
	28	None	0.68b/2 to 0.85b/2	1 at 0.68b/2	None	0	0	0	On	Upper 1/4-inch fuselage spoiler 8.6 inches from duct exit	C_L, C_D, at M = 0.85 and 0.92 (table V)
	29	None	0.68b/2 to 0.85b/2	1 at 0.68b/2	None	0	0	0	On	Upper 1/4-inch fuselage spoiler 3.25 inches from duct exit	C_L and C_D (table V)
	30	None	0.68b/2 to 0.85b/2	1 at 0.68b/2	None	0	0	0	On	Upper 1/8-inch fuselage spoiler 3.25 inches from duct exit	C_L and C_D (table V)
	31	None	0.68b/2 to 0.85b/2	1 at 0.68b/2	None	0	0	0	On	Lower 1/8-inch fuselage spoiler 2.5 inches from duct exit	C_L and C_D (table V)
	32	None	None	None	None	0	0	0	On	Fuselage faired at aft end to sting exit	C_L, C_D, M = 0.50 and 0.92 (table V)
	33	None	0.68b/2 to 0.85b/2	1 at 0.68b/2	None	0	0	0	On	Upper 1/4-inch fuselage fence 0 inch from duct exit	C_L and C_D (table V)
	34	None	0.68b/2 to 0.85b/2	1 at 0.68b/2	None	0	0	0	On	Upper 1/4-inch fuselage fence 3.25 inches from duct exit	C_L and C_D (table V)
27	35	None	None	None	None	0	0	0	On	Transition strip at $0.05\bar{c}$	
28	36	None	None	None	None	--	---	--	--	Body-canopy alone	
29	20	None	0.68b/2 to 0.85b/2	1 at 0.68b/2	None	0	0	0	On	Lateral data	
	20	None	0.68b/2 to 0.85b/2	1 at 0.68b/2	None	5	-5	0	On	Lateral data	C_L, C_D, C_m (table VI)
	20	None	0.68b/2 to 0.85b/2	1 at 0.68b/2	None	10	-10	0	On	Lateral data	C_L, C_D, C_m (table VI)
30	27	None	0.68b/2 to 0.85b/2	1 at 0.68b/2	60°	0	0	0	On	Lateral data	
	27	None	0.68b/2 to 0.85b/2	1 at 0.68b/2	60°	0	0	10	On	Lateral data	C_L, C_D, C_m (table VII)
	24	None	0.68b/2 to 0.85b/2	1 at 0.68b/2	30°	0	0	0	On	Lateral data	C_L, C_D, C_m (table VII)
31	20	None	0.68b/2 to 0.85b/2	1 at 0.68b/2	None	0	0	0	On	Lateral data, $\alpha = 0^{\circ}$	
	20	None	0.68b/2 to 0.85b/2	1 at 0.68b/2	None	0	0	0	On	Lateral data, $\alpha = 4^{\circ}$	
	20	None	0.68b/2 to 0.85b/2	1 at 0.68b/2	None	0	0	0	On	Lateral data, $\alpha = 6^{\circ}$	
	20	None	0.68b/2 to 0.85b/2	1 at 0.68b/2	None	0	0	0	On	Lateral data, $\alpha = 12^{\circ}$	
32	10	1 at 0.63b/2, 3 at 0.55b/2	None	None	None	--	---	0	On	Elevator effectiveness	
	20	None	0.68b/2 to 0.85b/2	1 at 0.68b/2	None	--	---	0	On	Elevator effectiveness	
33	20	None	0.68b/2 to 0.85b/2	1 at 0.68b/2	None	--	---	0	On	Helix angle and rate of roll	
34	10	1 at 0.63b/2, 3 at 0.55b/2	None	None	None	--	---	0	On	Lift-drag ratios	
	20	None	0.68b/2 to 0.85b/2	1 at 0.68b/2	None	--	---	0	On	Lift-drag ratios	
35	10	1 at 0.63b/2, 3 at 0.55b/2	None	None	None	--	---	0	On	Summary	
	20	None	0.68b/2 to 0.85b/2	1 at 0.68b/2	None	--	---	0	On	Summary	

TABLE II.- ADDITIONAL DATA SUPPLEMENTING FIGURE 16

Configuration 7 M = 0.50			
α, deg	C_L	C_D	C_m
-2.11	-0.091	0.0199	-0.0062
-.06	-.019	.0168	-.0098
2.01	.065	.0174	-.0144
4.08	.155	.0227	-.0204
6.17	.256	.0348	-.0256
8.24	.350	.0538	-.0291
10.33	.443	.0786	-.0322
12.43	.543	.1123	-.0363
14.53	.646	.1559	-.0373
16.61	.716	.1982	-.0365
18.68	.760	.2420	-.0352
20.70	.818	.2911	-.0442
22.75	.886	.3537	-.0543
24.68	.827	.3695	-.0637

Configuration 8							
M = 0.50				M = 0.92			
α, deg	C_L	C_D	C_m	α, deg	C_L	C_D	C_m
-2.11	-0.074	0.0193	-0.0078	-2.31	-0.126	0.0231	-0.0028
-.05	-.001	.0167	-.0118	-1.24	-.076	.0200	-.0076
2.05	.109	.0188	-.0164	-.16	-.023	.0183	-.0123
4.09	.176	.0237	-.0226	.90	.027	.0180	-.0177
6.17	.271	.0361	-.0281	1.97	.083	.0190	-.0226
8.25	.368	.0556	-.0321	3.06	.143	.0219	-.0283
10.33	.456	.0803	-.0358	4.13	.202	.0267	-.0345
12.43	.550	.1138	-.0381	5.21	.261	.0334	-.0399
14.52	.648	.1556	-.0392	6.31	.319	.0432	-.0429
16.61	.732	.2015	-.0406	7.40	.372	.0547	-.0464
18.72	.797	.2527	-.0331	8.46	.427	.0686	-.0526
20.75	.840	.3013	-.0407	9.57	.476	.0843	-.0541
22.78	.883	.3531	-.0452	10.62	.524	.1024	-.0587
24.71	.851	.3807	-.0607	11.69	.574	.1216	-.0649
				12.79	.625	.1433	-.0680
				13.85	.666	.1649	-.0710
				14.85	.762	.1992	-.0958
				15.97	.786	.2207	-.0895

TABLE III.- ADDITIONAL DATA SUPPLEMENTING FIGURE 19

Configuration 15										
M = 0.50				M = 0.85			M = 0.92			
α, deg	C_L	C_D	C_m	α, deg	C_L	C_D	α, deg	C_L	C_D	C_m
-2.11	-0.086	0.0160	-0.0048	-2.28	-0.118	0.0187	-2.29	-0.124	0.0198	-0.0016
-.06	-.019	.0126	-.0093	-1.21	-.066	.0157	-1.23	-.076	.0166	-.0066
2.02	.066	.0136	-.0134	-0.14	-.023	.0141	-.14	-.021	.0151	-.0113
4.08	.162	.0185	-.0190	.93	.032	.0138	.91	.027	.0146	-.0163
6.18	.269	.0324	-.0241	2.00	.078	.0146	1.99	.081	.0159	-.0206
8.27	.358	.0508	-.0264	3.08	.134	.0176	3.07	.143	.0191	-.0267
10.36	.463	.0789	-.0282	4.16	.189	.0216	4.15	.203	.0240	-.0324
12.46	.561	.1134	-.0320	5.23	.247	.0283	5.25	.265	.0313	-.0370
14.54	.648	.1533	-.0343	6.32	.304	.0370	6.35	.323	.0416	-.0399
16.63	.736	.2006	-.0359	7.42	.354	.0481	7.41	.386	.0535	-.0472
18.73	.829	.2567	-.0394	8.52	.410	.0610	8.50	.447	.0688	-.0524
20.81	.908	.3163	-.0434	9.61	.462	.0761	9.58	.502	.0856	-.0583
22.87	.967	.3773	-.0477	10.73	.514	.0936	10.65	.563	.1053	-.0654
24.85	.952	.4140	-.0513	11.84	.569	.1141	11.62	.630	.1282	-.0869
				12.93	.626	.1367	12.71	.684	.1521	-.0899
				14.03	.666	.1584	13.73	.754	.1819	-.1061
				15.11	.694	.1793	14.77	.801	.2077	-.1132
				16.14	.734	.2040				
				17.21	.781	.2322				
				18.26	.831	.2638				
				19.28	.845	.2855				
				20.28	.864	.3110				
				21.25	.852	.3238				
				22.16	.841	.3423				

Configuration 16 M = 0.85		
α, deg	C_L	C_D
-2.28	-0.111	0.0212
-1.21	-.065	.0189
-.14	-.016	.0175
.92	.033	.0172
1.99	.083	.0183
3.07	.135	.0206
4.15	.188	.0246
5.22	.246	.0317
6.31	.305	.0406
7.39	.360	.0511
8.51	.406	.0643
9.59	.461	.0797
10.69	.513	.0963
11.79	.560	.1145
12.88	.614	.1359
13.95	.682	.1636
15.04	.721	.1866
16.11	.763	.2130
17.17	.796	.2363
18.23	.842	.2689
19.28	.846	.2879
20.30	.849	.3074
21.14	.808	.3134
22.15	.817	.3346
23.05	.781	.3404

Configuration 17 M = 0.85		
α, deg	C_L	C_D
-2.29	-0.113	0.0215
-1.22	-.064	.0187
-.15	-.020	.0170
.91	.029	.0168
1.98	.081	.0179
3.06	.138	.0207
4.14	.192	.0249
5.22	.251	.0315
6.30	.304	.0400
7.39	.349	.0501
8.47	.402	.0631
9.55	.455	.0775
10.65	.507	.0941
11.73	.551	.1132
12.79	.601	.1345
13.87	.655	.1577
14.96	.710	.1840
16.03	.761	.2111
17.10	.792	.2356
18.17	.800	.2562
19.20	.804	.2749
20.21	.811	.2955
21.12	.788	.3074
22.07	.775	.3199
23.05	.789	.3443

Configuration 18 M = 0.85		
α, deg	C_L	C_D
-2.28	-0.109	0.0209
-1.22	-.063	.0187
-.14	-.013	.0170
.92	.035	.0168
1.99	.083	.0181
3.07	.139	.0206
4.14	.195	.0249
5.22	.256	.0319
6.31	.303	.0395
7.40	.350	.0498
8.49	.404	.0628
9.58	.455	.0771
10.69	.531	.0988
11.77	.569	.1174
12.86	.625	.1392
13.93	.671	.1613
15.01	.719	.1875
16.08	.749	.2106
17.17	.784	.2358
18.21	.800	.2572
19.24	.820	.2807
20.27	.840	.3055
21.22	.828	.3193
22.14	.813	.3338
23.04	.801	.3485

TABLE IV.- ADDITIONAL DATA SUPPLEMENTING FIGURE 24

Configuration 26 M = 0.92			
α, deg	C_L	C_D	C_m
-2.26	-0.137	0.0252	0.0042
-1.20	-.083	.0214	-.0024
-.13	-.031	.0195	-.0073
.93	.020	.0187	-.0123
2.01	.078	.0198	-.0175
3.09	.141	.0232	-.0238
4.17	.206	.0284	-.0318
5.24	.271	.0365	-.0388
6.30	.334	.0475	-.0470
7.43	.382	.0574	-.0457
8.51	.440	.0713	-.0512
9.60	.492	.0864	-.0538
10.62	.568	.1087	-.0698
11.65	.634	.1307	-.0846
12.69	.700	.1555	-.0961
13.68	.770	.1859	-.1147
14.83	.798	.2067	-.1054

[redacted]

TABLE V.- ADDITIONAL DATA SUPPLEMENTING FIGURE 26

Configuration 28						
M = 0.85			M = 0.92			
α, deg	C_L	C_D	α, deg	C_L	C_D	C_m
-2.33	-0.117	0.0245	-2.37	-0.122	0.0279	-0.0107
-1.26	-.069	.0216	-1.32	-.072	.0249	-.0173
-.19	-.021	.0200	-.25	-.019	.0236	-.0225
.87	.024	.0196	.81	.028	.0244	-.0264
1.93	.075	.0212	1.88	.074	.0271	-.0299
3.02	.130	.0236	2.96	.136	.0289	-.0370
4.09	.183	.0275	4.04	.191	.0335	-.0425
5.17	.243	.0341	5.11	.251	.0393	-.0482
6.26	.295	.0424	6.21	.313	.0483	-.0516
7.35	.351	.0531	7.32	.369	.0588	-.0544
8.46	.400	.0653	8.44	.419	.0718	-.0539
9.56	.450	.0798	9.54	.478	.0878	-.0576
10.66	.497	.0953	10.58	.551	.1096	-.0712
11.78	.555	.1162	11.63	.607	.301	-.0799
12.87	.610	.1380	12.66	.679	.1595	-.0951
13.98	.653	.1601	13.73	.730	.1819	-.0997
15.08	.680	.1807	14.76	.788	.2113	-.1105
16.11	.718	.2061				
17.17	.766	.2344				
18.22	.807	.2623				

Configuration 29 M = 0.85		
α, deg	C_L	C_D
-2.28	-0.130	0.0274
-1.21	-.084	.0243
-.13	-.031	.0223
.92	.012	.0213
2.00	.064	.0222
3.08	.119	.0242
4.15	.174	.0280
5.25	.233	.0348
6.34	.284	.0428
7.44	.340	.0534
8.54	.393	.0666
9.65	.444	.0815
10.75	.501	.0998
11.85	.557	.1196
12.92	.618	.1422
14.02	.661	.1643
15.12	.720	.1924
16.16	.736	.2120
17.24	.799	.2453
18.29	.839	.2737

Configuration 30 M = 0.85		
[redacted]	[redacted]	[redacted]
[redacted]	[redacted]	[redacted]
21.22	.842	.3251

[redacted]		
[redacted]	[redacted]	[redacted]
[redacted]	[redacted]	[redacted]

TABLE V.- ADDITIONAL DATA SUPPLEMENTING FIGURE 26 - Concluded

Configuration 32										
M = 0.85			M = 0.50				M = 0.92			
α, deg	C_L	C_D	α, deg	C_L	C_D	C_m	α, deg	C_L	C_D	C_m
-2.29	-0.106	0.0211	-2.13	-0.089	0.0220	-0.0099	-2.33	-0.125	0.0239	-0.0060
-1.23	-.060	.0183	-.07	-.010	.0175	-.0145	-1.26	-.073	.0204	-.0111
-.16	-.013	.0169	1.99	.073	.0183	-.0193	-.19	-.023	.0187	-.0157
.90	.037	.0170	4.06	.164	.0240	-.0260	.87	.029	.0185	-.0210
1.96	.087	.0182	6.15	.273	.0380	-.0319	1.94	.083	.0200	-.0265
3.04	.144	.0213	8.24	.374	.0582	-.0362	3.02	.146	.0235	-.0326
4.11	.198	.0256	10.34	.459	.0841	-.0329	4.09	.207	.0283	-.0395
5.19	.255	.0327	12.44	.536	.1162	-.0301	5.18	.269	.0354	-.0450
6.26	.311	.0419	14.53	.633	.1569	-.0337	6.27	.331	.0450	-.0506
7.37	.366	.0532	16.61	.727	.2054	-.0388	7.35	.384	.0568	-.0537
8.46	.389	.0641	16.68	.811	.2564	-.0443	8.46	.428	.0698	-.0529
9.56	.436	.0785	20.73	.860	.3051	-.0477	9.55	.472	.0852	-.0536
10.67	.486	.0945	22.83	.965	.3824	-.0561	10.59	.551	.1080	-.0694
11.76	.558	.1173	24.84	.982	.4325	-.0612	11.58	.624	.1314	-.0884
12.84	.614	.1383					12.64	.688	.1554	-.0978
13.92	.688	.1663					13.71	.735	.1787	-.1010
15.00	.729	.1891					14.74	.788	.2058	-.1120
16.09	.780	.2173								
17.15	.801	.2398								
18.20	.826	.2632								
19.22	.861	.2924								
20.22	.879	.3172								
21.22	.884	.3390								
22.05	.856	.3491								
23.00	.824	.3557								

Configuration 33 M = 0.85		
α, deg	C_L	C_D
-2.29	-0.115	0.0210
-1.23	-.066	.0182
-.15	-.020	.0167
.91	.029	.0162
1.99	.080	.0174
3.07	.134	.0200
4.15	.193	.0246
5.23	.247	.0314
6.33	.298	.0391
7.42	.354	.0504
8.52	.407	.0632
9.62	.459	.0783
10.73	.505	.0945
11.82	.585	.1188
12.90	.636	.1408
14.01	.675	.1620
15.08	.731	.1892
16.14	.741	.2077
17.18	.774	.2313
18.25	.822	.2616
19.27	.852	.2882
20.29	.876	.3153
21.13	.818	.3159
22.17	.842	.3444

Configuration 34 M = 0.85		
α, deg	C_L	C_D
-2.29	-0.111	0.0208
-1.22	-.065	.0181
-.15	-.017	.0165
.91	.029	.0162
1.99	.082	.0177
3.07	.137	.0201
4.14	.191	.0245
5.23	.247	.0312
6.32	.300	.0398
7.43	.358	.0511
8.53	.410	.0638
9.62	.459	.0787
10.74	.512	.0962
11.82	.579	.1180
12.90	.640	.1414
14.01	.676	.1624
15.09	.701	.1830
16.15	.744	.2092
17.21	.811	.1795
18.26	.840	.2681
19.28	.862	.2935
20.30	.881	.3185
21.19	.848	.3282
22.14	.845	.3454

TABLE VI.- ADDITIONAL DATA SUPPLEMENTING FIGURE 29

Configuration 20, $\delta_e = \pm 5^\circ$											
M = 0.50				M = 0.85				M = 0.92			
α, deg	C_L	C_D	C_m	α, deg	C_L	C_D	C_m	α, deg	C_L	C_D	C_m
-3.44	-0.149	0.0264	-0.0050	-3.56	-0.185	0.0299	-0.0031	-3.61	-0.203	0.0320	0.0023
-1.37	-.069	.0193	-.0099	-2.46	-.133	.0242	-.0068	-2.50	-.149	.0263	-.0009
.82	.013	.0172	-.0145	-1.38	-.085	.0208	-.0108	-1.40	-.099	.0231	-.0061
2.90	.098	.0203	-.0196	-.29	-.035	.0188	-.0149	-.32	-.046	.0200	-.0120
4.99	.194	.0277	-.0245	.79	.013	.0181	-.0179	.78	.004	.0203	-.0163
7.08	.290	.0427	-.0274	1.88	.063	.0188	-.0214	1.88	.063	.0215	-.0218
9.17	.385	.0638	-.0284	2.98	.117	.0206	-.0256	2.99	.123	.0235	-.0277
11.28	.484	.0935	-.0298	4.06	.172	.0245	-.0297	4.11	.192	.0289	-.0361
13.37	.582	.1313	-.0331	5.17	.228	.0309	-.0341	5.21	.246	.0349	-.0397
15.47	.677	.1753	-.0371	6.27	.282	.0390	-.0362	6.33	.309	.0444	-.0451
17.57	.764	.2249	-.0405	7.38	.336	.0494	-.0385	7.45	.371	.0562	-.0517
19.67	.865	.2877	-.0450	8.51	.403	.0643	-.0403	8.55	.429	.0702	-.0588
21.76	.940	.3505	-.0492	9.58	.443	.0773	-.0407	9.67	.494	.0885	-.0650
23.78	.954	.3950	-.0508	10.69	.487	.0927	-.0400	10.76	.568	.1127	-.0846
24.68	.873	.3853	-.0663	11.82	.550	.1140	-.0428	11.87	.624	.1337	-.0886
				12.91	.609	.1366	-.0486	12.97	.677	.1569	-.0940
				14.01	.669	.1615	-.0552	14.07	.739	.1858	-.1055
				15.13	.715	.1862	-.0535				
				16.18	.727	.2052	-.0470				
				17.26	.764	.2310	-.0502				
				18.34	.814	.2624	-.0587				
				19.38	.838	.2873	-.0628				
				20.41	.845	.3074	-.0636				
				21.43	.861	.3330	-.0679				
				22.35	.825	.3425	-.0782				

Configuration 20, $\delta_e = \pm 10^\circ$											
M = 0.50				M = 0.85				M = 0.92			
α, deg	C_L	C_D	C_m	α, deg	C_L	C_D	C_m	α, deg	C_L	C_D	C_m
-2.13	-0.117	0.0292	-0.0074	-2.30	-0.141	0.0315	-0.0027	-2.33	-0.155	0.0327	-0.0015
-.07	-.043	.0246	-.0119	-1.22	-.095	.0285	-.0078	-1.24	-.102	.0292	-.0049
2.01	-.038	.0247	-.0165	-.14	-.046	.0265	-.0120	-.15	-.051	.0270	-.0112
4.09	.129	.0282	-.0219	.95	.003	.0261	-.0158	.94	.005	.0276	-.0169
6.19	.228	.0396	-.0258	2.05	.057	.0269	-.0207	2.06	.065	.0292	-.0234
8.29	.323	.0575	-.0274	3.14	.117	.0292	-.0266	3.17	.132	.0321	-.0314
10.39	.423	.0839	-.0290	4.23	.169	.0319	-.0294	4.28	.196	.0365	-.0385
12.48	.513	.1153	-.0312	5.34	.224	.0383	-.0334	5.39	.250	.0421	-.0419
14.59	.616	.1567	-.0348	6.45	.282	.0470	-.0369	6.50	.316	.0520	-.0486
16.68	.715	.2056	-.0386	7.55	.336	.0577	-.0383	7.61	.374	.0656	-.0549
18.81	.824	.2660	-.0442	8.64	.384	.0697	-.0388	8.72	.436	.0786	-.0635
20.86	.878	.3180	-.0456	9.75	.432	.0841	-.0379	9.84	.495	.0960	-.0666
22.93	.934	.3770	-.0492	10.86	.477	.0998	-.0372	10.96	.552	.1157	-.0689
24.84	.866	.3917	-.0678	11.97	.538	.1209	-.0404	12.21	.618	.1413	-.0850
				13.10	.621	.1488	-.0531	13.35	.688	.1714	-.1010
				14.19	.664	.1698	-.0527	14.45	.744	.1990	-.1120
				15.29	.707	.1940	-.0518	15.56	.790	.2240	-.1160
				16.38	.745	.2206	-.0509				
				17.44	.768	.2434	-.0500				
				18.50	.803	.2699	-.0539				
				19.56	.826	.2945	-.0589				
				20.59	.841	.3176	-.0617				
				21.60	.846	.3390	-.0640				
				22.52	.811	.3455	-.0684				
				23.46	.787	.3577	-.0773				

TABLE VII.- ADDITIONAL DATA SUPPLEMENTING FIGURE 30

Configuration 27, $\delta_r = 10^\circ$											
M = 0.50				M = 0.85				M = 0.92			
α, deg	C_L	C_D	C_m	α, deg	C_L	C_D	C_m	α, deg	C_L	C_D	C_m
-2.10	-0.107	0.0287	0.0014	-2.26	-0.138	0.0300	0.0044	-2.31	-0.157	0.0320	0.0078
-.04	-.037	.0240	-.0026	-1.18	-.089	.0265	.0004	-1.21	-.100	.0251	.0031
2.05	.054	.0247	-.0071	-.09	-.038	.0245	-.0036	-.12	-.049	.0246	-.0022
4.13	.141	.0286	-.0124	1.00	.014	.0235	-.0075	.98	.004	.0235	-.0070
6.21	.240	.0405	-.0161	2.08	.060	.0239	-.0113	2.09	.062	.0244	-.0121
8.32	.337	.0596	-.0174	3.19	.120	.0264	-.0161	3.21	.128	.0273	-.0187
10.42	.433	.0868	-.0179	4.30	.179	.0306	-.0206	4.33	.195	.0325	-.0265
12.51	.534	.1209	-.0209	5.38	.226	.0361	-.0229	5.43	.256	.0409	-.0343
14.63	.641	.1649	-.0254	6.48	.276	.0438	-.0241	6.55	.315	.0509	-.0358
16.73	.745	.2164	-.0307	7.58	.327	.0542	-.0262	7.66	.373	.0626	-.0428
18.84	.839	.2726	-.0364	8.69	.387	.0684	-.0287	8.77	.433	.0773	-.0491
20.92	.918	.3336	-.0411	9.80	.435	.0834	-.0287	9.89	.497	.0954	-.0568
22.95	.946	.3818	-.0447	10.91	.489	.1013	-.0287	11.00	.558	.1155	-.0638
24.99	.967	.4328	-.0484	12.01	.543	.1205	-.0320	12.08	.623	.1379	-.0810
				13.12	.606	.1441	-.0388	13.19	.686	.1636	-.0909
				14.22	.662	.1695	-.0438	14.28	.754	.1953	-.1090
				15.35	.724	.1983	-.0480	15.37	.809	.2233	-.1152
				16.43	.754	.2216	-.0463				
				17.49	.789	.2474	-.0488				
				18.56	.823	.2741	-.0539				
				19.59	.845	.2989	-.0598				
				20.65	.870	.3267	-.0640				
				21.66	.882	.3510	-.0674				
				22.60	.859	.3639	-.0759				
				23.54	.823	.3691	-.0811				

Configuration 24, $\delta_r = 10^\circ$											
M = 0.50				M = 0.85				M = 0.92			
α, deg	C_L	C_D	C_m	α, deg	C_L	C_D	C_m	α, deg	C_L	C_D	C_m
-2.09	-0.094	0.0246	-0.0015	-2.25	-0.119	0.0255	0.0001	-2.28	-0.131	0.0266	0.0032
-.02	-.012	.0212	-.0060	-1.15	-.070	.0223	-.0040	-1.18	-.078	.0234	-.0016
2.05	.066	.0219	-.0098	-.07	-.022	.0206	-.0076	-.08	-.029	.0212	-.0063
4.13	.160	.0272	-.0154	1.02	.033	.0202	-.0115	1.00	.024	.0207	-.0115
6.24	.255	.0403	-.0194	2.11	.077	.0213	-.0148	2.12	.081	.0223	-.0164
8.33	.355	.0595	-.0208	3.20	.132	.0235	-.0191	3.23	.145	.0258	-.0228
10.43	.454	.0866	-.0220	4.30	.189	.0279	-.0235	4.35	.213	.0313	-.0316
12.55	.563	.1236	-.0253	5.39	.242	.0345	-.0267	5.46	.279	.0404	-.0405
14.64	.662	.1668	-.0301	6.52	.302	.044	-.0287	6.57	.333	.0492	-.0436
16.76	.777	.2225	-.0352	7.61	.351	.0545	-.0310	7.70	.398	.0626	-.0490
18.85	.867	.2791	-.0404	8.73	.408	.0682	-.0313	8.79	.453	.0768	-.0537
20.95	.946	.3415	-.0442	9.81	.456	.0827	-.0325	9.90	.519	.0960	-.0623
23.00	.988	.3967	-.0478	10.94	.513	.1019	-.0337	11.00	.579	.1163	-.0724
24.93	.928	.4175	-.0610	12.07	.578	.1241	-.0362	12.11	.649	.1413	-.0865
				13.16	.630	.1451	-.0413	13.20	.698	.1639	-.0934
				14.27	.690	.1724	-.0464	14.32	.768	.1950	-.1074
				15.37	.736	.1978	-.0472				
				16.44	.769	.2225	-.0485				
				17.50	.791	.2453	-.0497				
				18.58	.841	.2767	-.0581				
				19.62	.861	.3012	-.0615				
				20.64	.874	.3245	-.0649				
				21.65	.878	.3445	-.0687				
				22.61	.863	.3628	-.0767				
				23.54	.828	.3688	-.0810				

 [redacted]

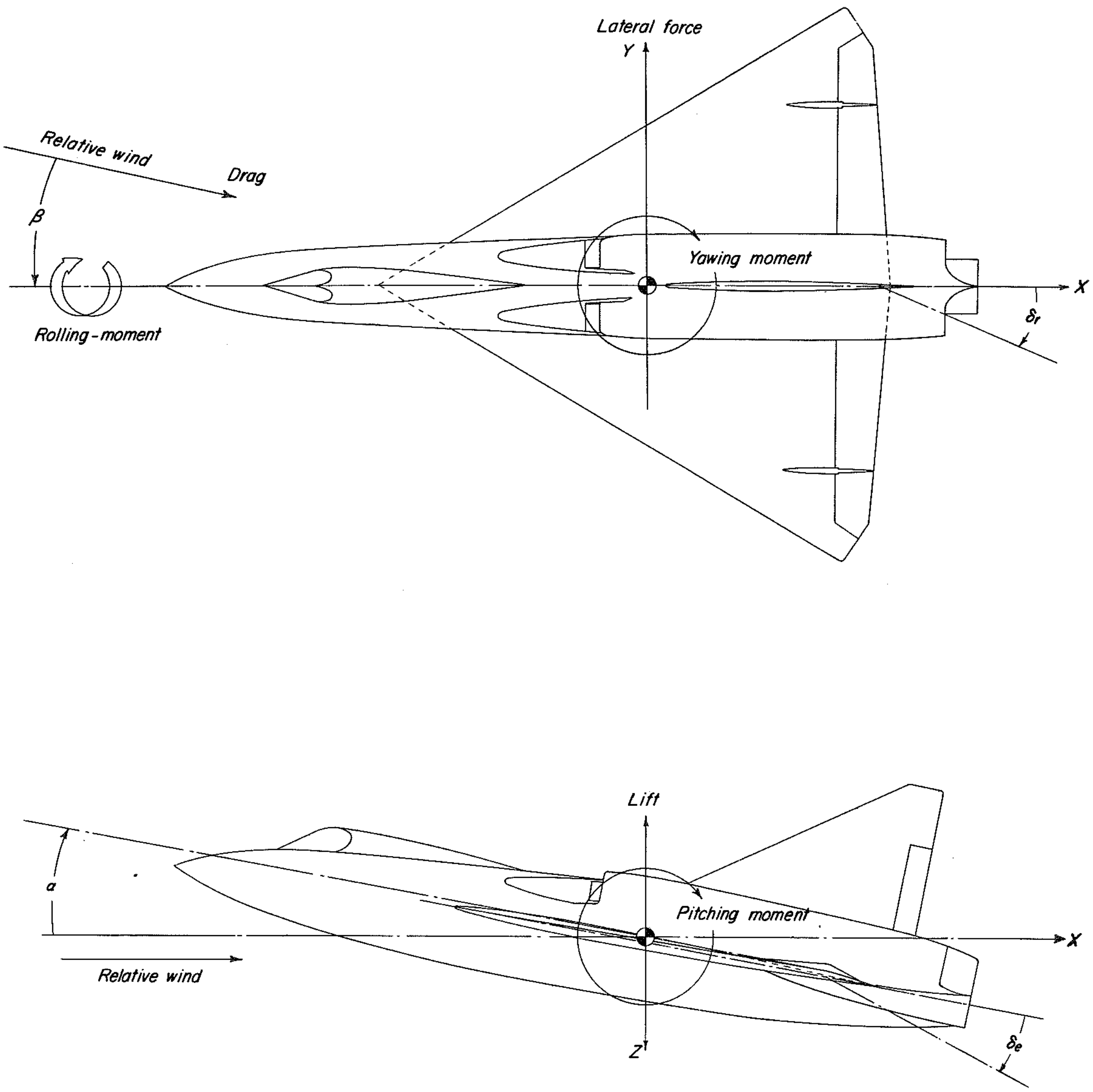

Figure 1.- System of axes used. Positive direction of forces, moments, and angles are indicated by arrows.

[redacted]

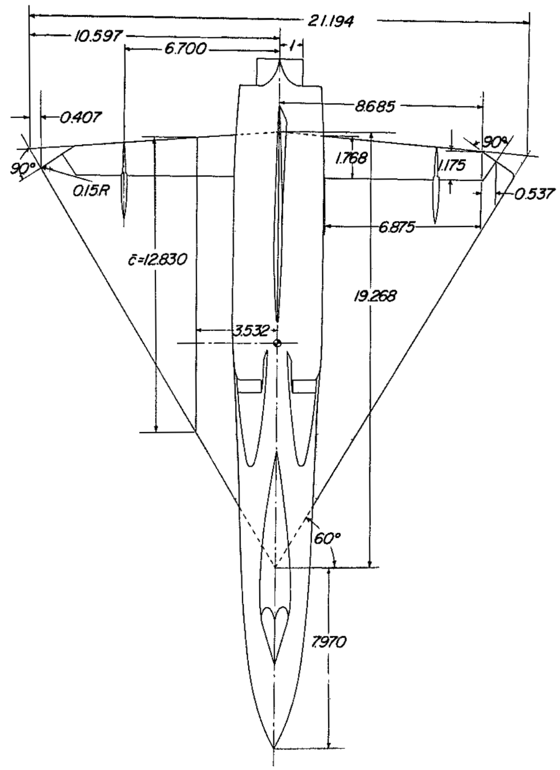

Physical Characteristics

Wing	
Leading-edge sweep, deg	60
Area, sq ft	1.42
Aspect ratio	2.18
Span, ft	1.76
Mean aerodynamic chord, ft	1.069
Incidence, deg	0
Dihedral, deg	1.5
Airfoil section parallel to free stream	
Root	NACA 65 - 003.3
Tip	NACA 65 - 004
Vertical tail	
Leading-edge sweep, deg	56
Area, sq ft	.20
Aspect ratio	1.0

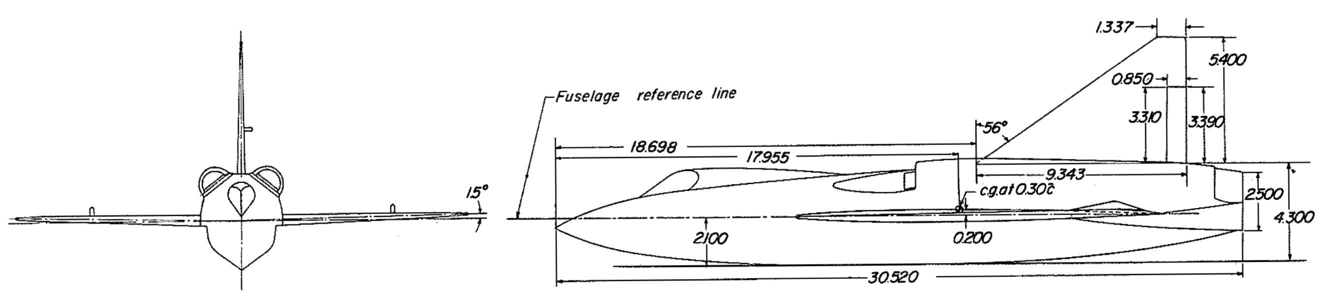

Figure 2.- General arrangement of test model. (All dimensions in inches.)

 [redacted]

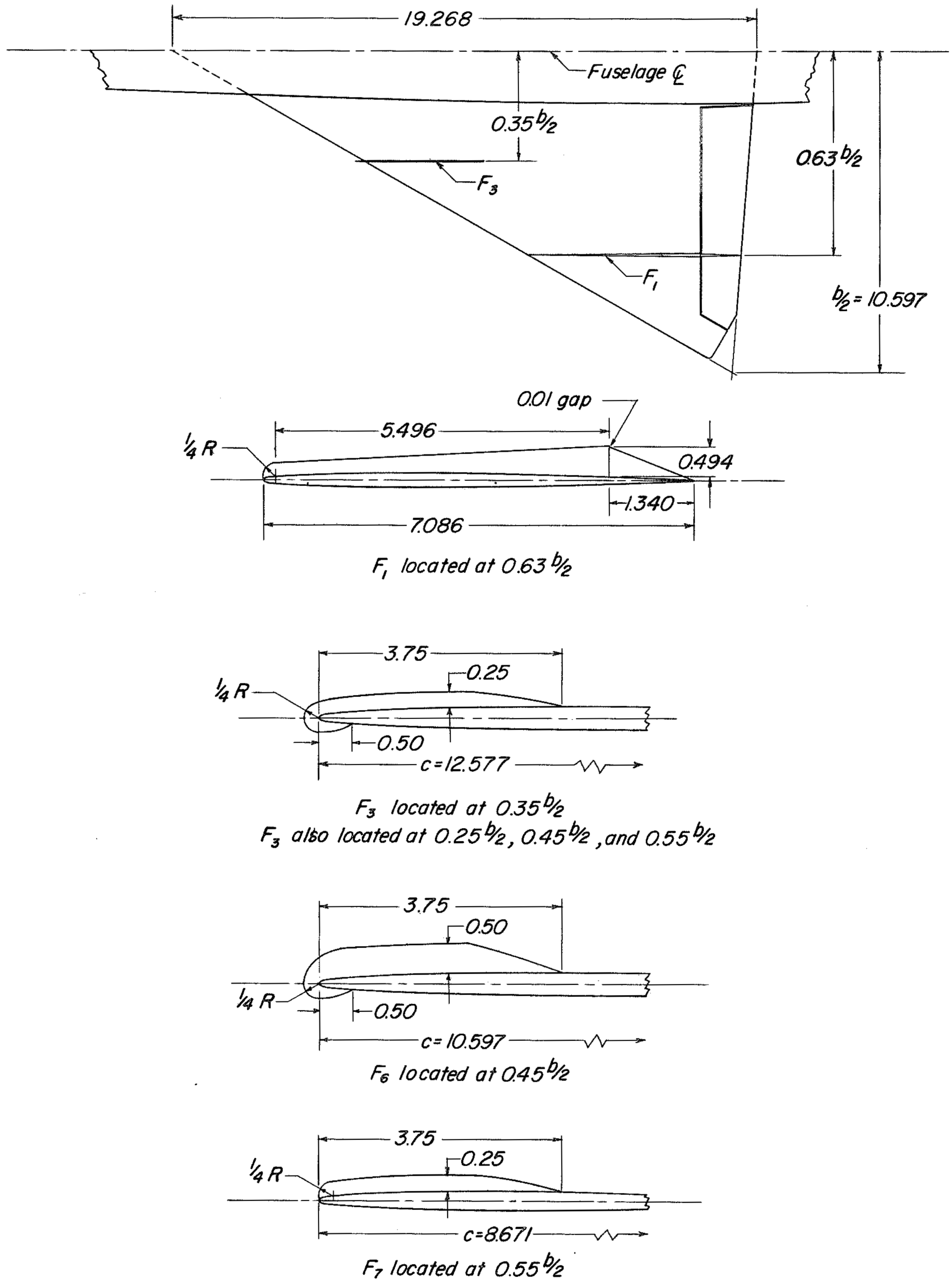

Figure 3.- Details of various wing fence configurations. (All dimensions in inches.)

[redacted]

[redacted]

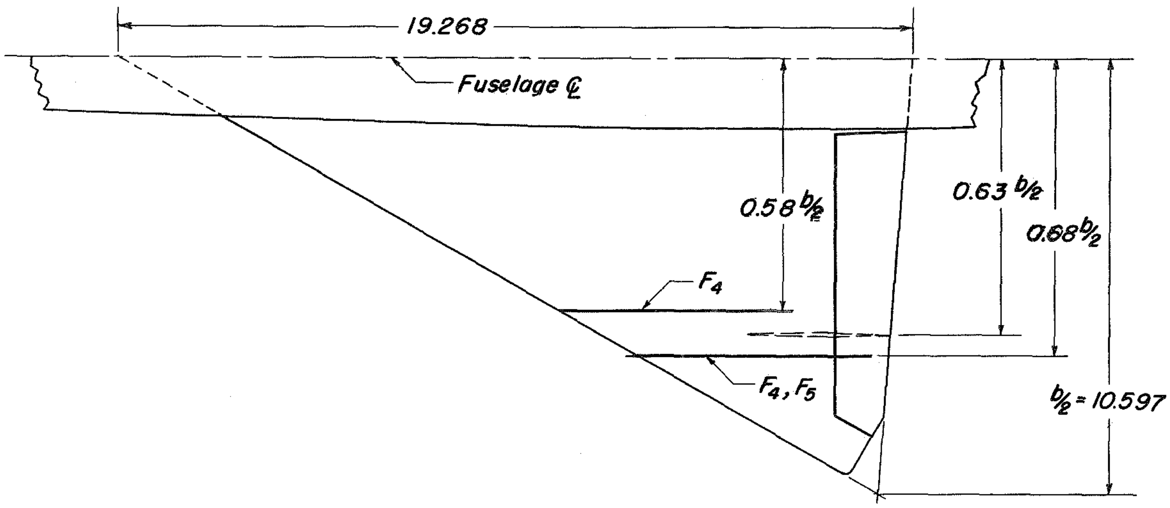

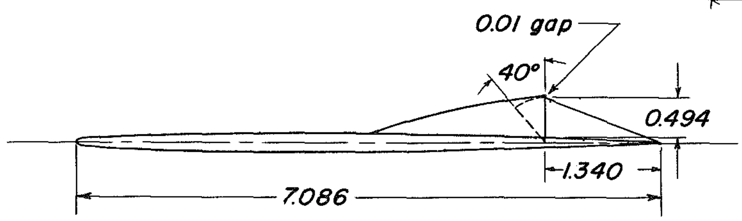

Elevon actuator and fairing located at 0.63 b/2

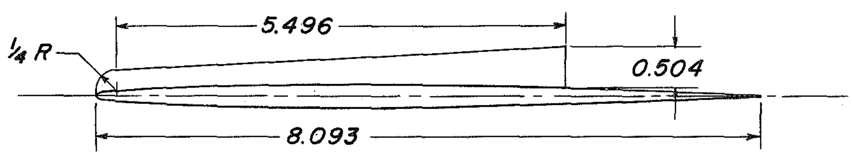

F_4 located at 0.58 b/2, elevon actuator and fairing removed
(F_4 also located at 0.63 b/2 and 0.68 b/2, elevon actuator and fairing removed and at 0.68 b/2 with elevon actuator and fairing installed.)

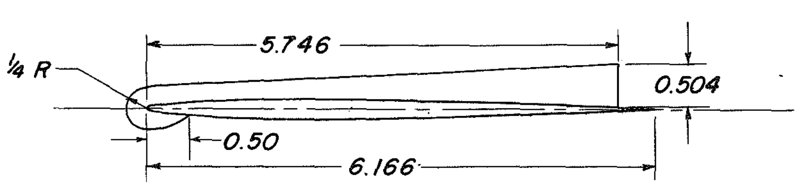

F_5 located at 0.68 b/2

Figure 3.- Concluded.

[redacted]

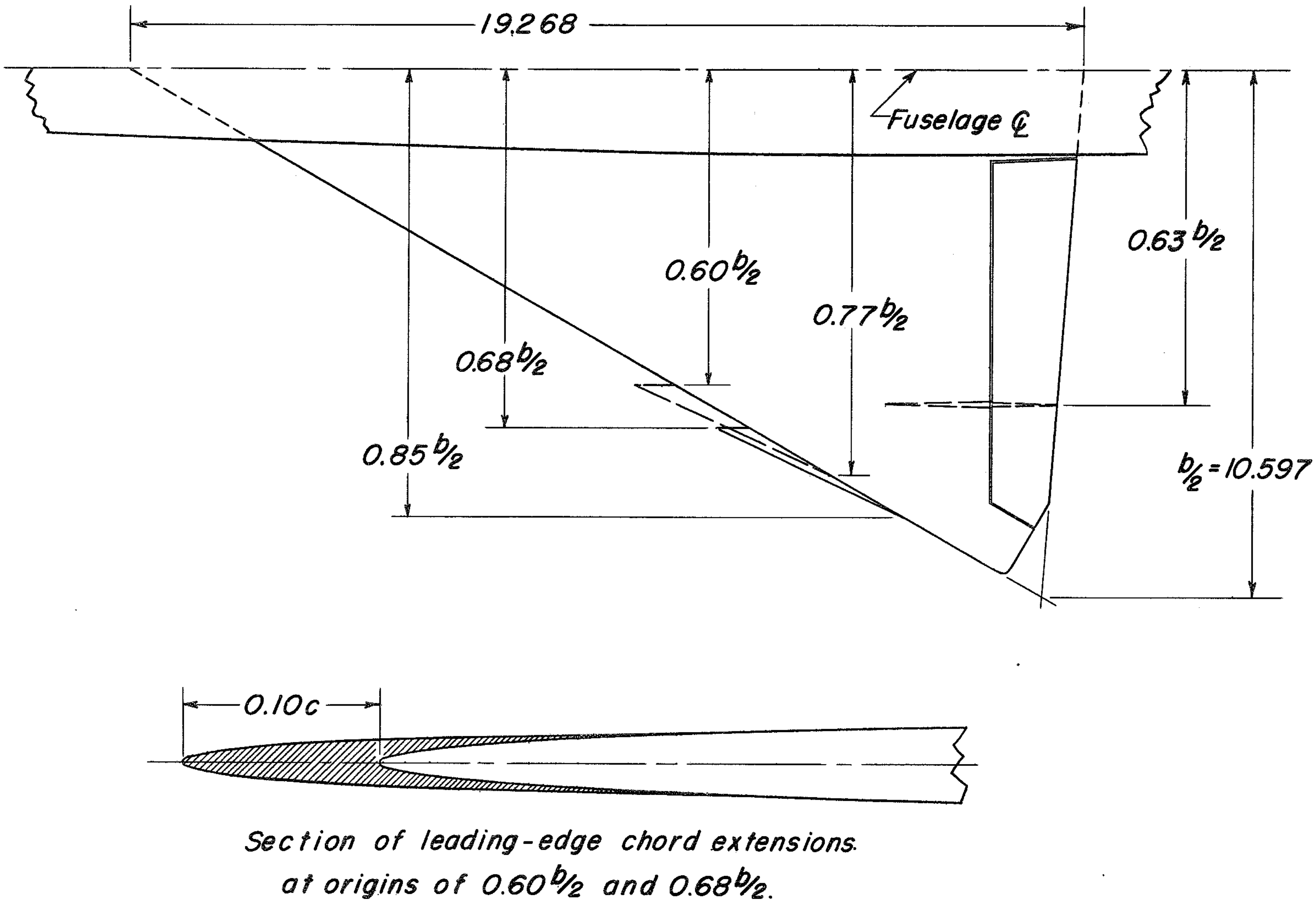

Figure 4.- Details of leading-edge chord-extensions originating at 0.60b/2 and 0.68b/2. (All dimensions in inches.)

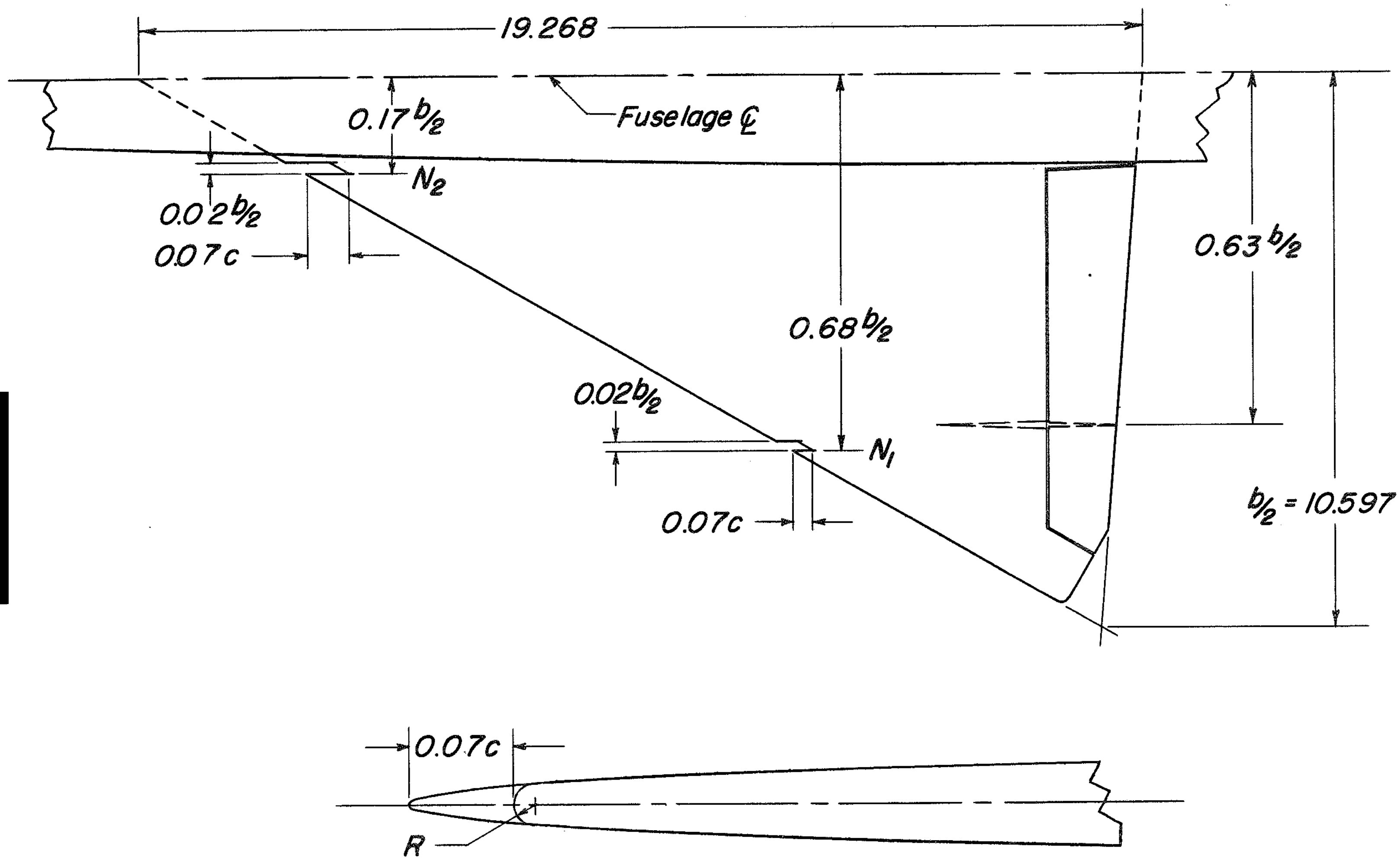

Detail of 0.07c leading-edge notches.

Figure 5.- Details of leading-edge notches located at 0.17b/2 and 0.68b/2. (All dimensions in inches.)

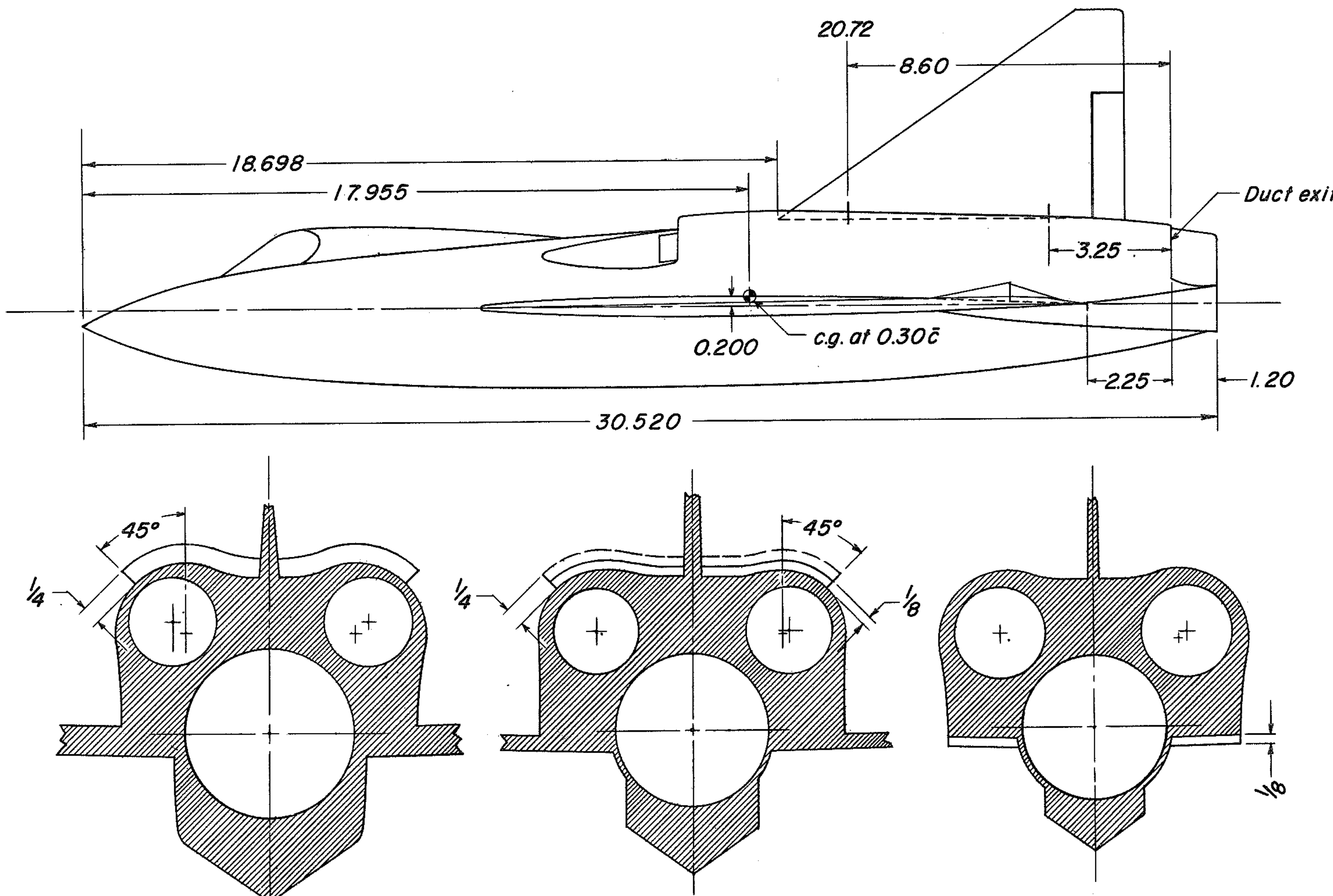

Section view at 8.60 from duct exit showing upper fuselage spoiler

Section view at 3.25 from duct exit showing upper fuselage spoilers

Section view at 2.25 from duct exit showing lower fuselage spoiler

Figure 6.- Details of upper and lower fuselage spoilers. (All dimensions in inches.)

[redacted]

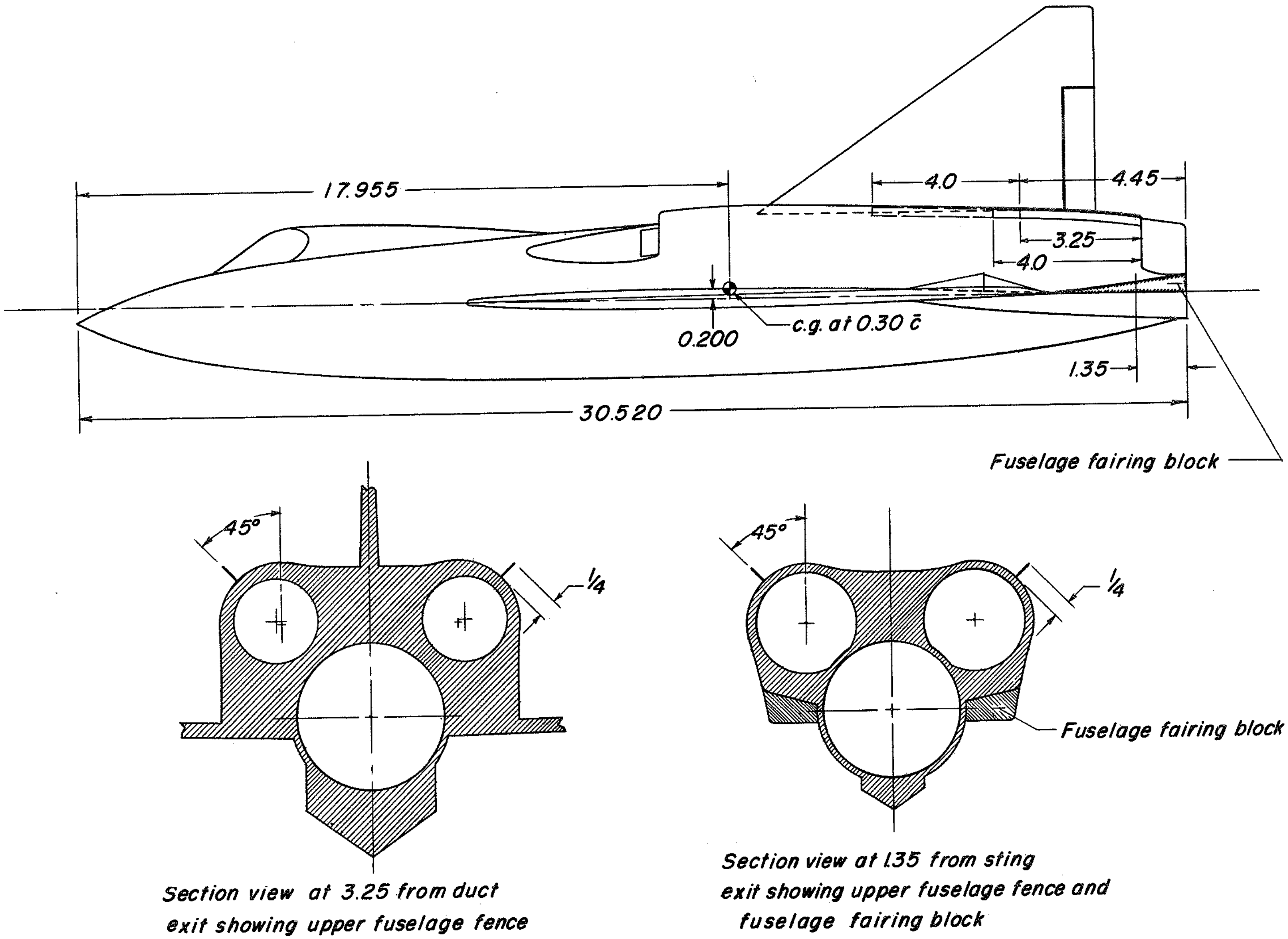

Figure 7.- Details of upper fuselage fences and fuselage fairing at aft end of model. (All dimensions in inches.)

[redacted]

[redacted]

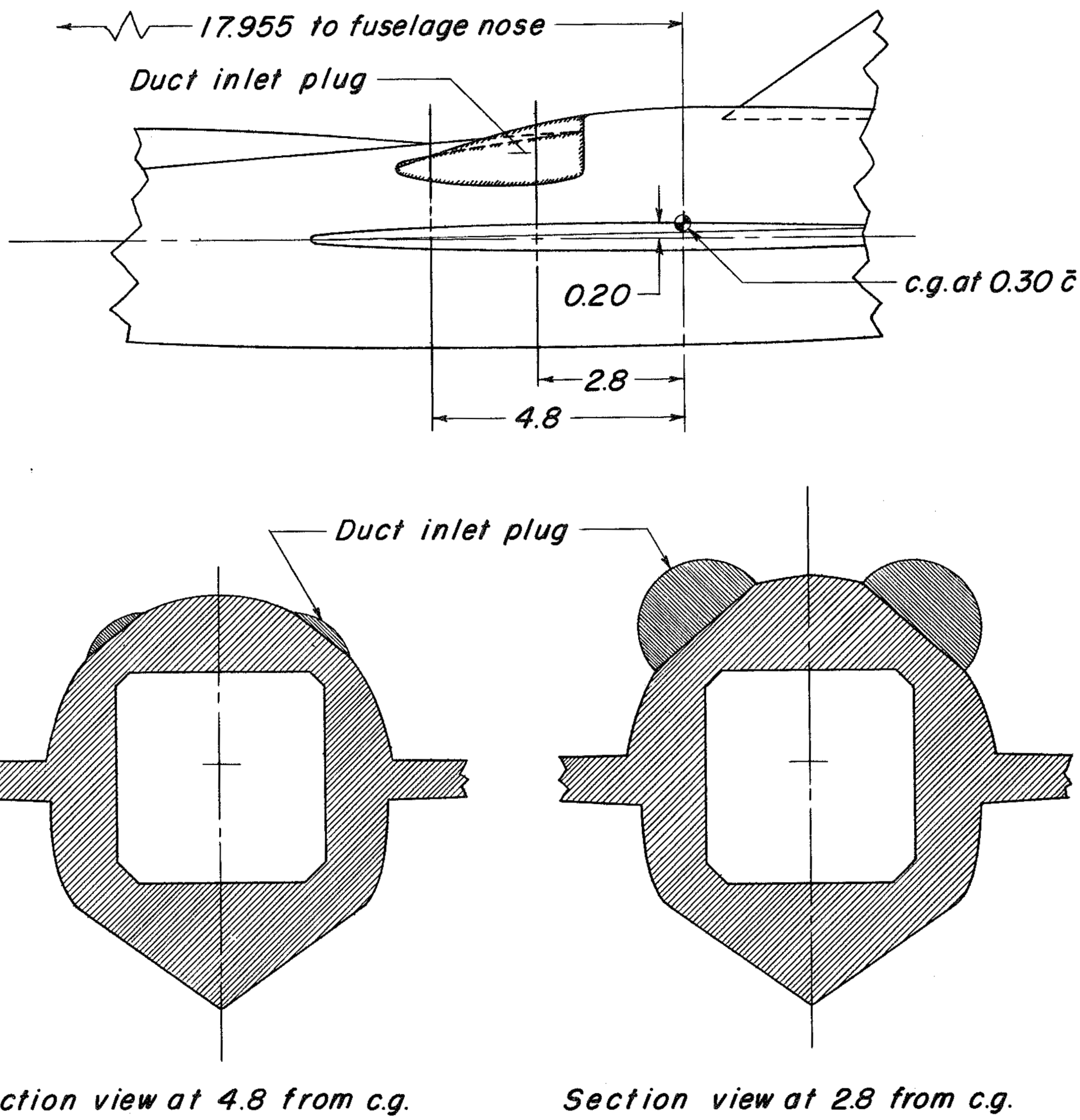

Figure 8.- Details of duct inlet plugs. (All dimensions in inches.)

[redacted]

[redacted]

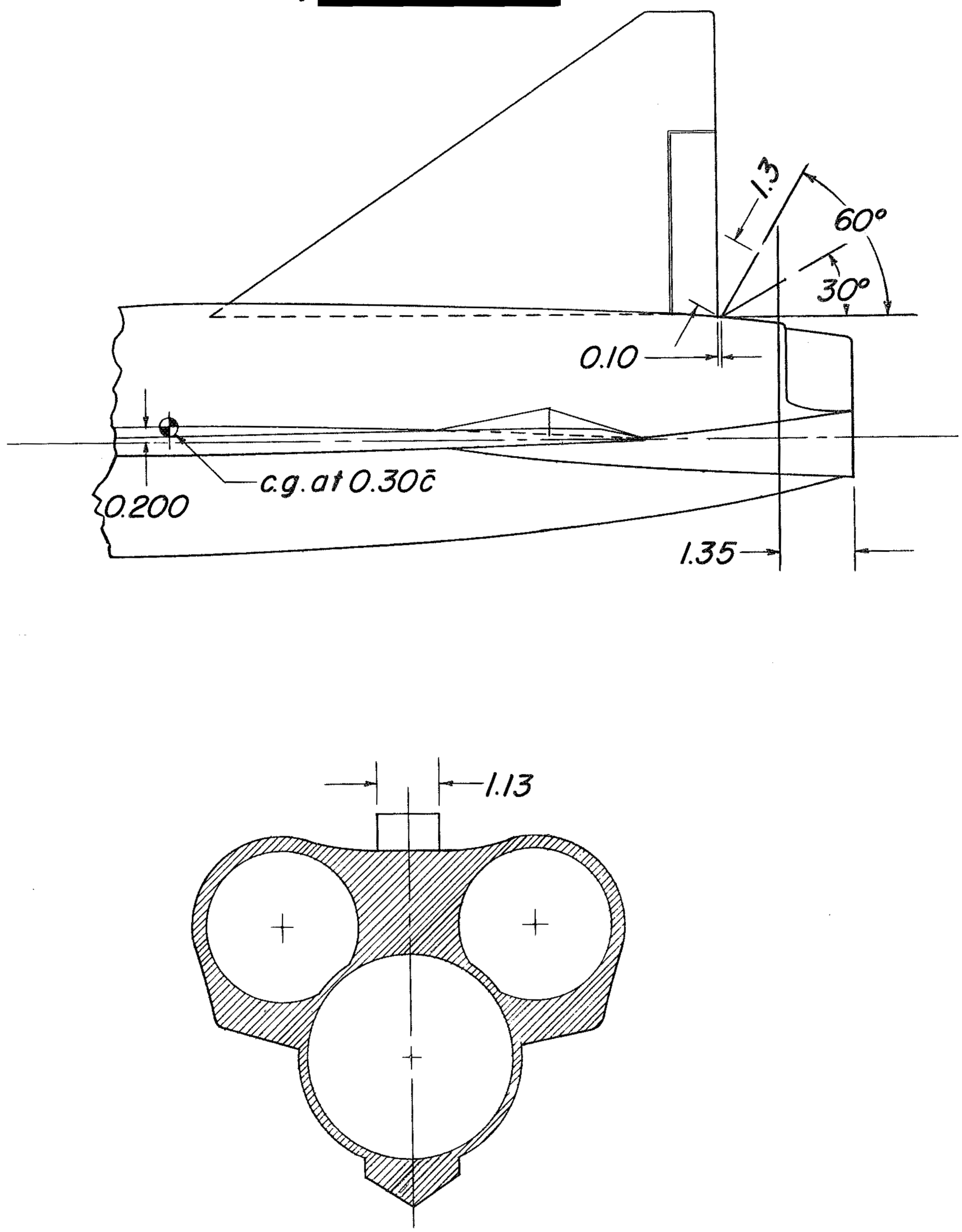

Section view at 1.35 from sting exit showing upper aft dive brake

Figure 9.- Details of upper aft fuselage dive brake. (All dimensions in inches.)

[redacted]

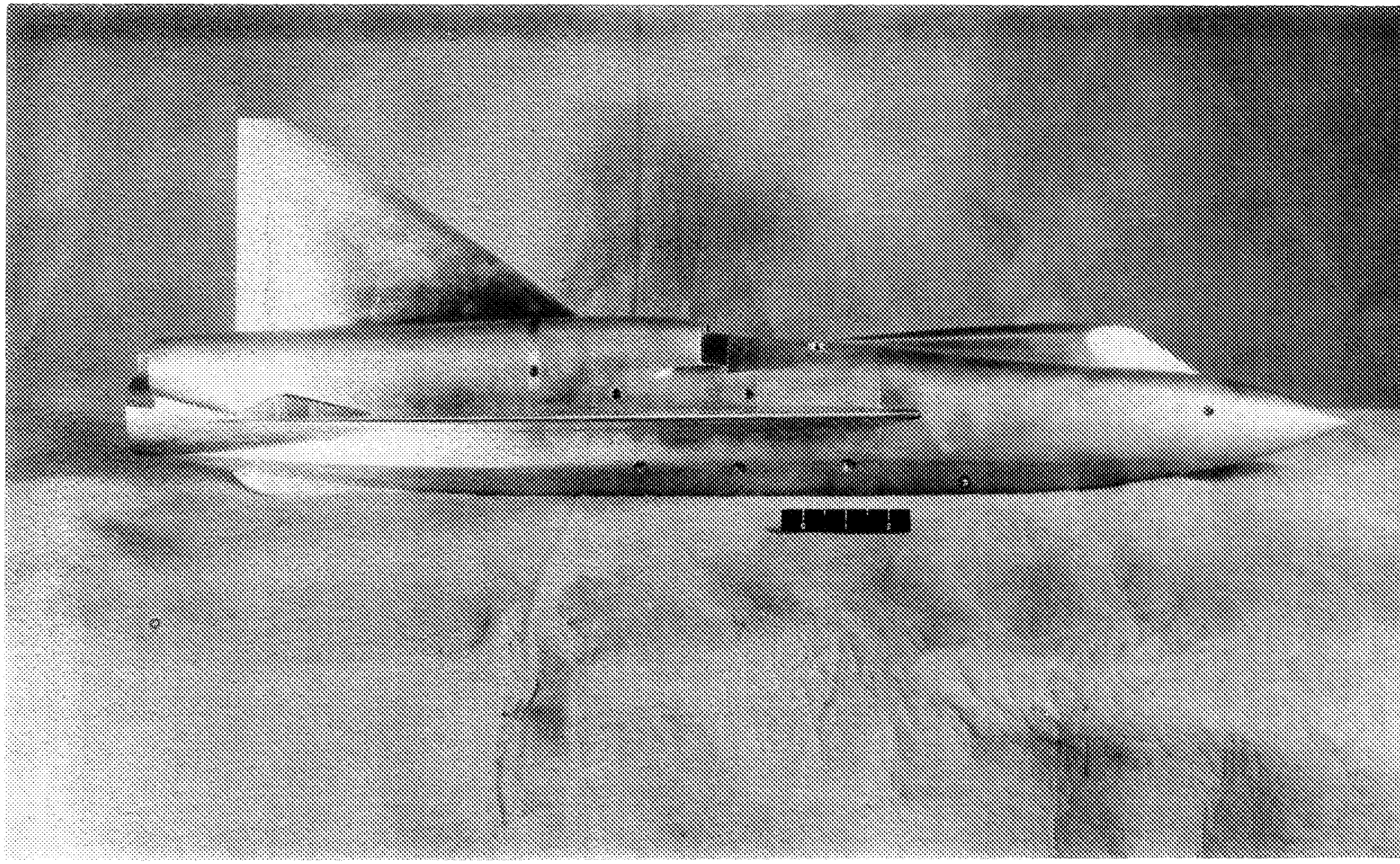

(a) Configuration BCWV, $\delta_e = 0^\circ$, $\delta_r = 0^\circ$.

L-78678

Figure 10.- Photographs of test model.

[redacted]

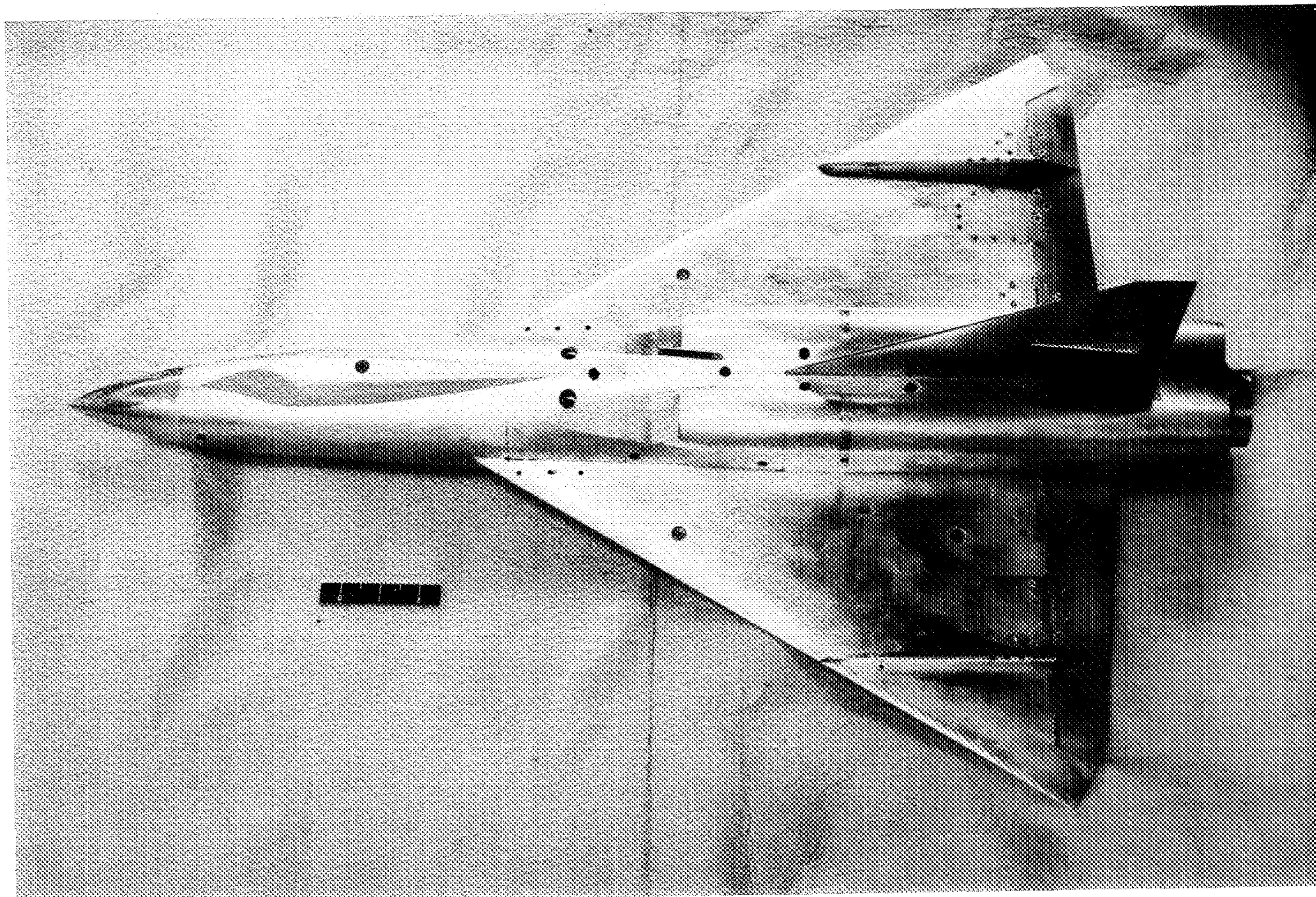

L-78681

(b) Configuration $BCW_{F_1}V$, $\delta_e = 0^{\circ}$, $\delta_r = 0^{\circ}$.

Figure 10.- Continued.

[redacted]

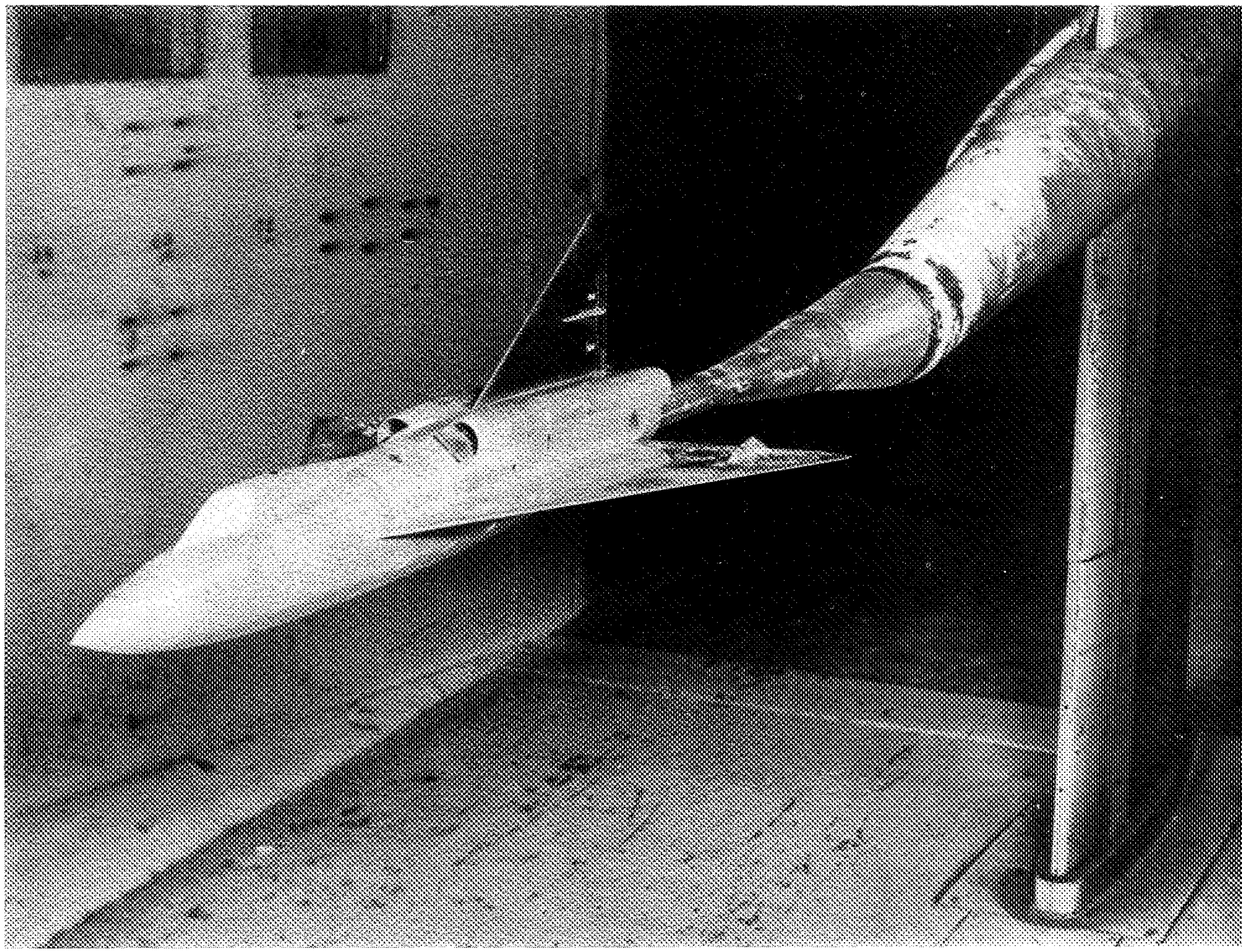

L-78683

(c) Configuration BCWV, $\delta_e = 0^\circ$, $\delta_r = 0^\circ$; mounted on sting in Langley high-speed 7- by 10-foot tunnel.

Figure 10.- Concluded.

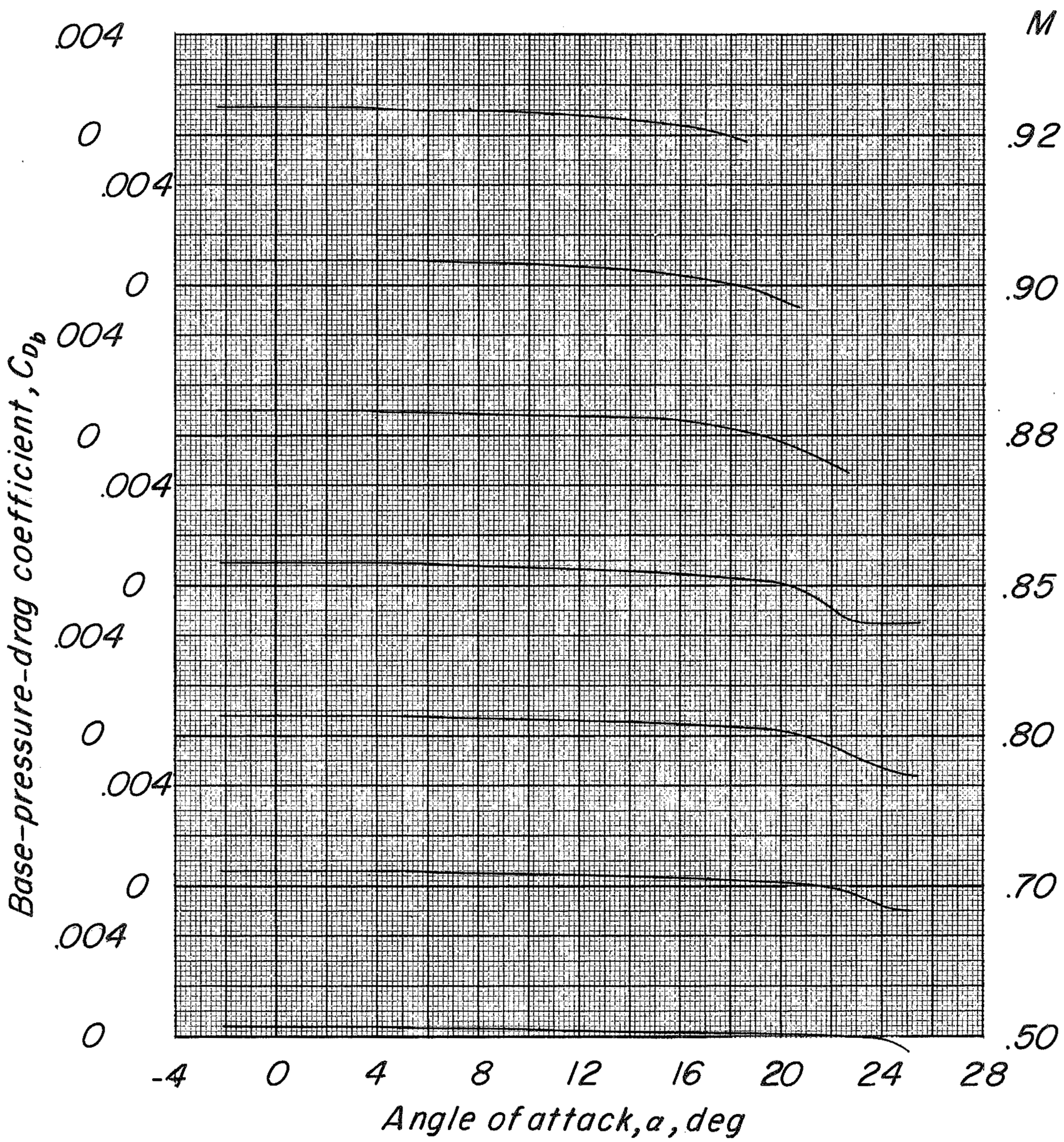

Figure 11.- Variation of base-pressure-drag coefficient with angle of attack and test Mach number.

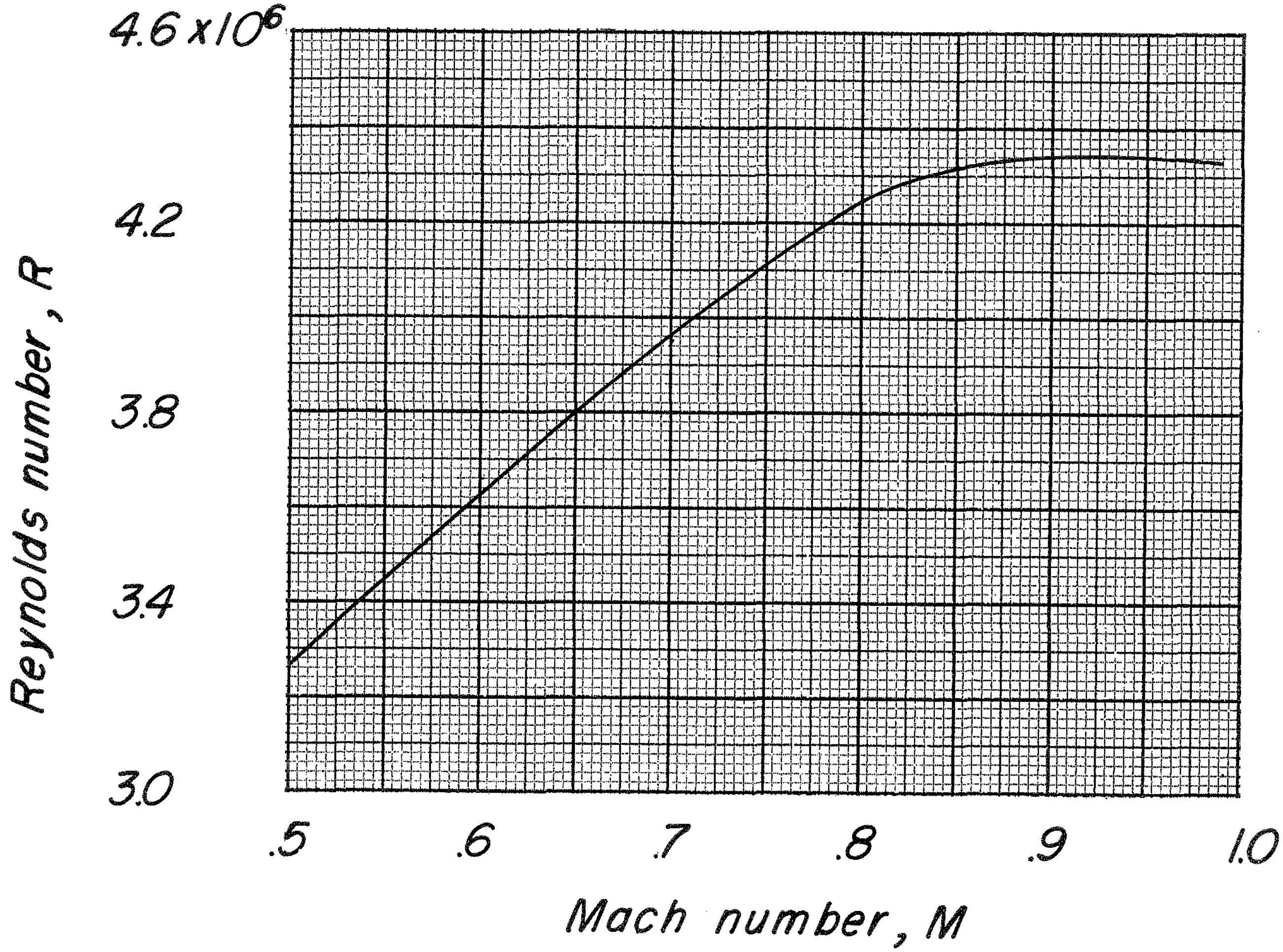

Figure 12.- Variation of test Reynolds number with Mach number based on wing mean aerodynamic chord.

[redacted]

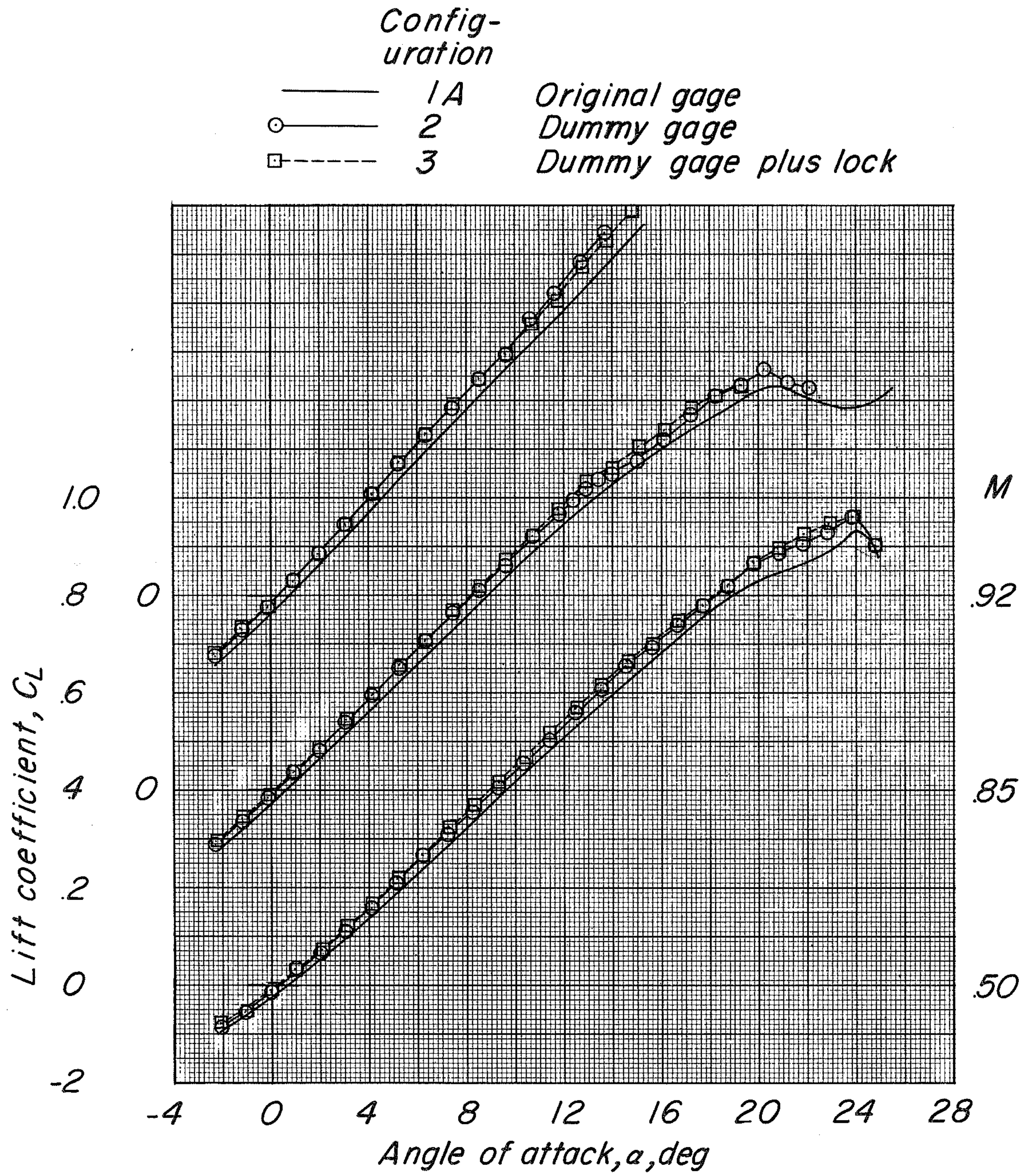

(a) Variation of C_L with α.

Figure 13.- Basic longitudinal characteristics of configuration $BCW_{F_1}V$, $\delta_e = 0^o$, $\delta_r = 0^o$ showing effects of the original elevon strain gage and a more rigid dummy elevon strain gage.

[redacted]

[redacted]

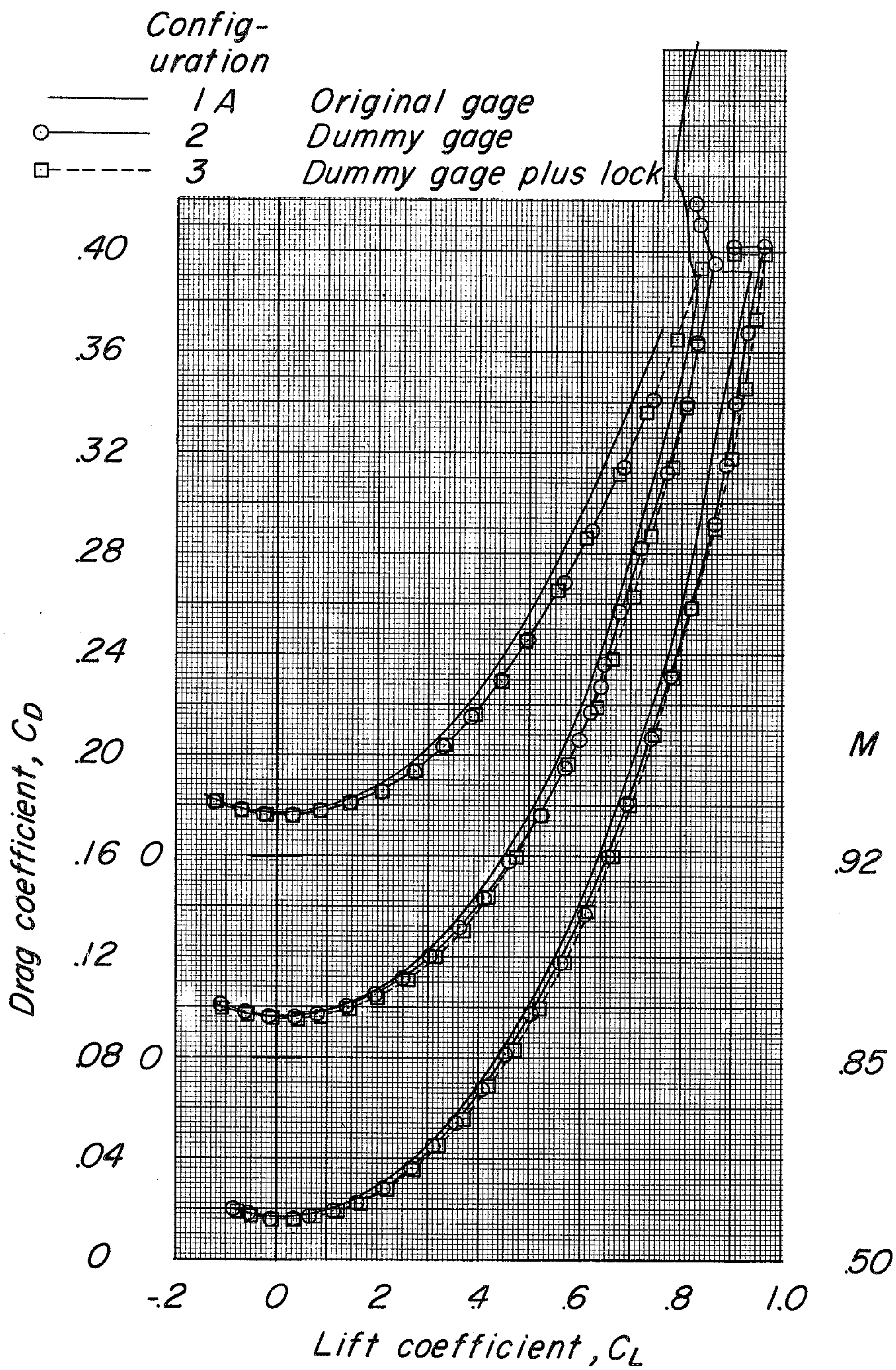

(b) Variation of C_D with C_L.

Figure 13.- Continued.

[redacted]

 [redacted]

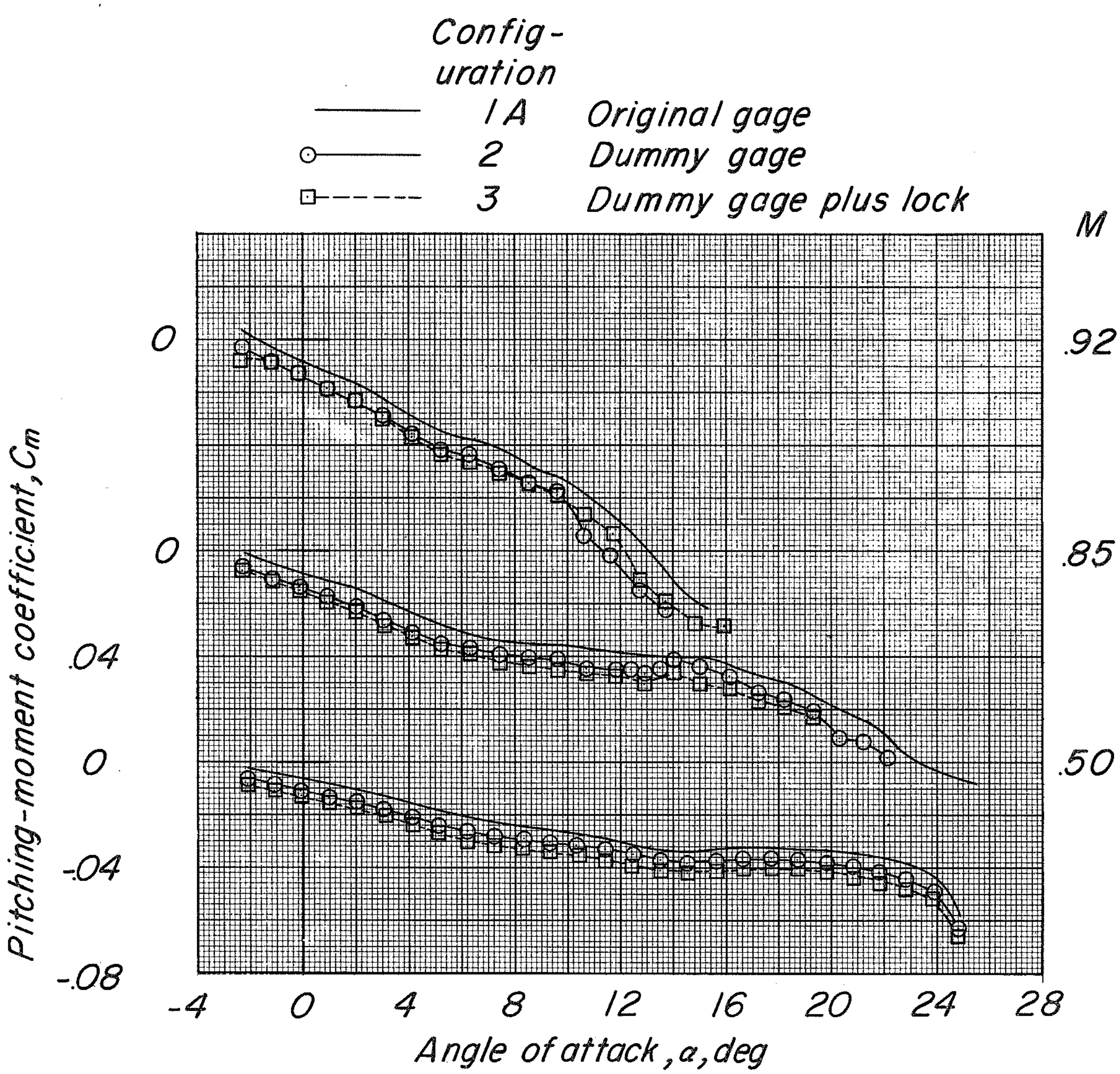

(c) Variation of C_m with α.

Figure 13.- Continued.

[redacted]

[redacted]

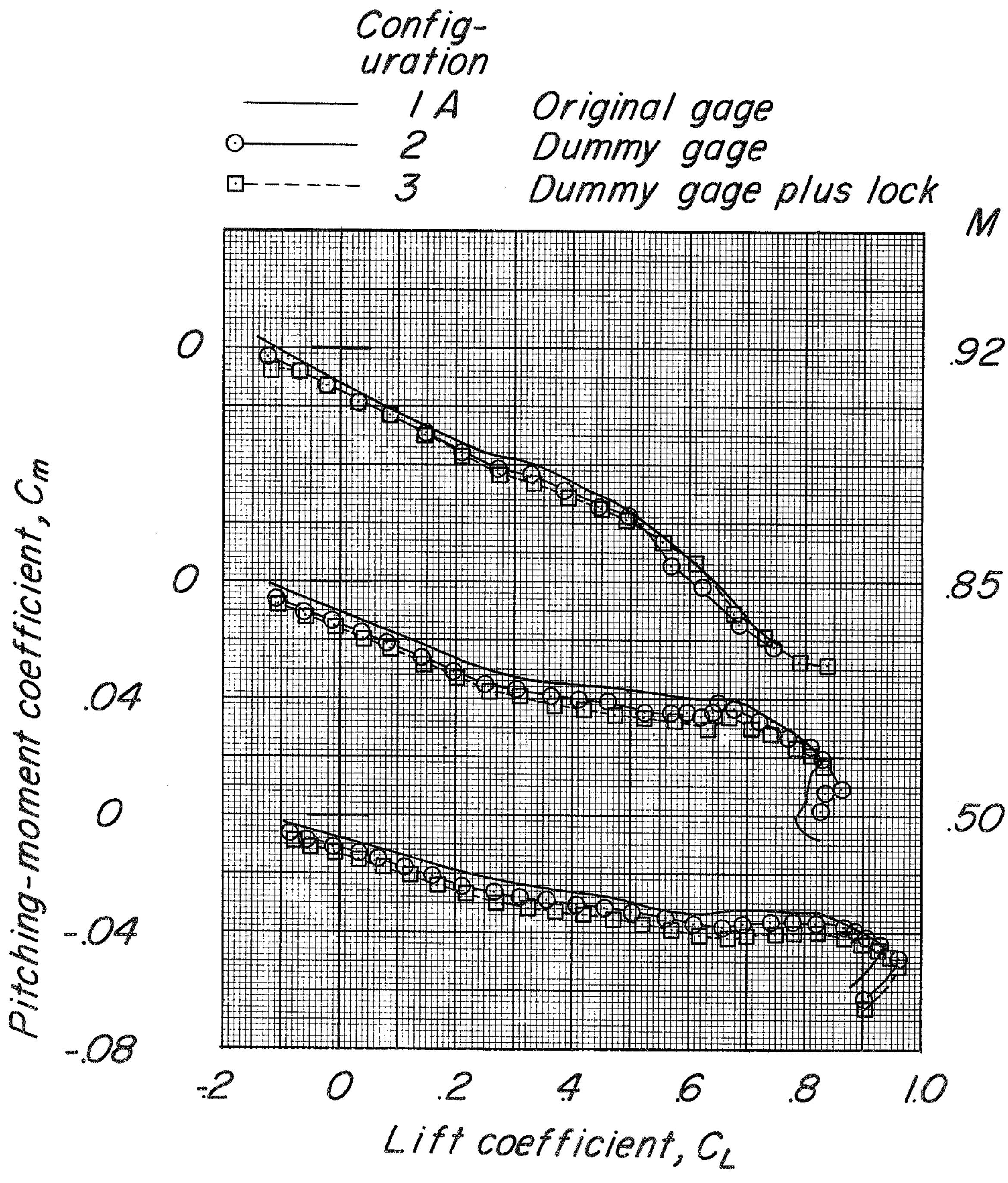

(d) Variation of C_m with C_L.

Figure 13.- Concluded.

[redacted]

[redacted]

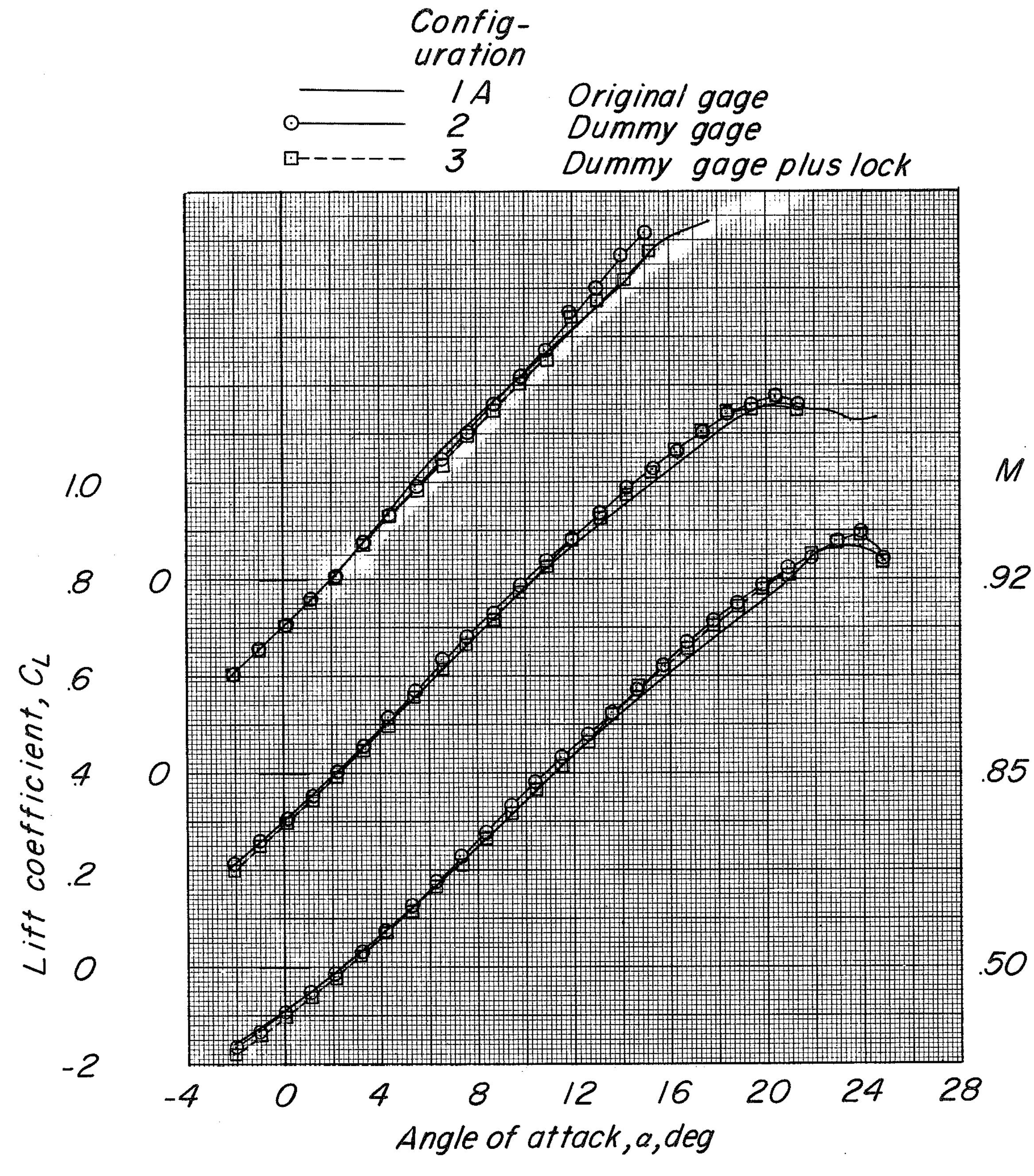

(a) Variation of C_L with α.

Figure 14.- Basic longitudinal characteristics of configuration $BCW_{F_1}V$, $\delta_e = -5^o$, $\delta_r = 0^o$ showing effects of the original elevon strain gage and a more rigid dummy elevon strain gage.

[redacted]

[redacted]

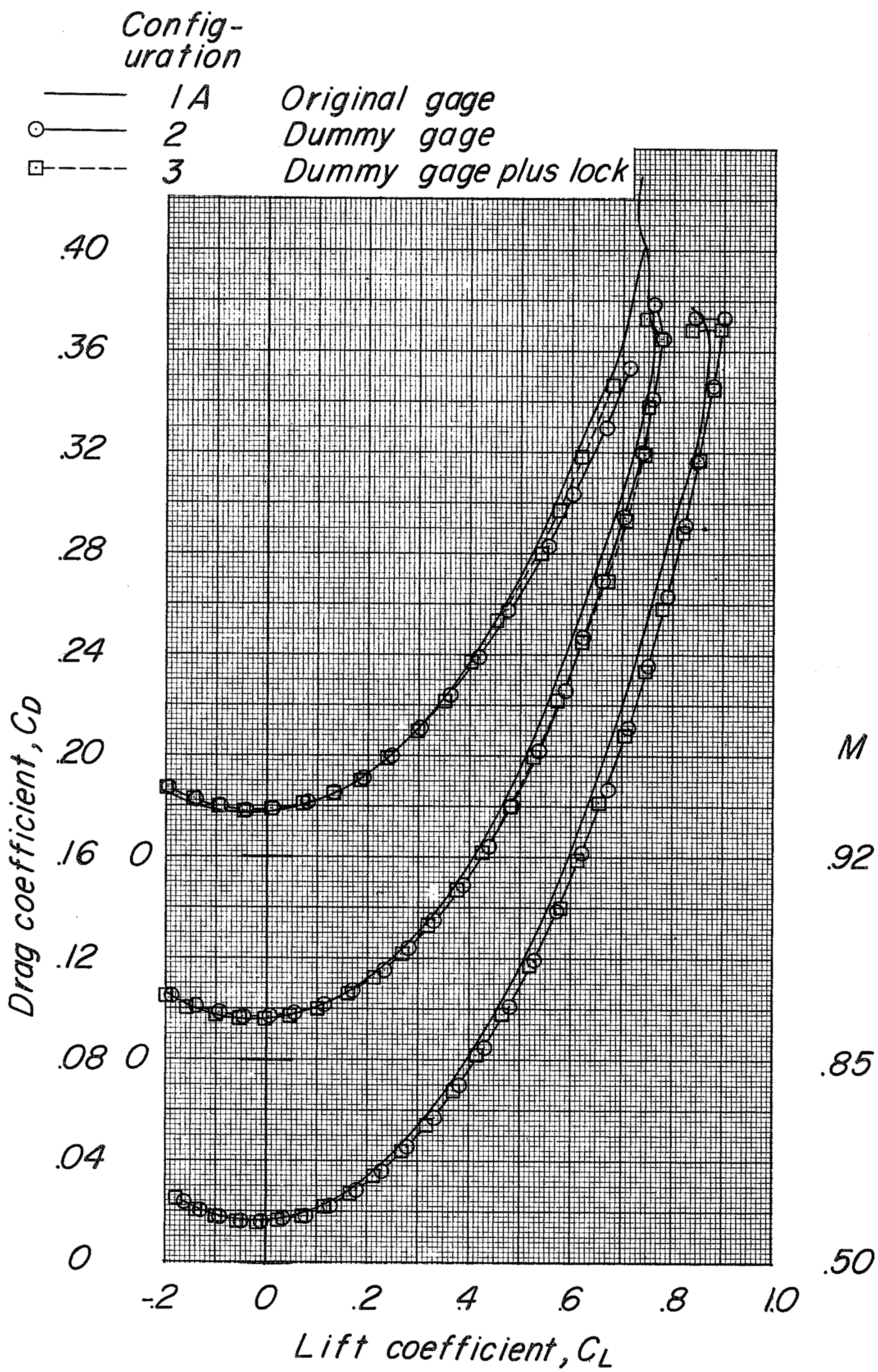

(b) Variation of C_D with C_L.

Figure 14.- Continued.

[redacted]

[redacted]

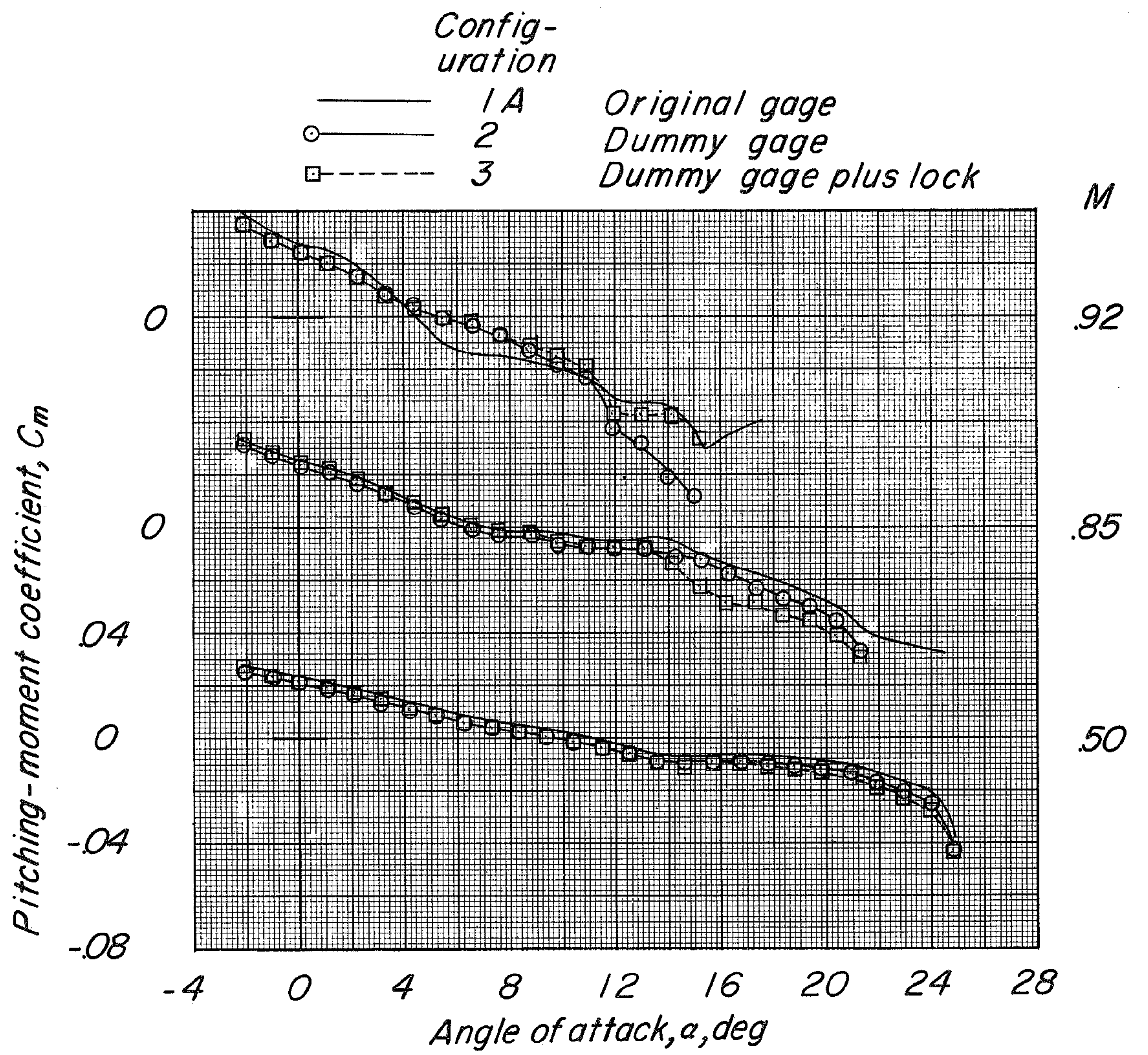

(c) Variation of C_m with α.

Figure 14.- Continued.

[redacted]

 [redacted]

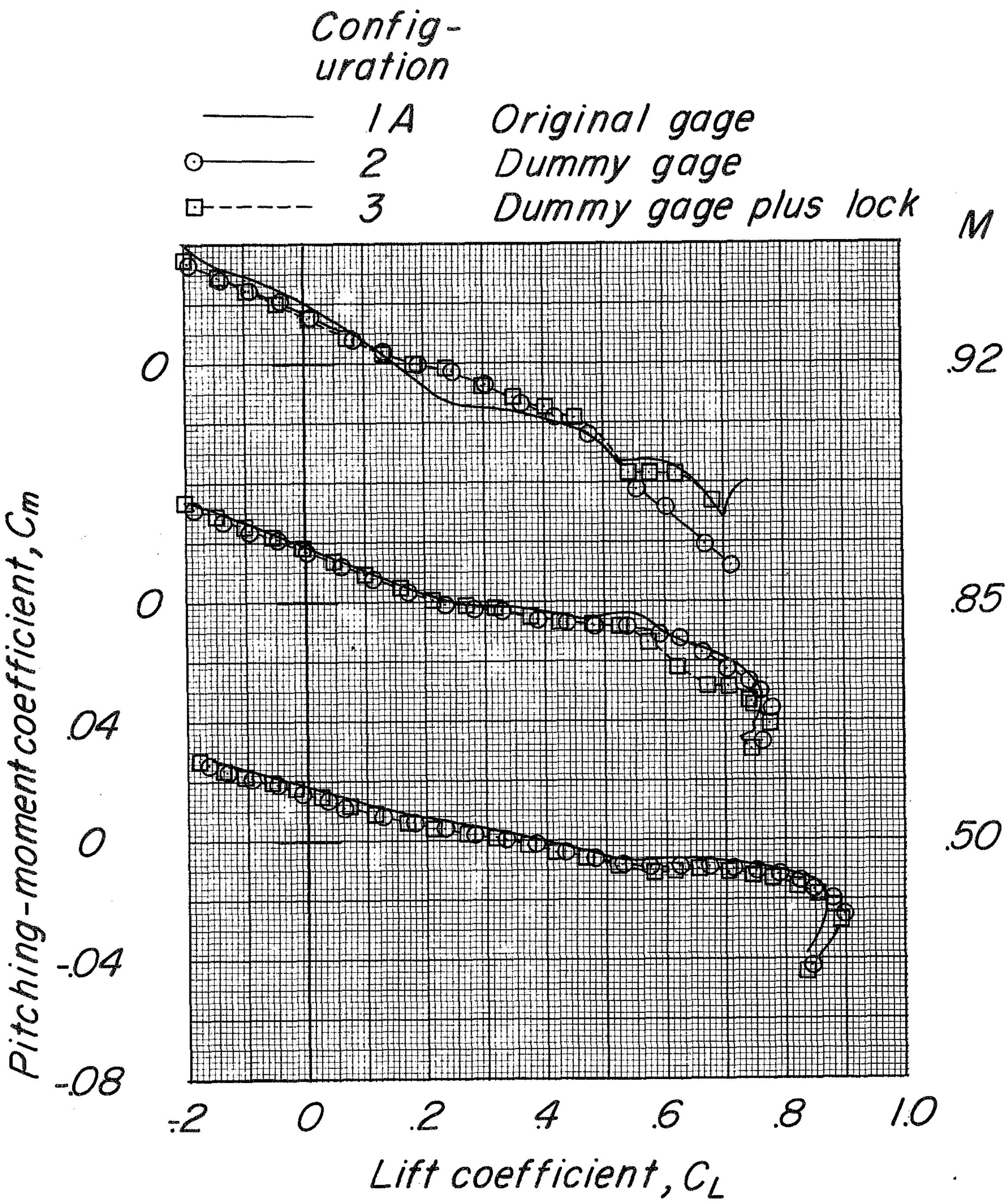

(d) Variation of C_m with C_L.

Figure 14.- Concluded.

[redacted]

 [redacted]

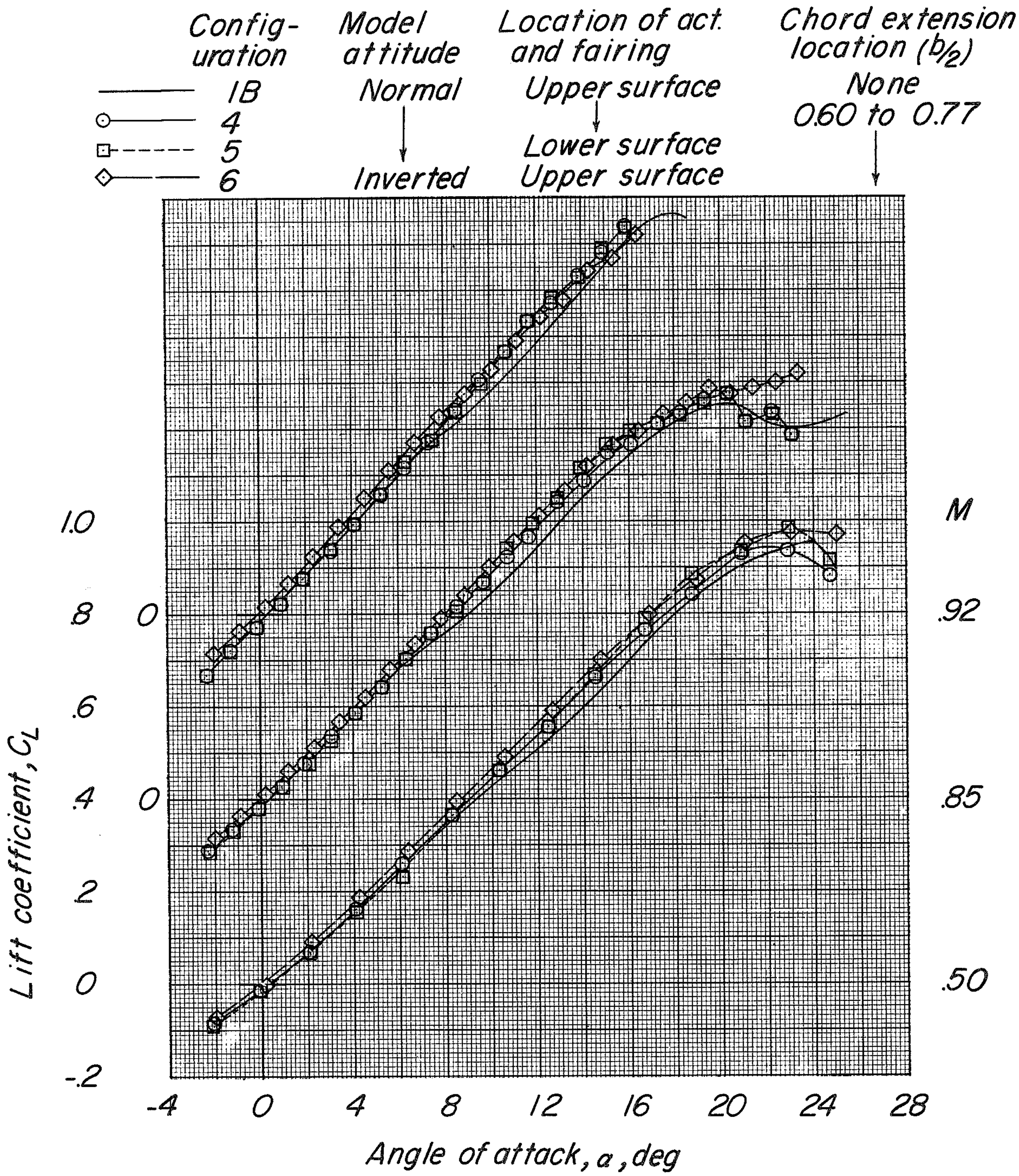

(a) Variation of C_L with α.

Figure 15.- Basic longitudinal characteristics of configuration BCWV with and without leading-edge chord-extension from 0.60b/2 to 0.77b/2, $\delta_e = 0^\circ$, $\delta_r = 0^\circ$ showing effects of changing the location of the elevon actuator and fairing and of inverting the model.

[redacted]

[redacted]

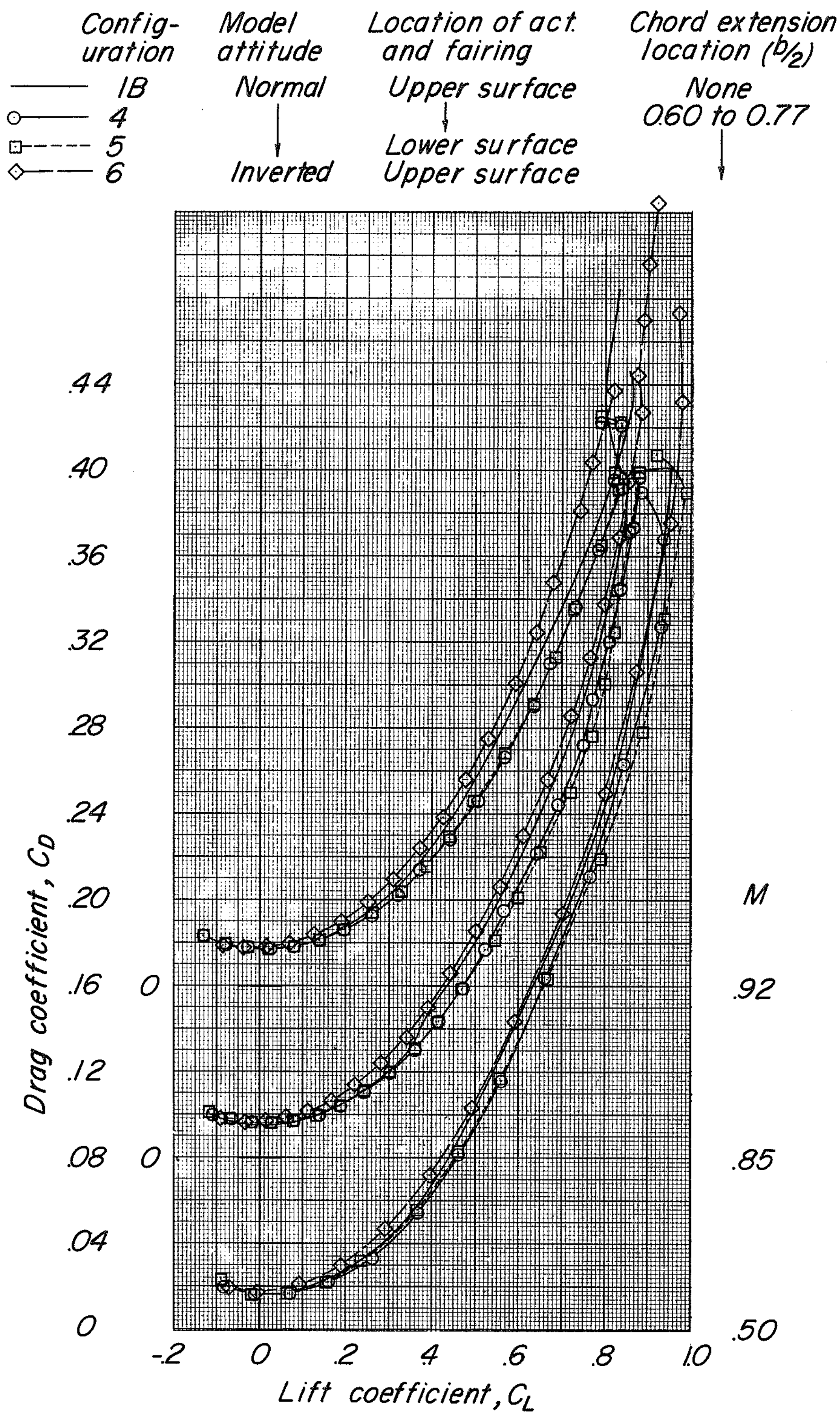

(b) Variation of C_D with C_L.

Figure 15.- Continued.

[redacted]

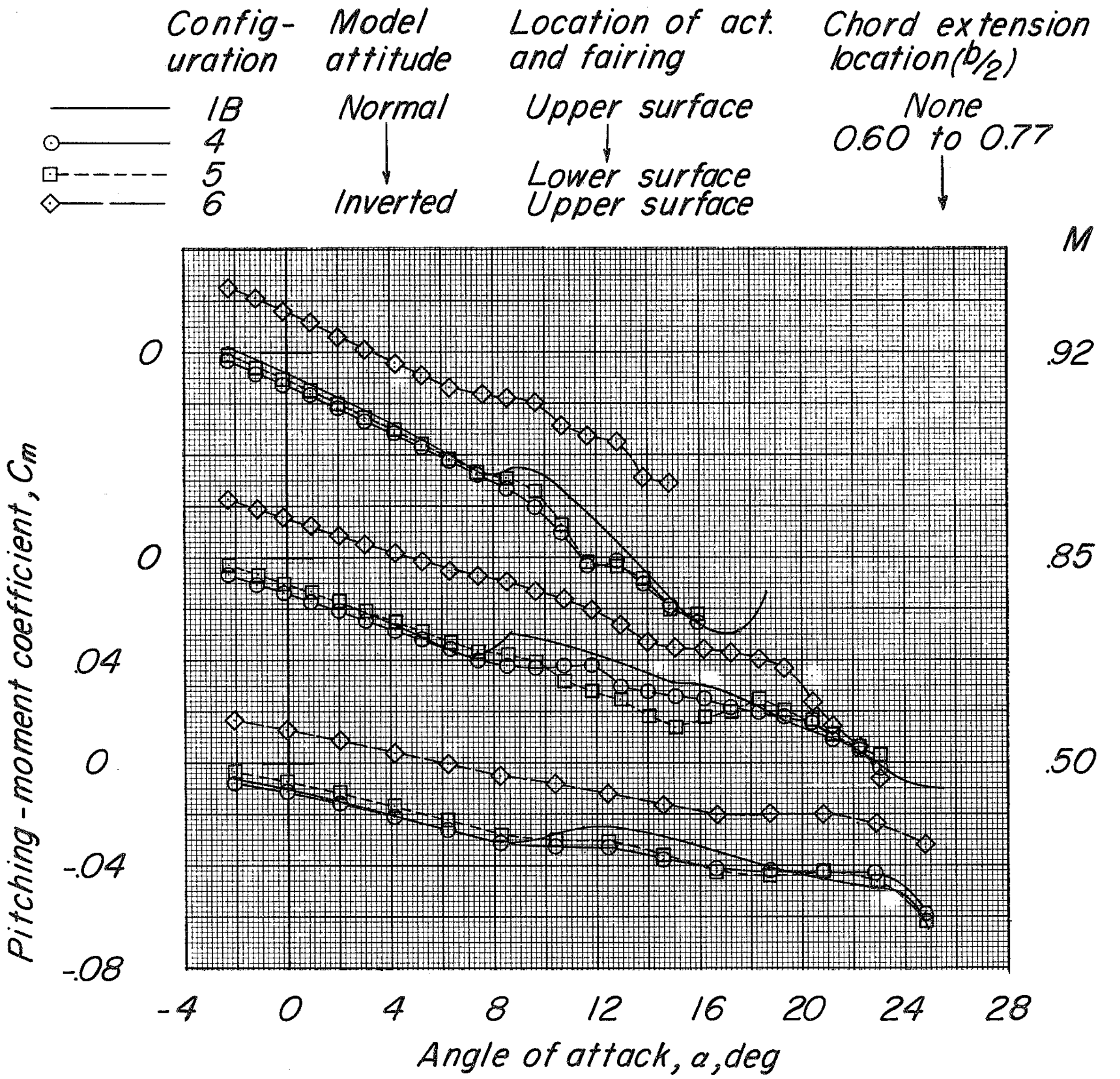

(c) Variation of C_m with α.

Figure 15.- Continued.

[redacted]

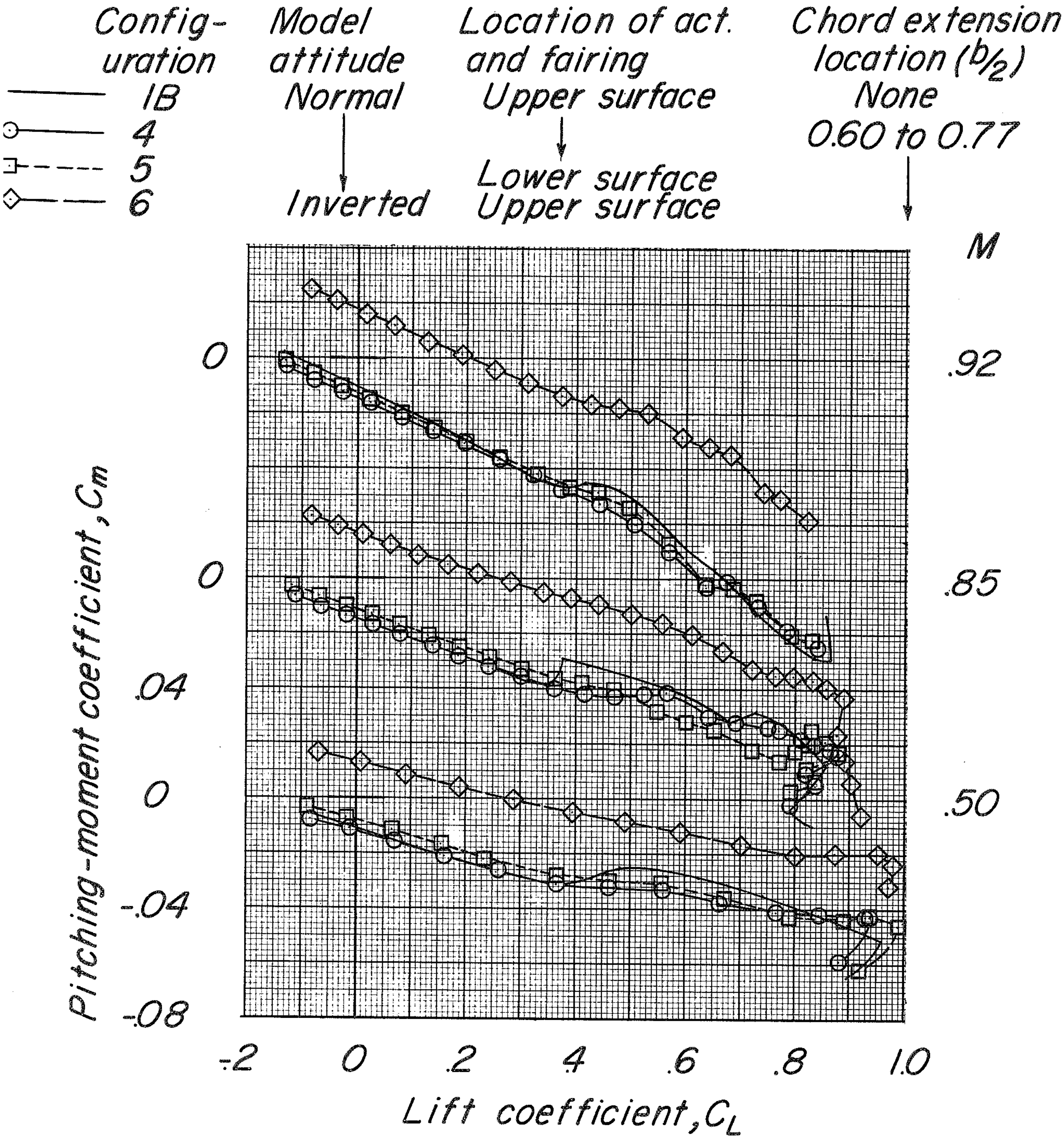

(d) Variation of C_m with C_L.

Figure 15.- Concluded.

[redacted]

 [redacted]

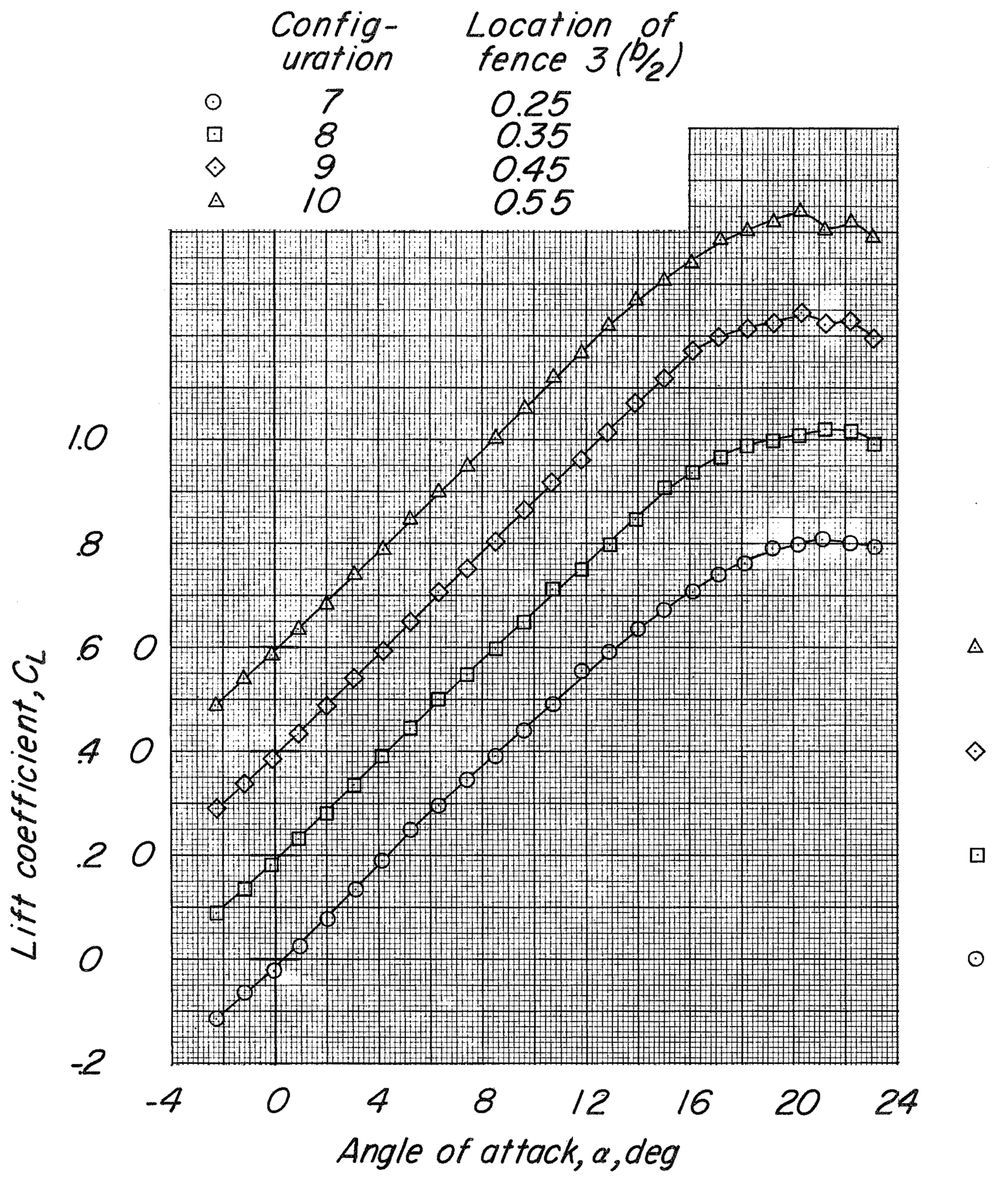

(a) Variation of C_L with α.

Figure 16.- Basic longitudinal characteristics of configuration $BCW_{F_{1+3}}V$, $\delta_e = 0^{\circ}$, $\delta_r = 0^{\circ}$ at a constant Mach number of 0.85 showing effects of changing spanwise location of fence 3. Fence 1 constant at 0.63b/2.

[redacted]

 [redacted]

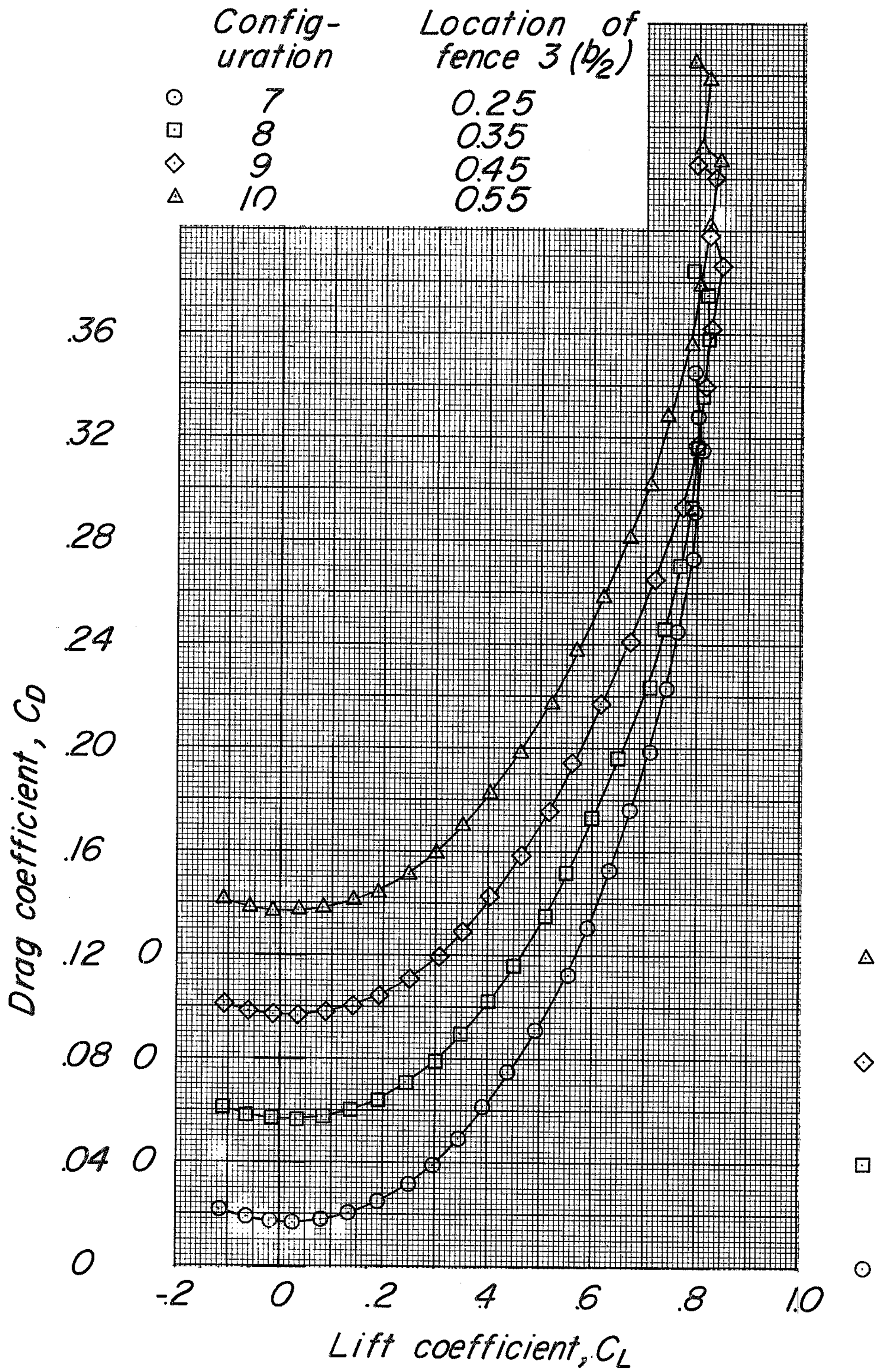

(b) Variation of C_D with C_L.

Figure 16.- Continued.

[redacted]

[redacted]

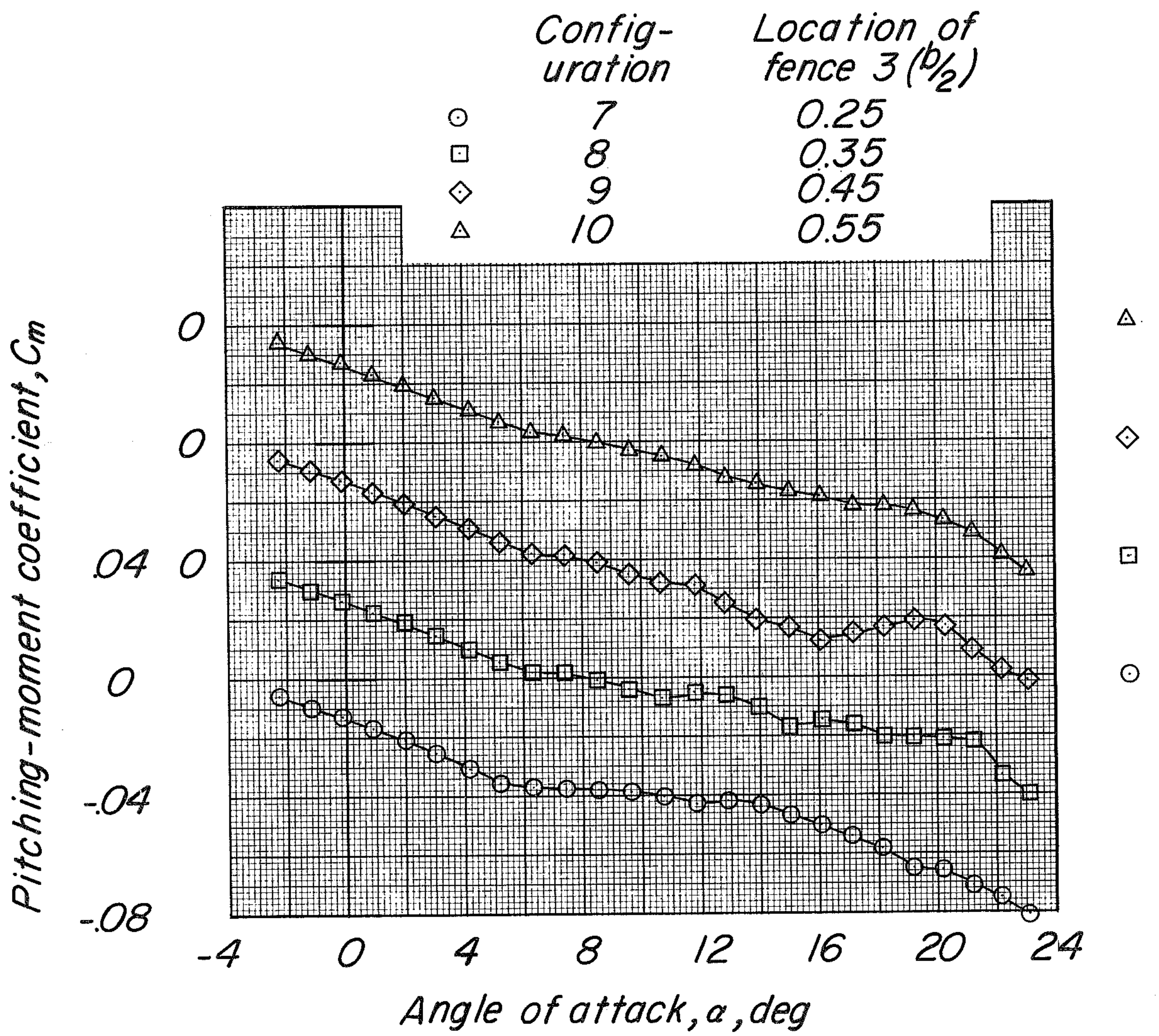

(c) Variation of C_m with α.

Figure 16.- Continued.

[redacted]

 [redacted]

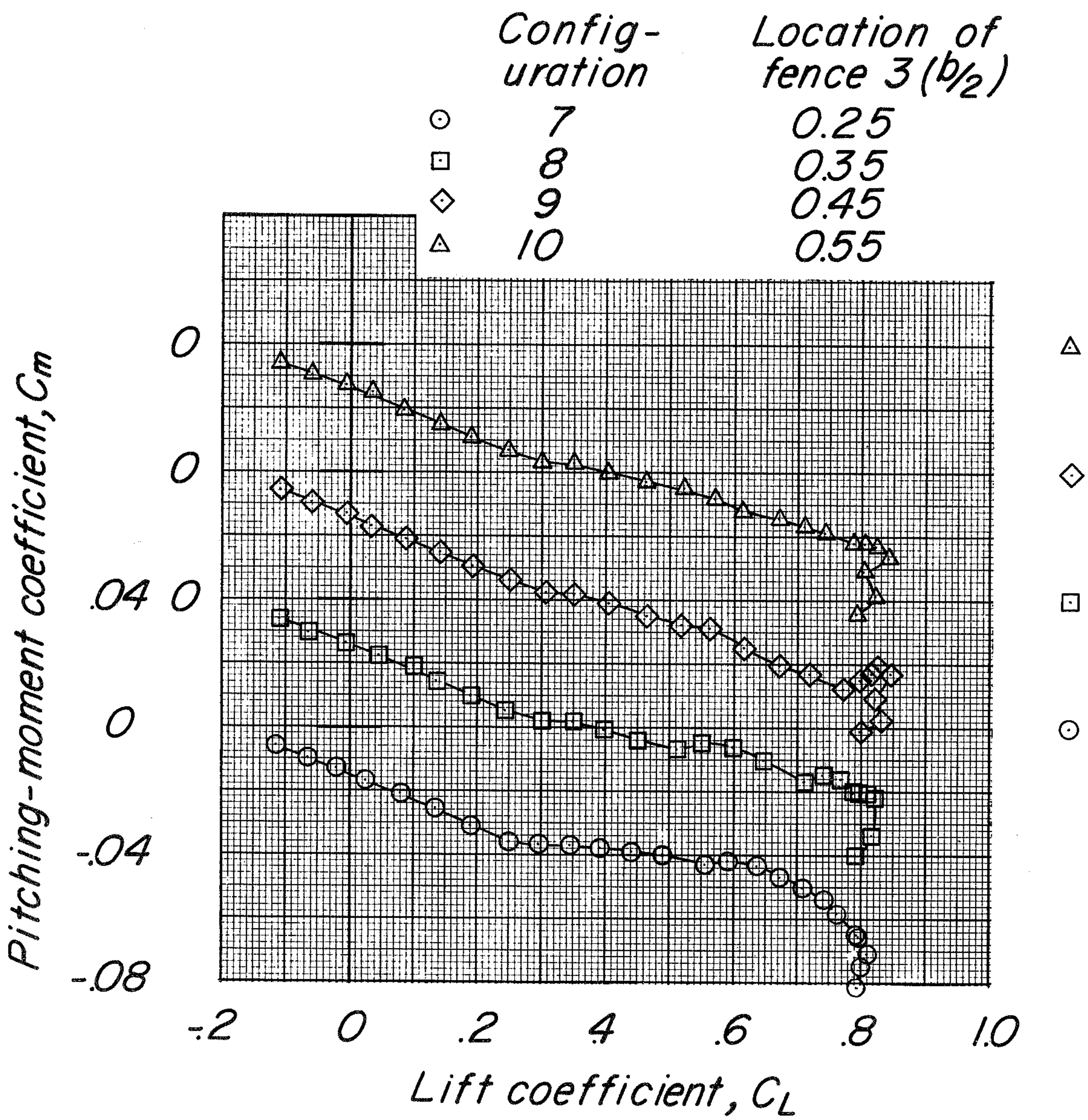

(d) Variation of C_m with C_L.

Figure 16.- Concluded.

[redacted]

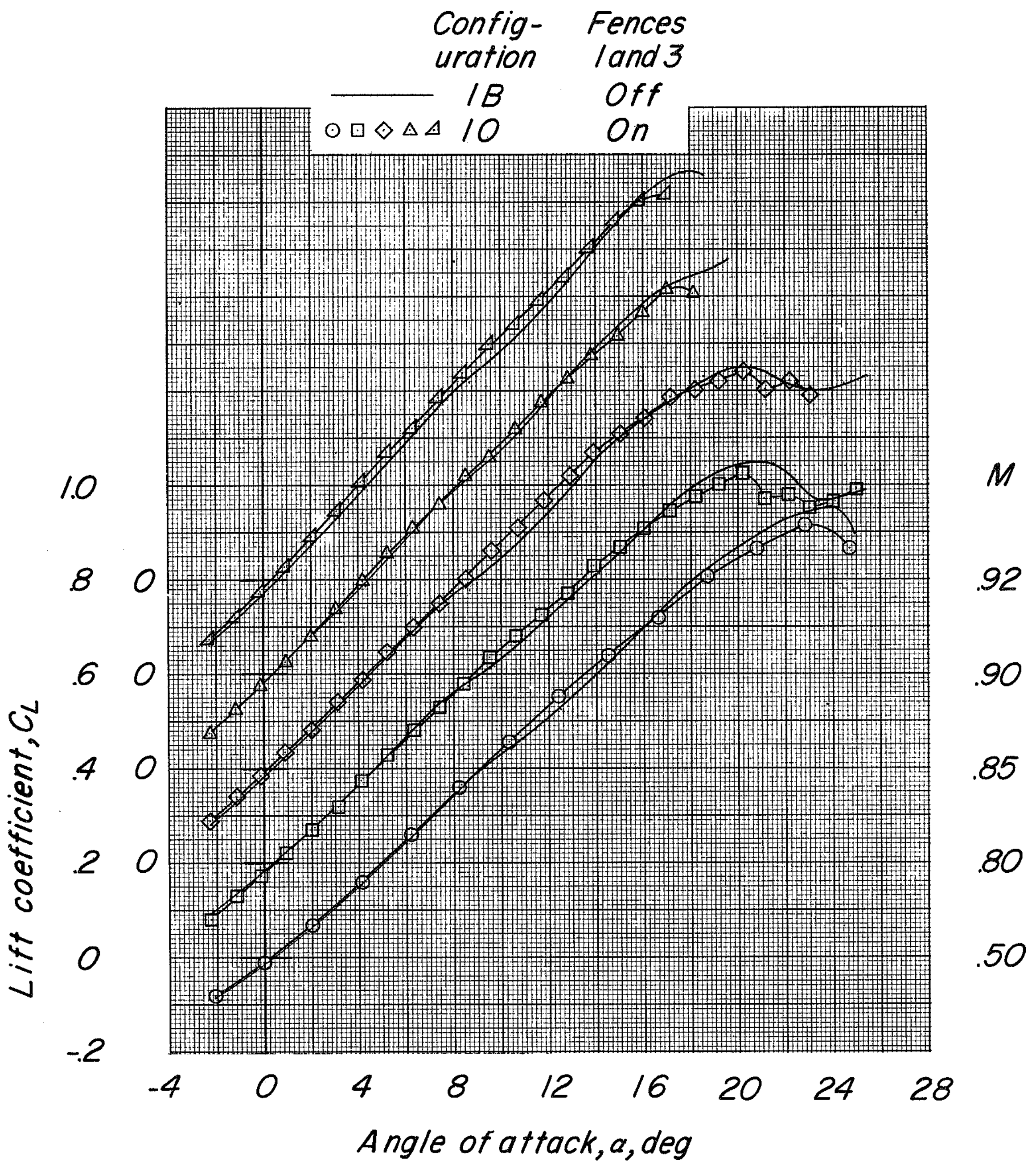

(a) Variation of C_L with α.

Figure 17.- Basic longitudinal characteristics of configurations 1B (basic model) and 10 (fences 1 and 3 located at 0.63b/2 and 0.55b/2, respectively).

[redacted]

[redacted]

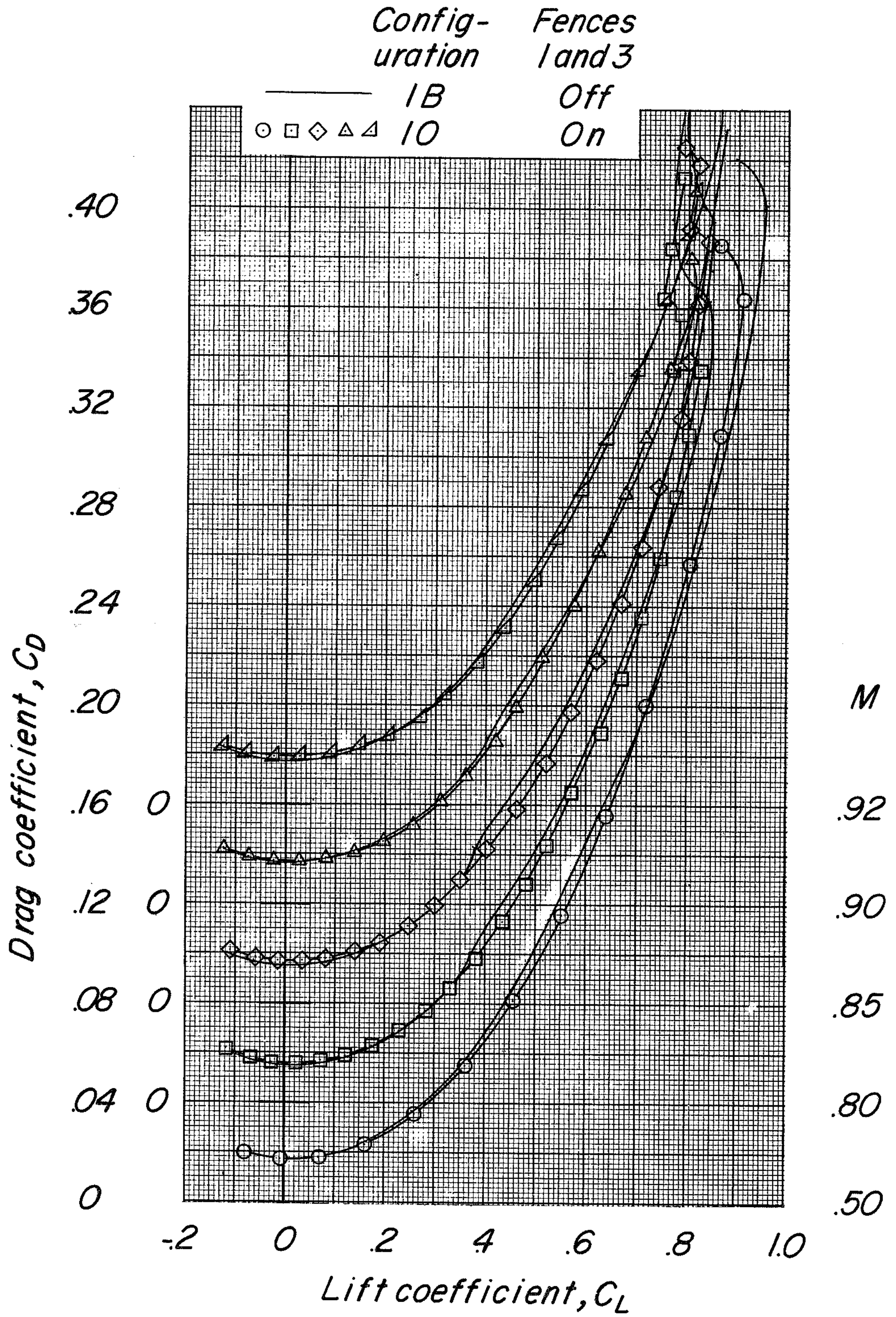

(b) Variation of C_D with C_L.

Figure 17.- Continued.

[redacted]

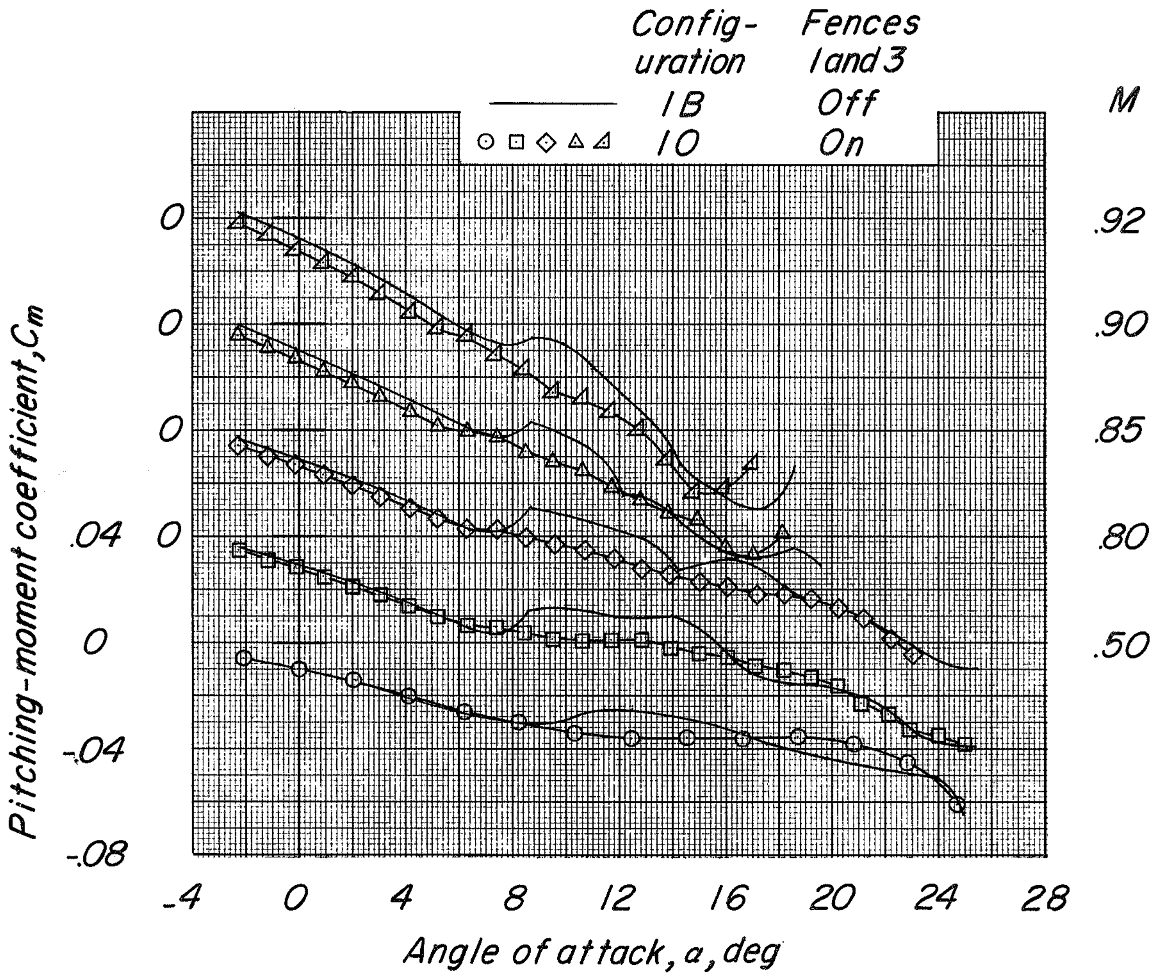

(c) Variation of C_m with α.

Figure 17.- Continued.

[redacted]

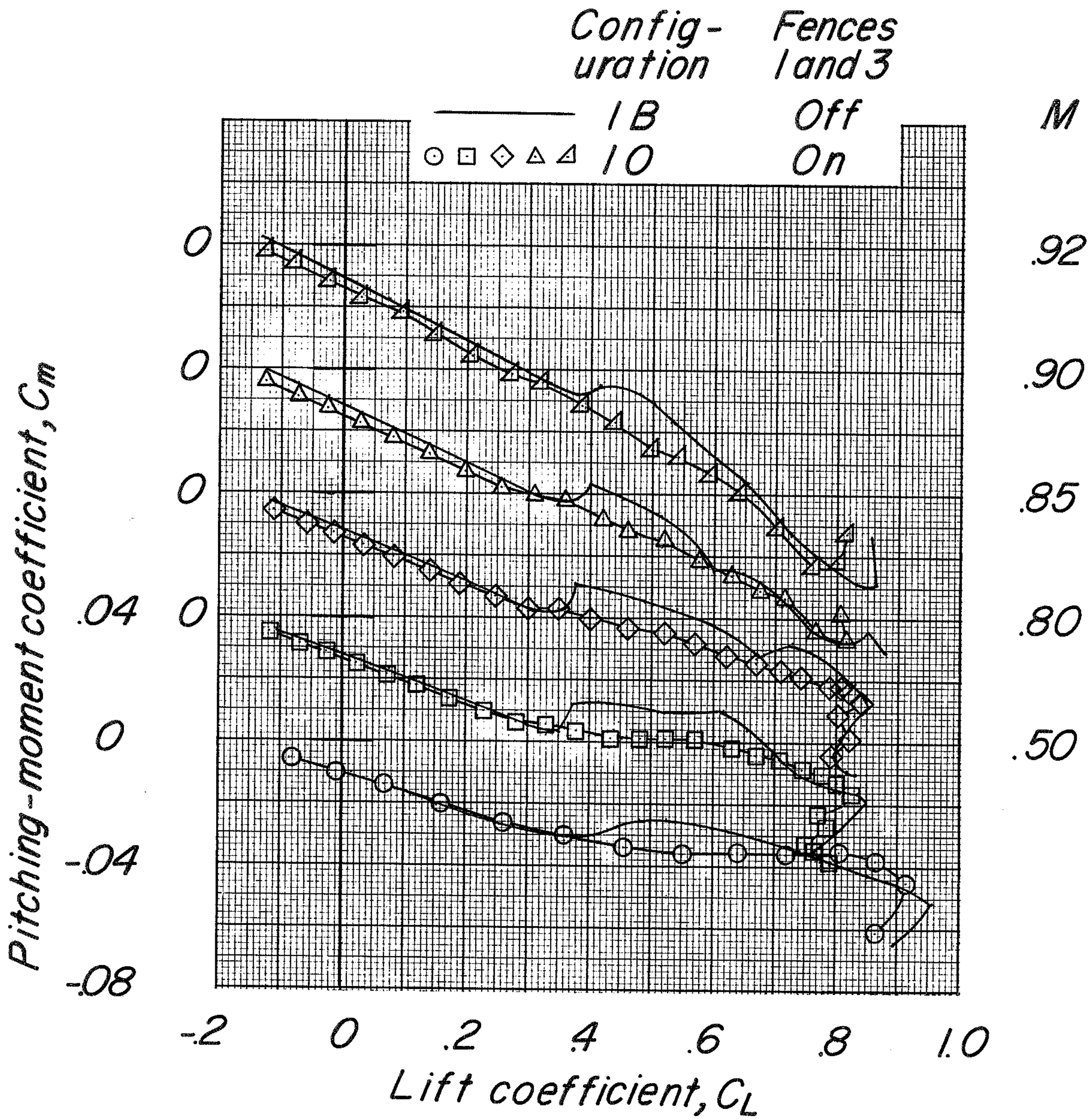

(d) Variation of C_m with C_L.

Figure 17.- Concluded.

 [redacted]

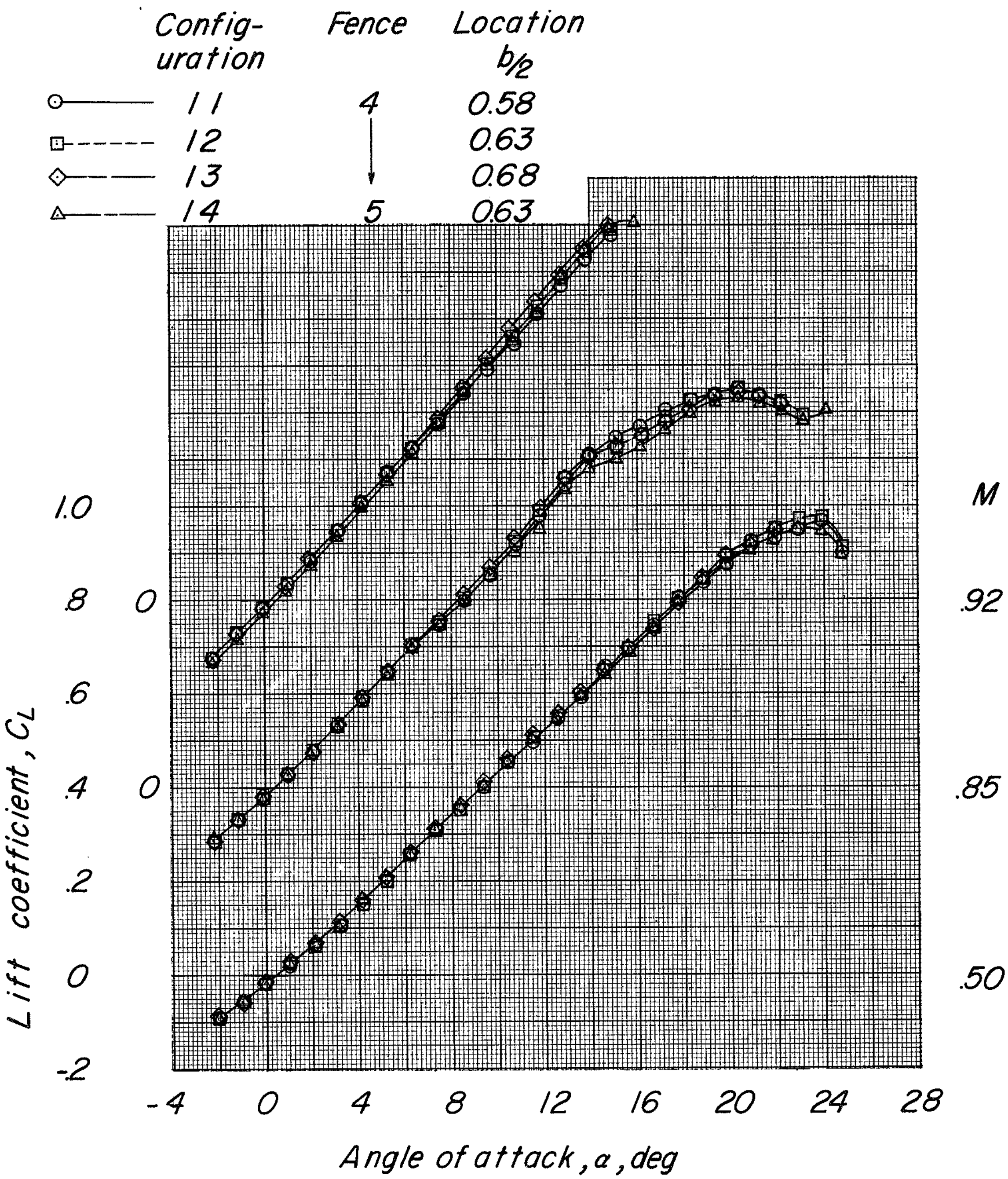

(a) Variation of C_L with α.

Figure 18.- Basic longitudinal characteristics of configuration BCWV, $\delta_e = 0^\circ$, $\delta_r = 0^\circ$ with elevon actuator and fairing removed showing effects of fence 4 at various spanwise locations and fence 5 at 0.63b/2.

[redacted]

[redacted]

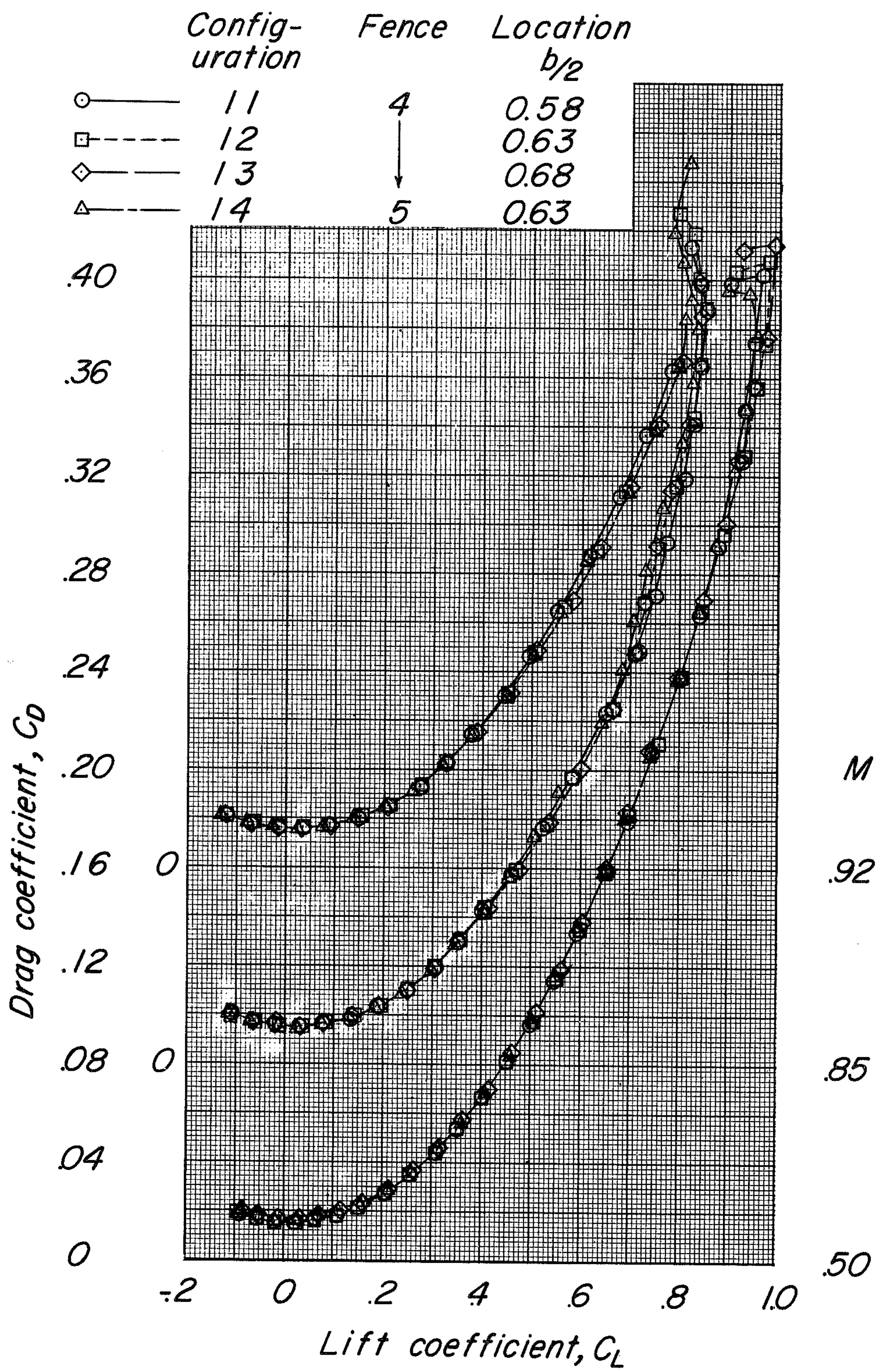

(b) Variation of C_D with C_L.

Figure 18.- Continued.

[redacted]

 [redacted]

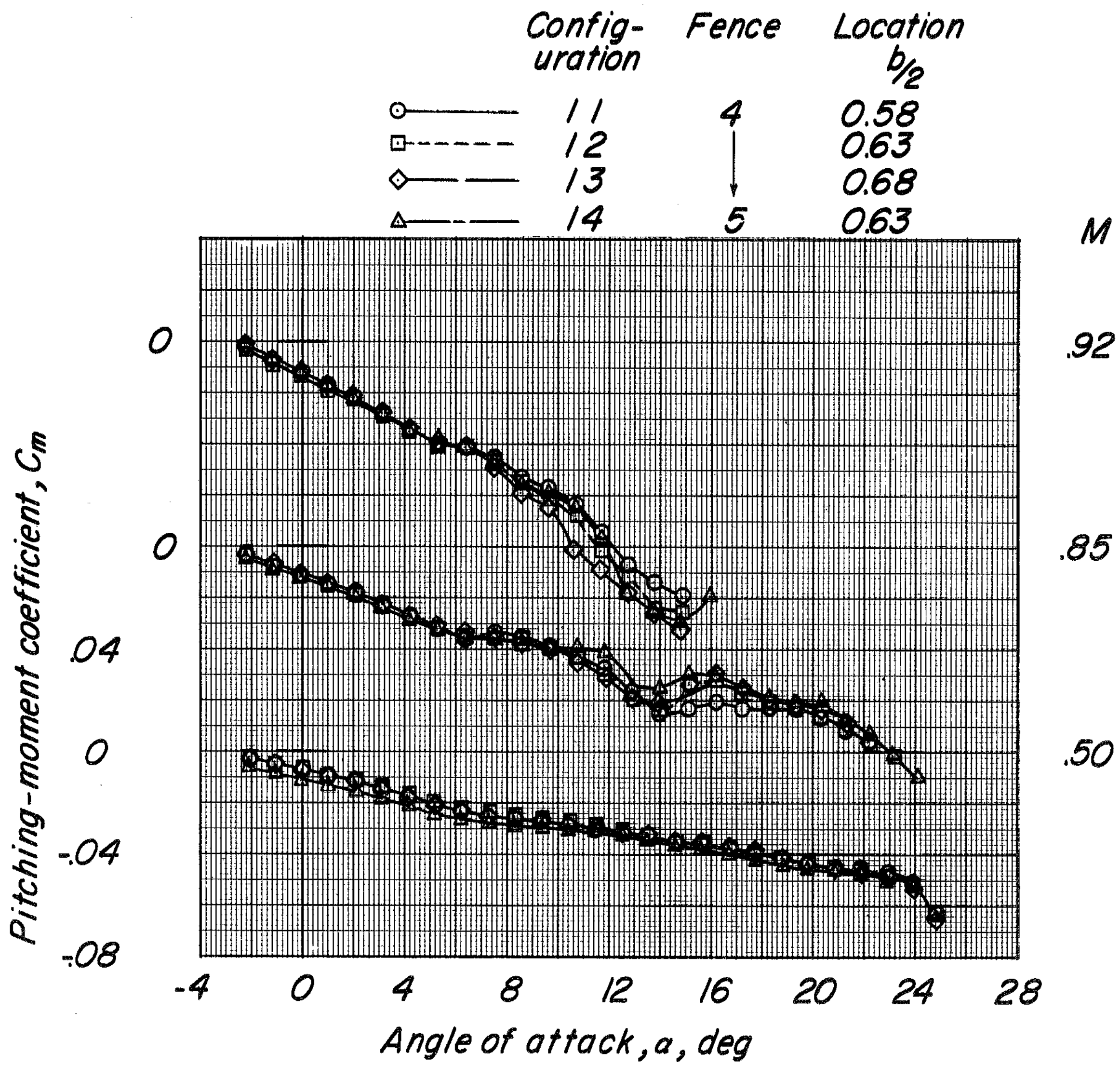

(c) Variation of C_m with α.

Figure 18.- Continued.

[redacted]

[redacted]

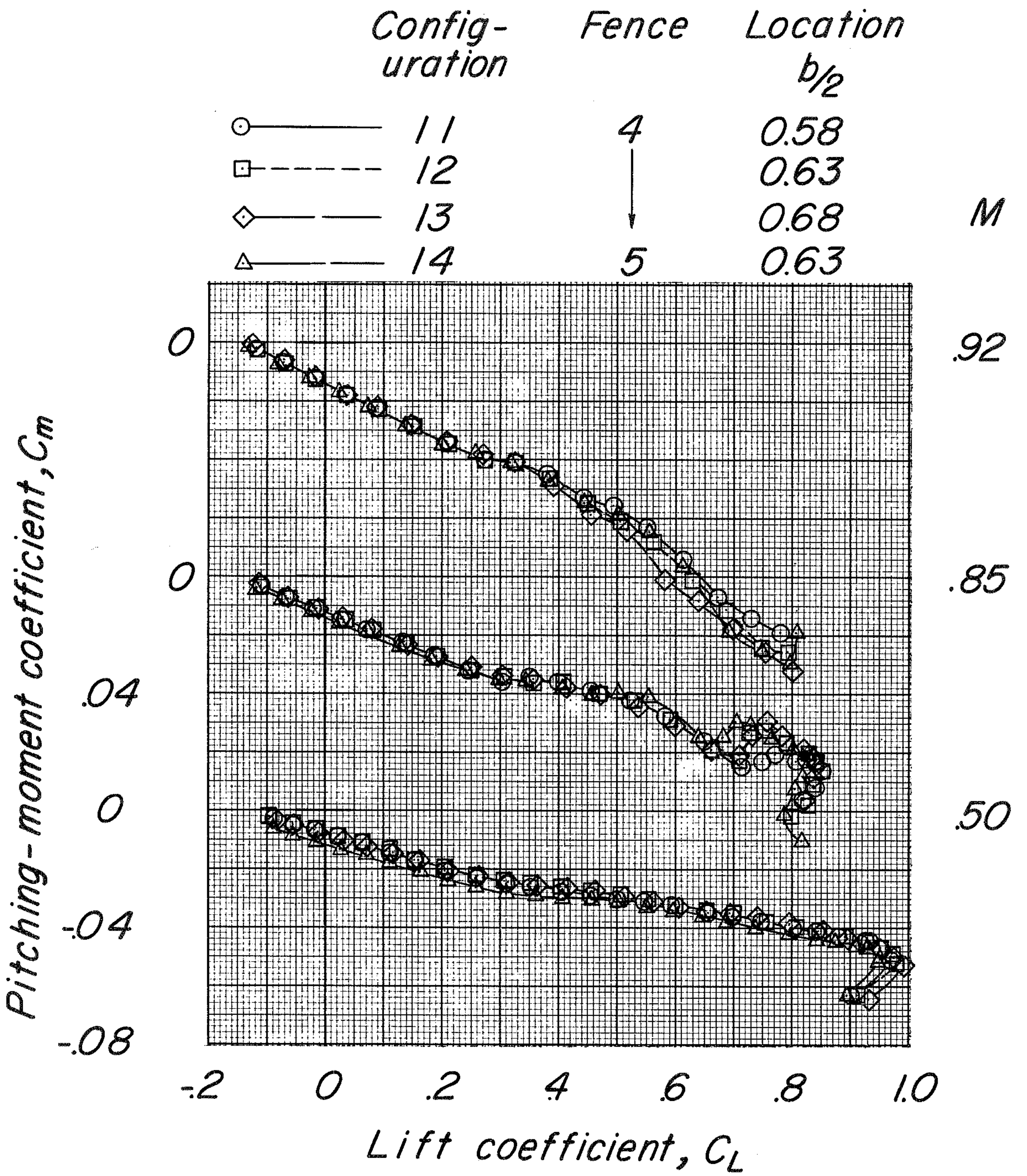

(d) Variation of C_m with C_L.

Figure 18.- Concluded.

[redacted]

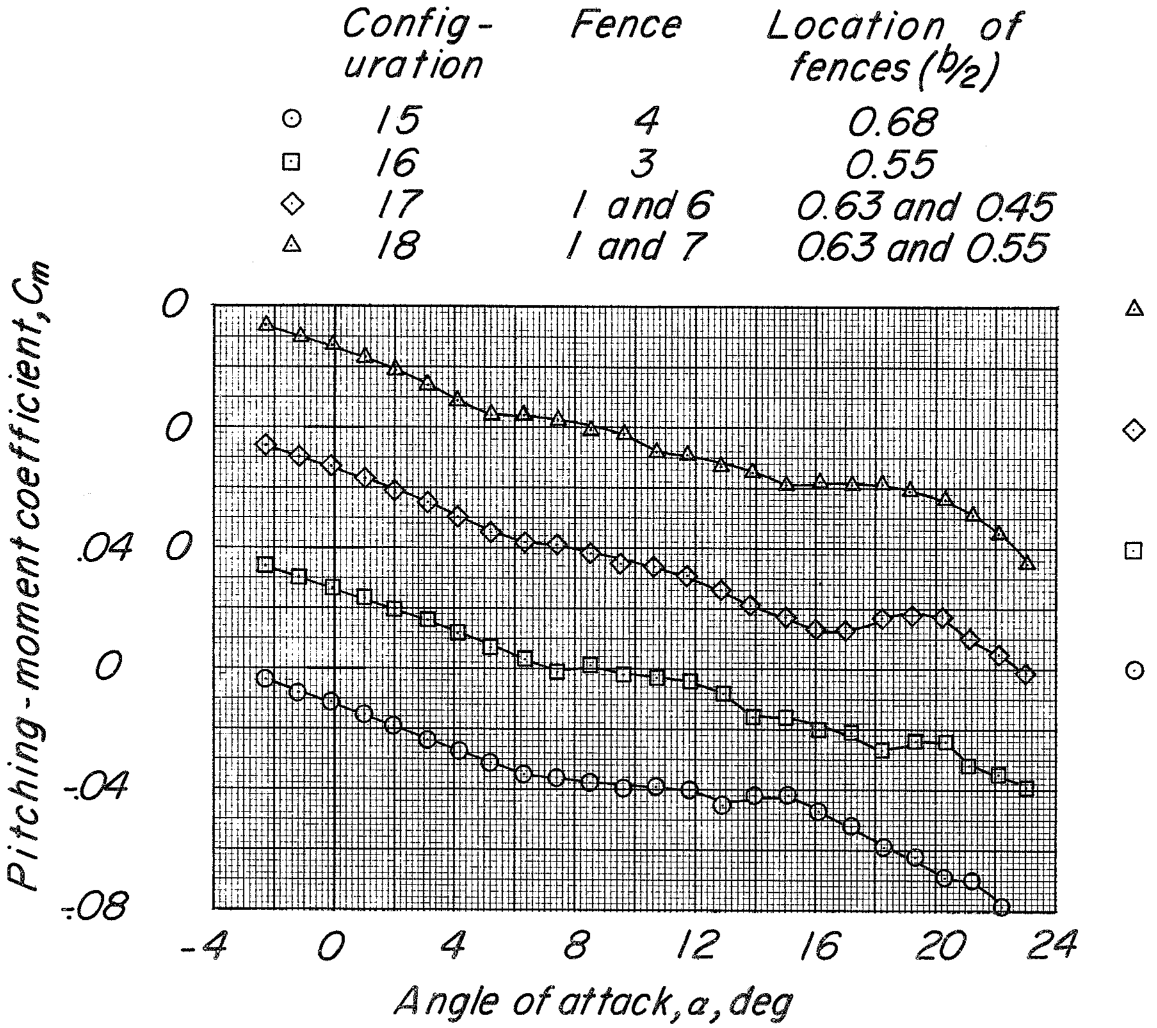

(a) Variation of C_m with α.

Figure 19.- Pitching-moment characteristics of configuration BCWV, $\delta_e = 0^\circ$, $\delta_r = 0^\circ$ at a constant Mach number of 0.85 showing effects of a number of fences and spanwise locations.

[redacted]

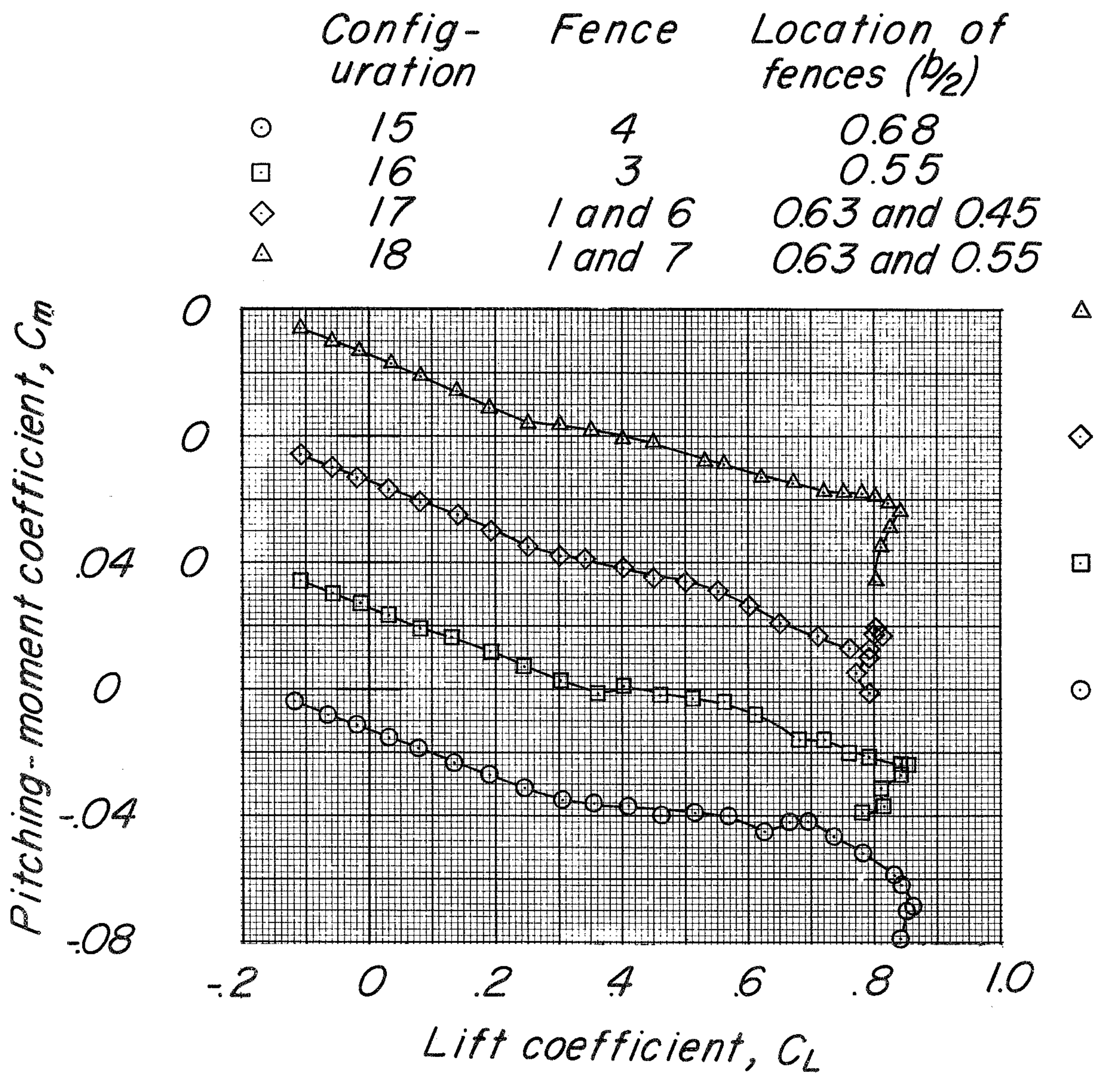

(b) Variation of C_m with C_L.

Figure 19.- Concluded.

[redacted]

 [redacted]

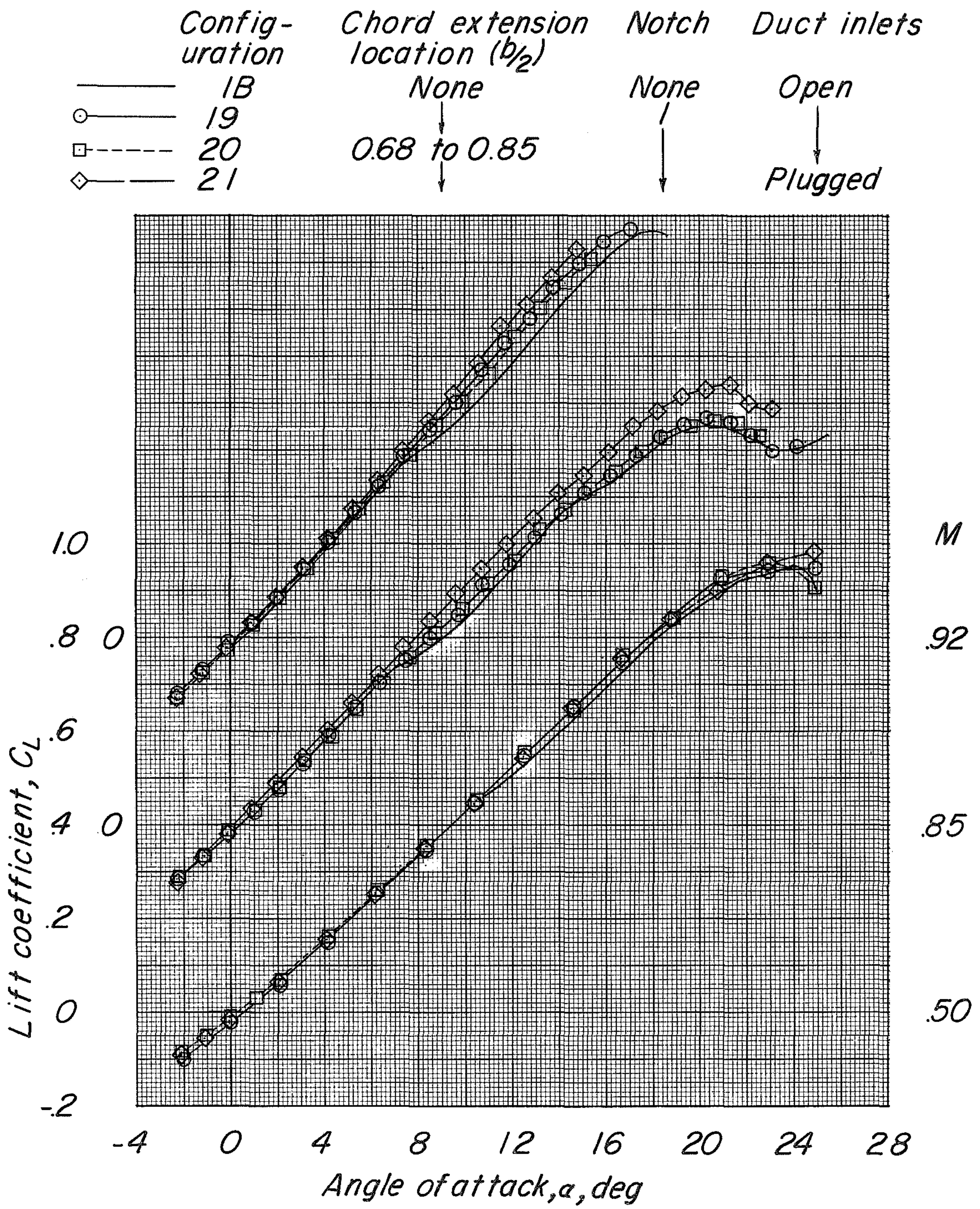

(a) Variation of C_L with α.

Figure 20.- Basic longitudinal characteristics of configuration BCWV, $\delta_e = 0^\circ$, $\delta_r = 0^\circ$ with and without leading-edge chord-extension and notch 1 and with the duct inlets open and plugged.

[redacted]

[redacted]

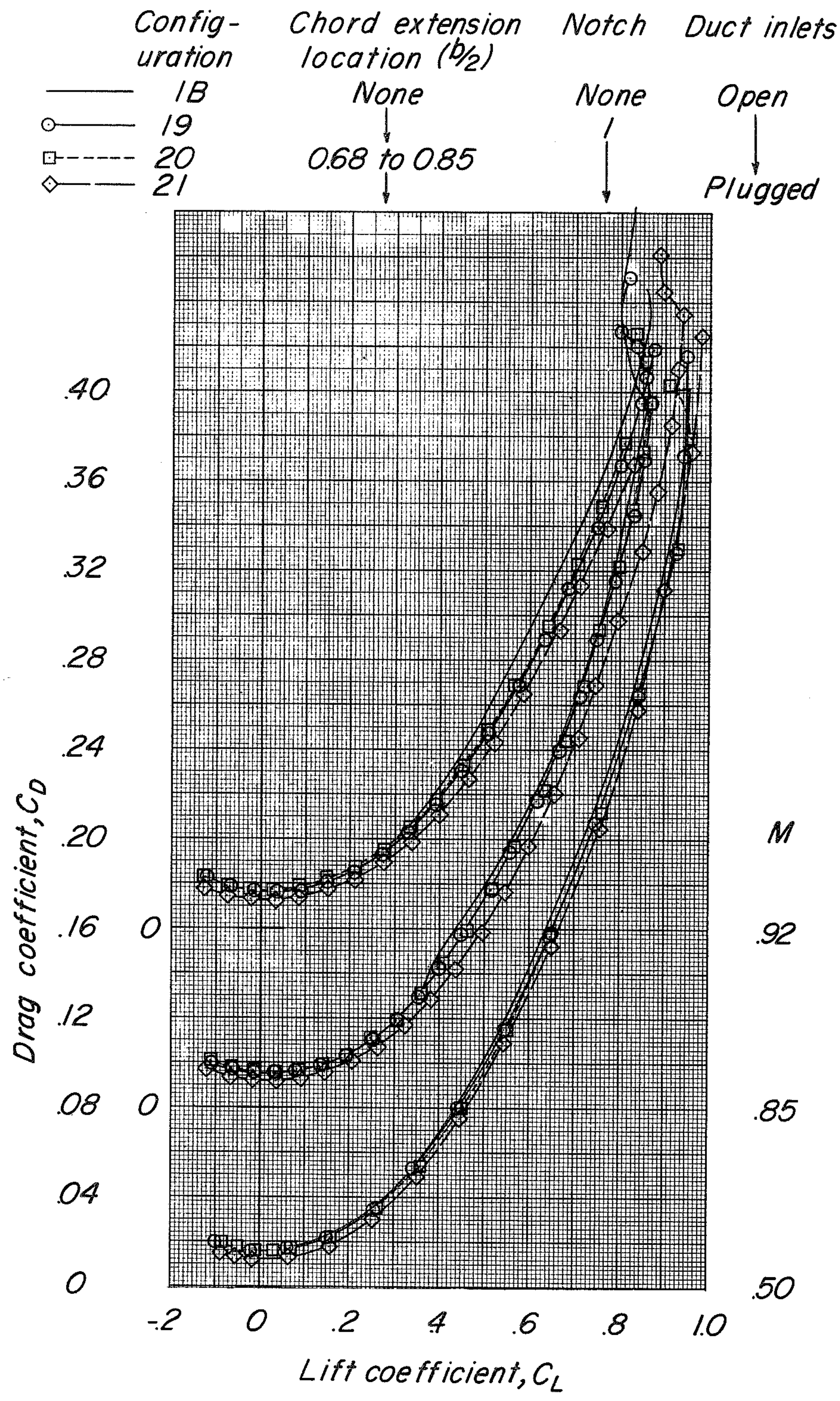

(b) Variation of C_D with C_L.

Figure 20.- Continued.

[redacted]

[redacted]

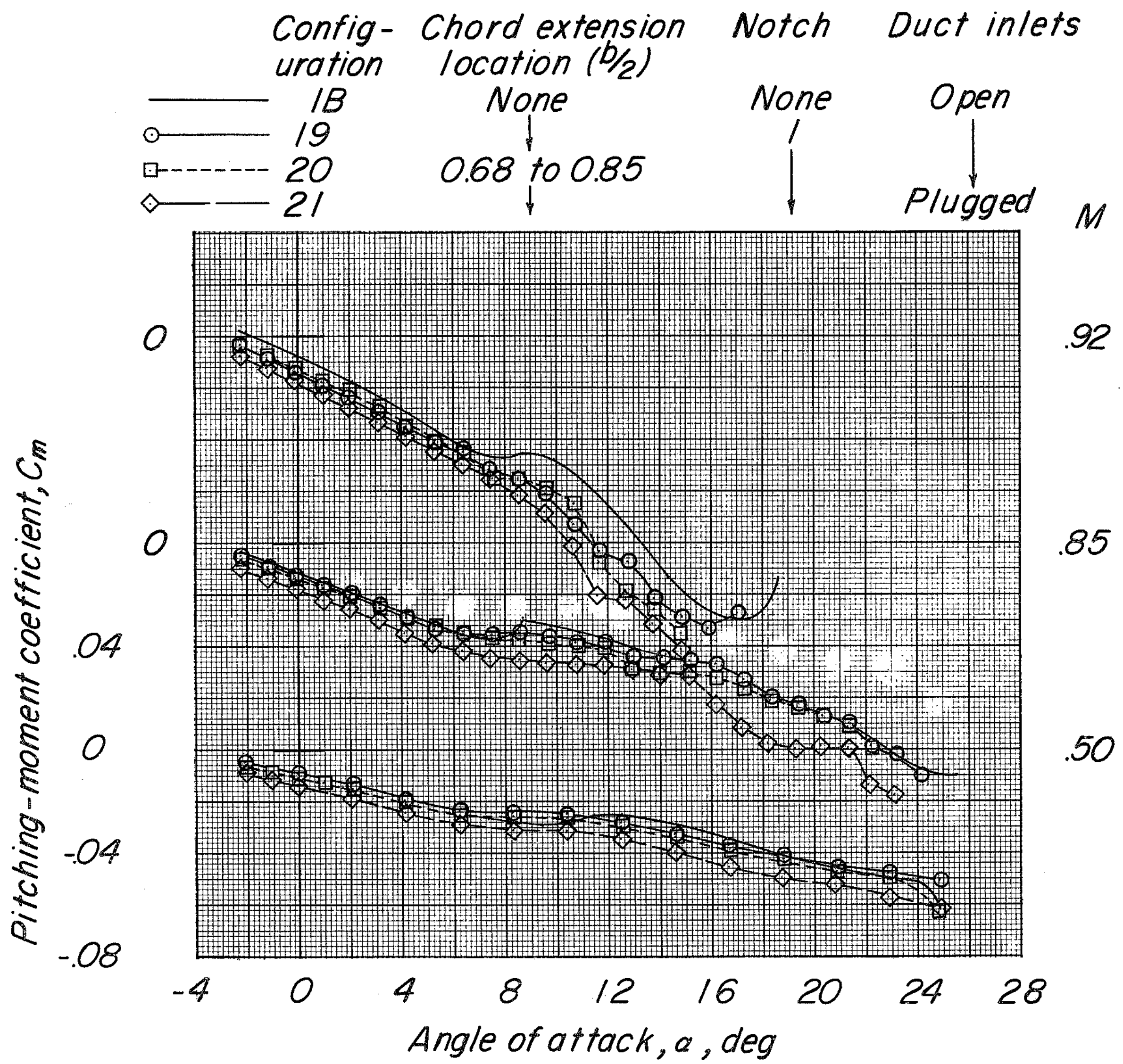

(c) Variation of C_m with α.

Figure 20.- Continued.

[redacted]

[redacted]

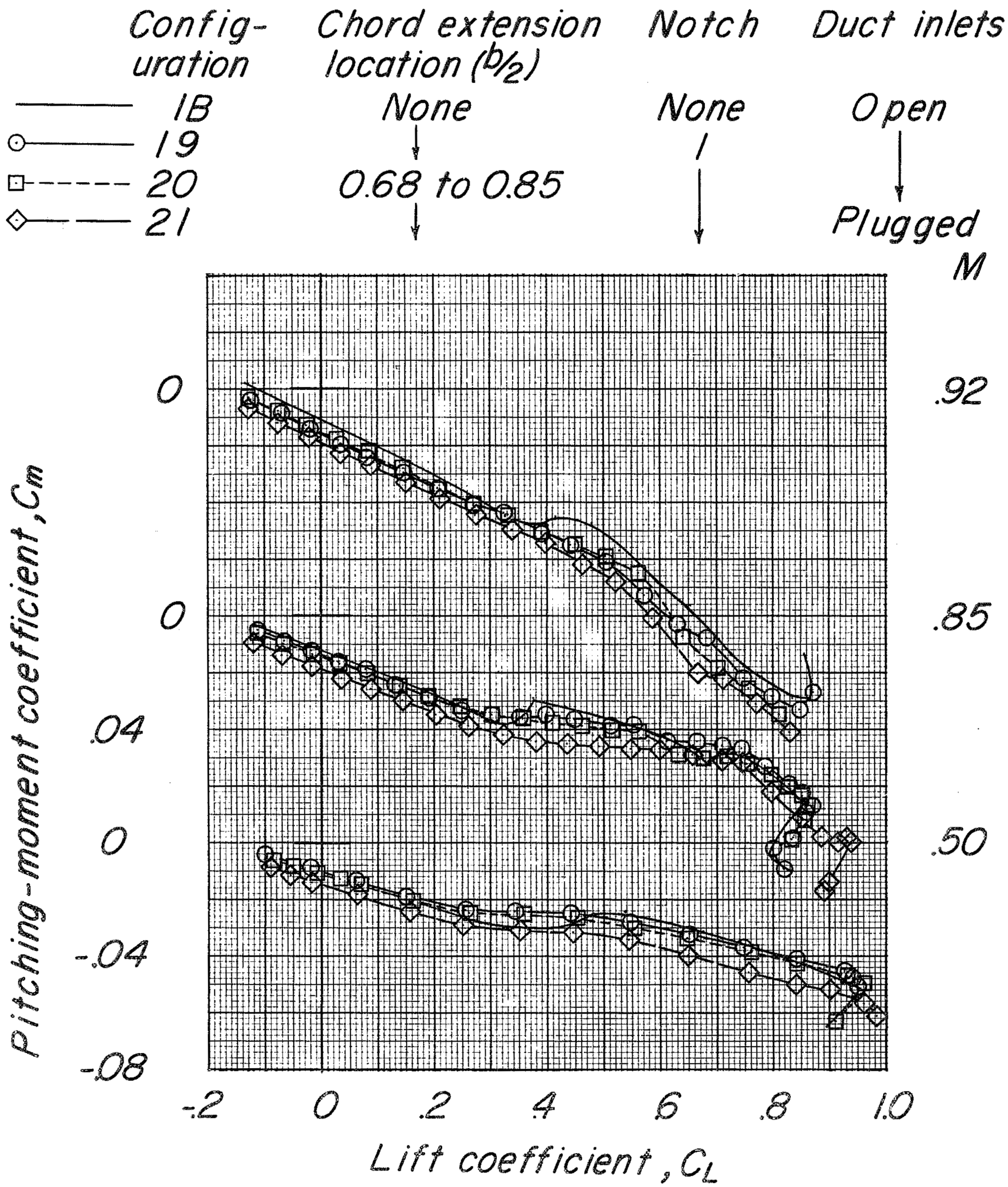

(d) Variation of C_m with C_L.

Figure 20.- Concluded.

[redacted]

 [redacted]

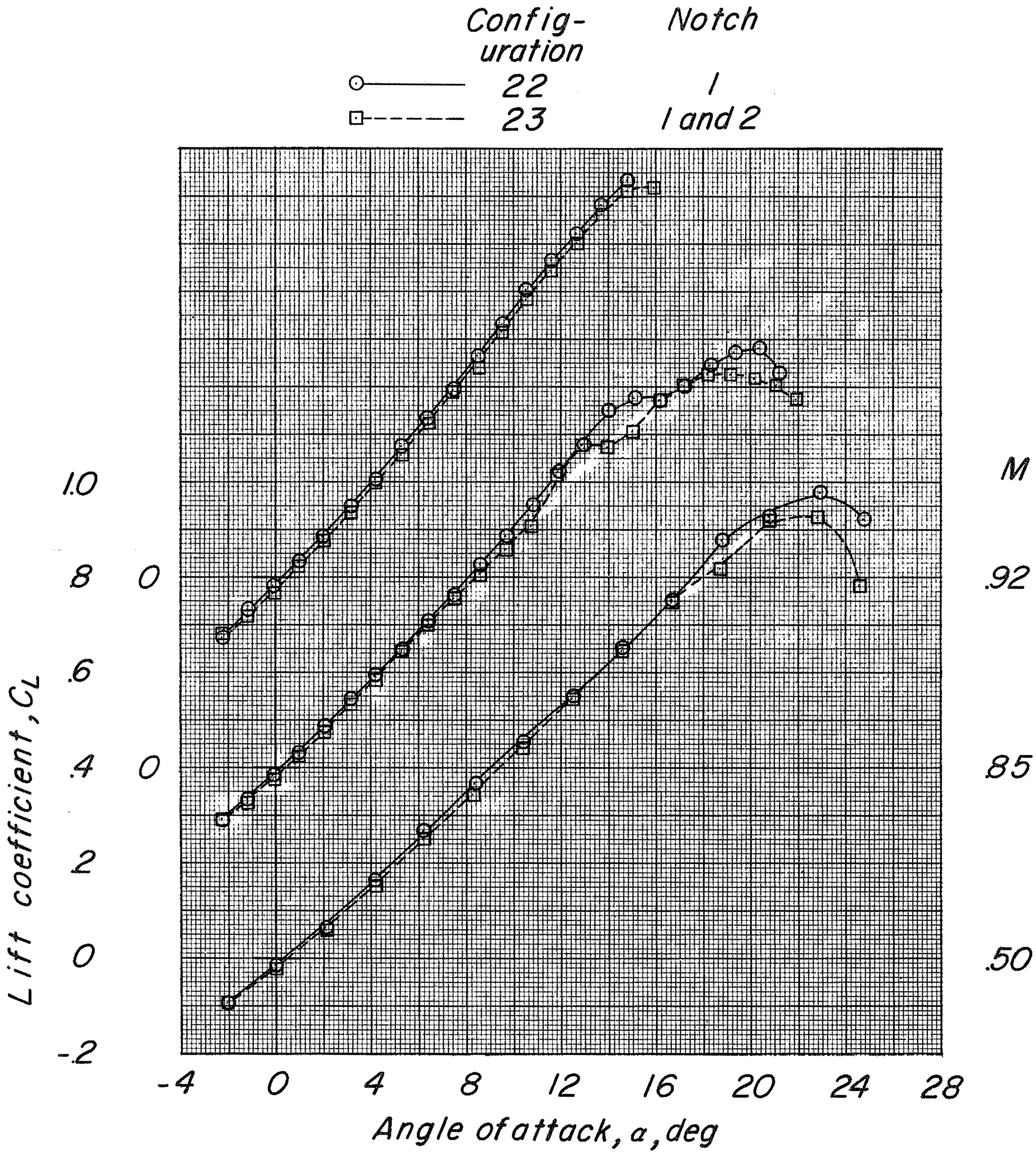

(a) Variation of C_L with α.

Figure 21.- Basic longitudinal characteristics of configuration BCWV, $\delta_e = 0^{\circ}$, $\delta_r = 0^{\circ}$ with a leading-edge chord-extension from 0.68b/2 to 0.85b/2 and with the elevon actuator and fairing removed showing the effects of two leading-edge notch arrangements.

[redacted]

[redacted]

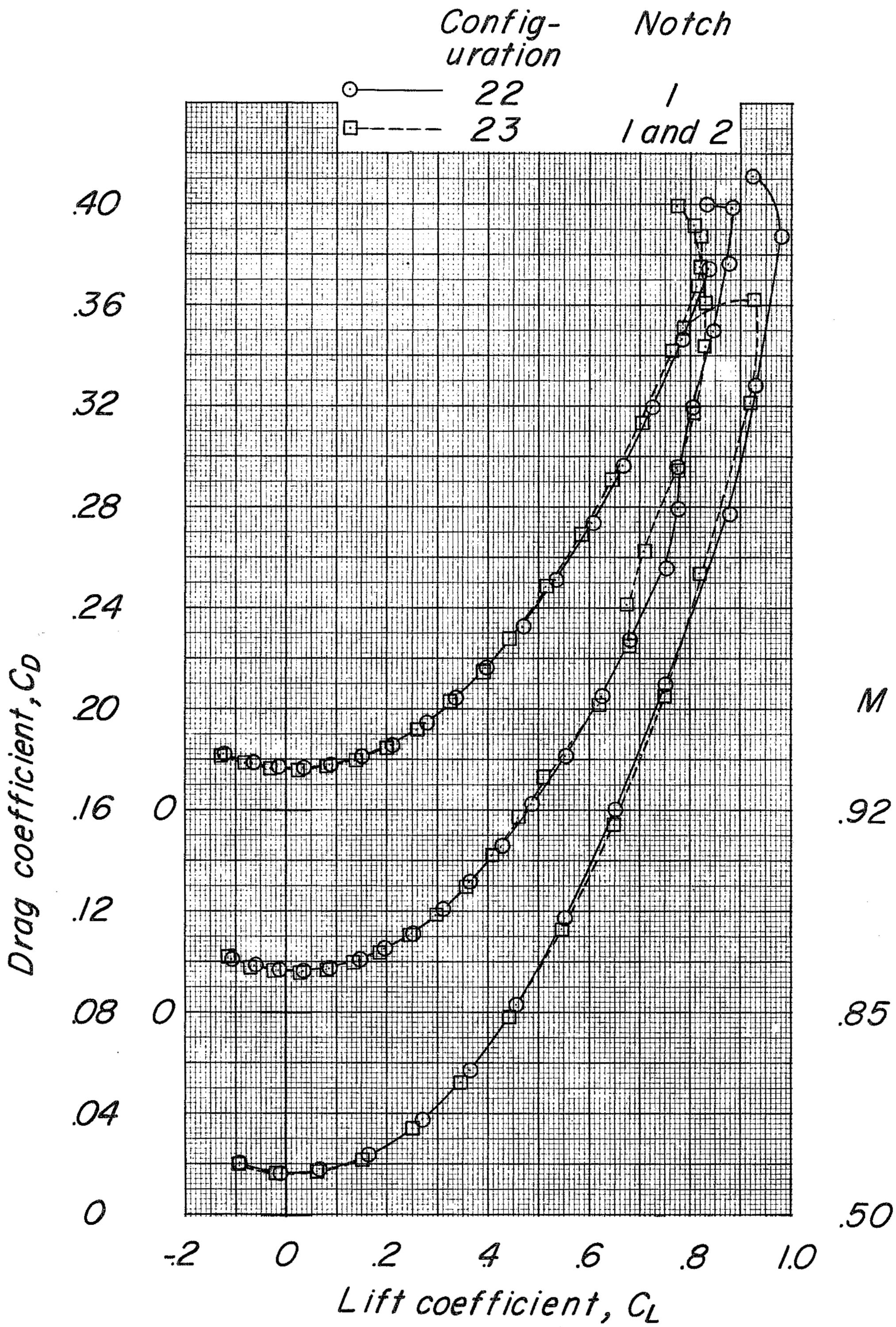

(b) Variation of C_D with C_L.

Figure 21.- Continued.

[redacted]

 [redacted]

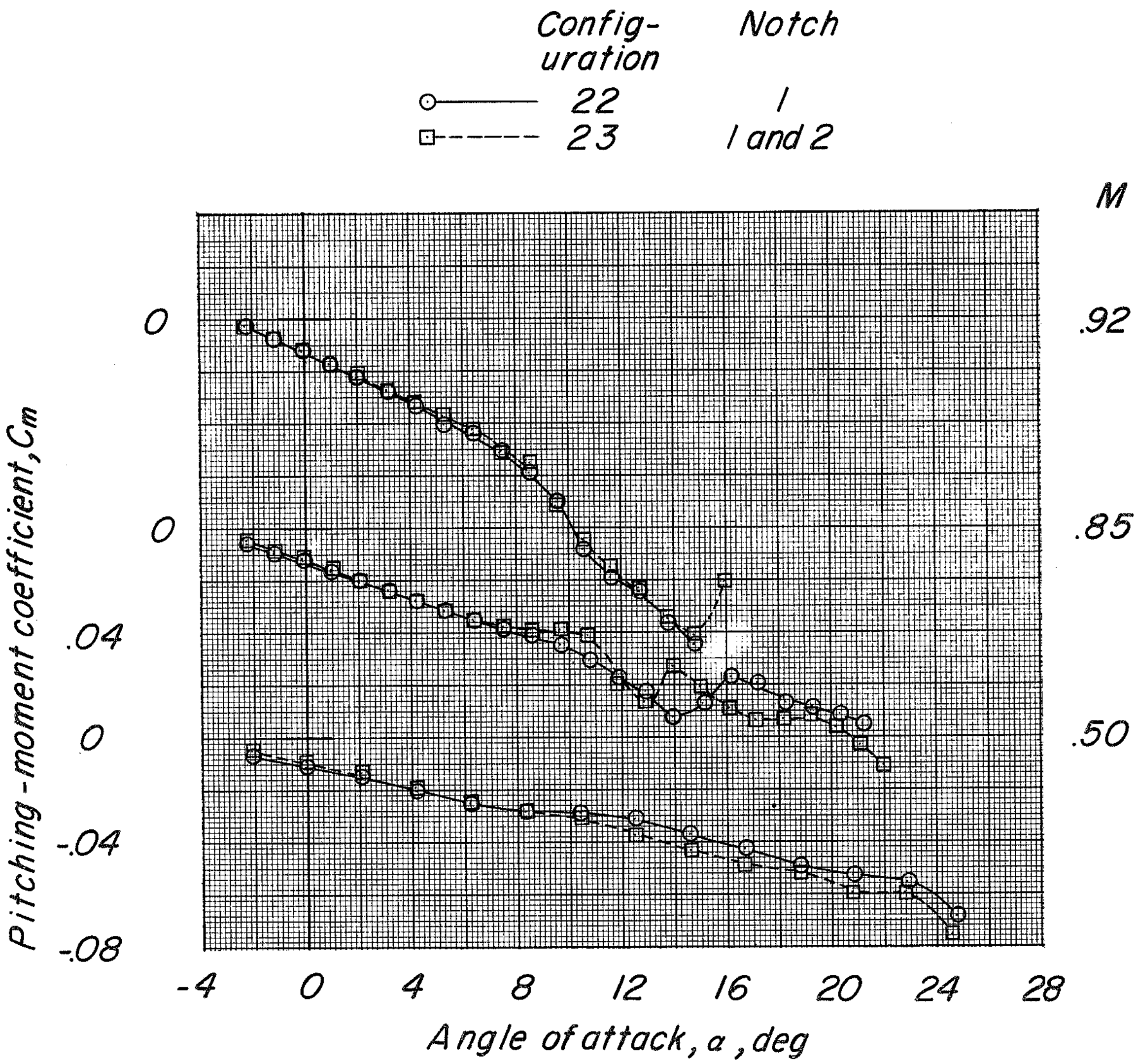

(c) Variation of C_m with α.

Figure 21.- Continued.

 [redacted]

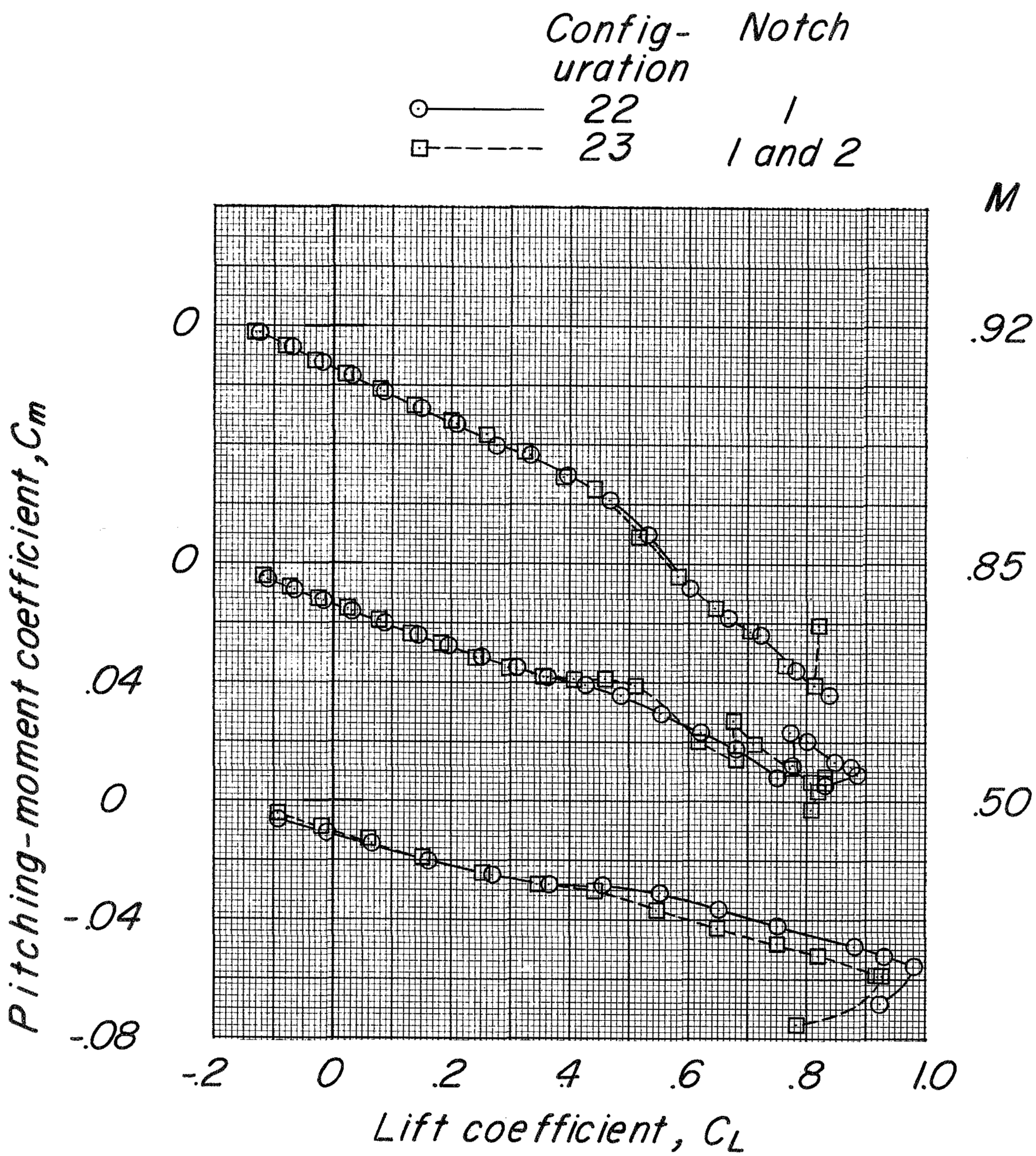

(d) Variation of C_m with C_L.

Figure 21.- Concluded.

[redacted]

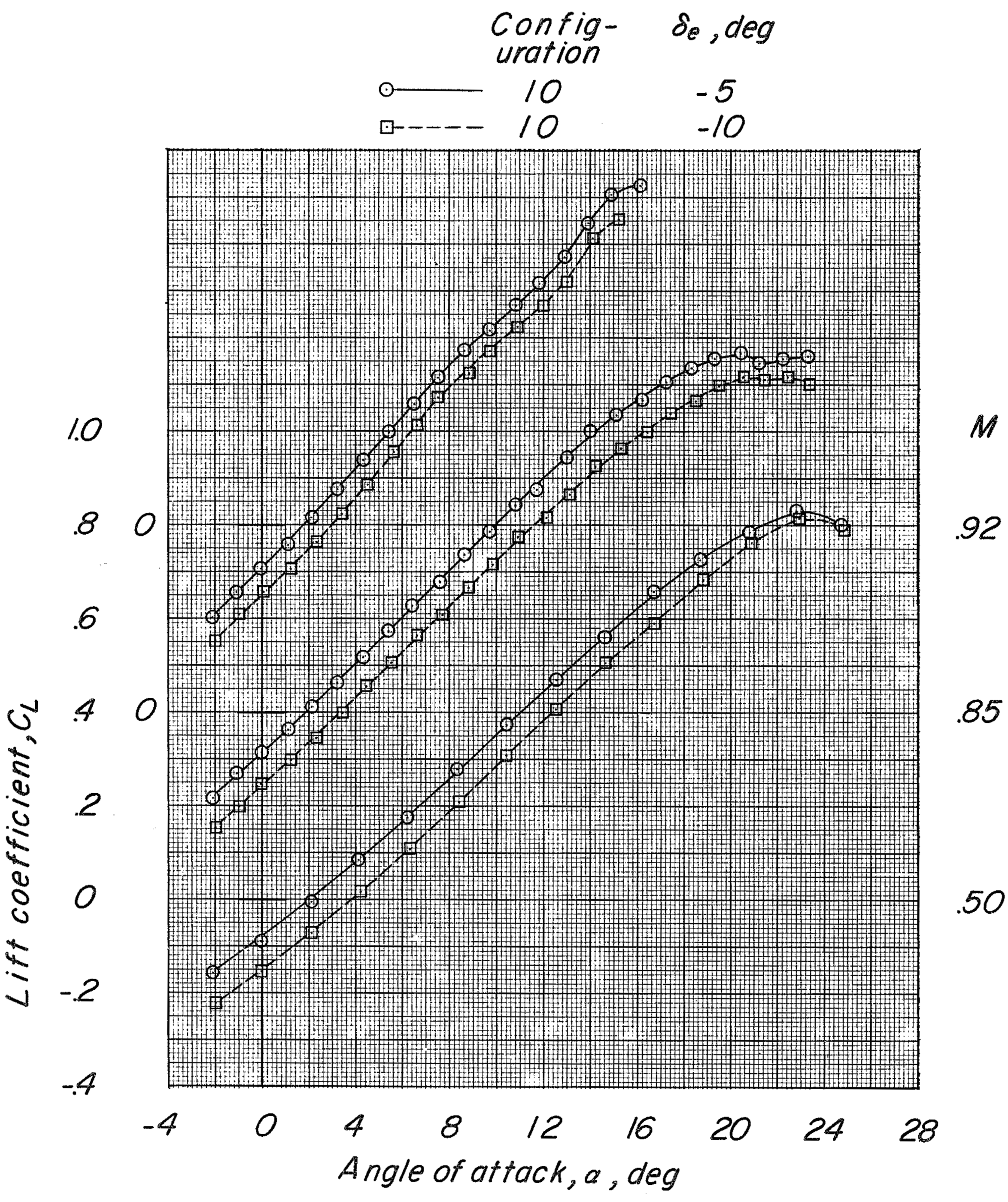

(a) Variation of C_L with α.

Figure 22.- Basic longitudinal characteristics of configuration $BCW_{F_{1+3}}V$, $\delta_r = 0^\circ$ showing effects of two elevon angles. Fences 1 and 3 located at 0.63b/2 and 0.55b/2, respectively.

[redacted]

 [redacted]

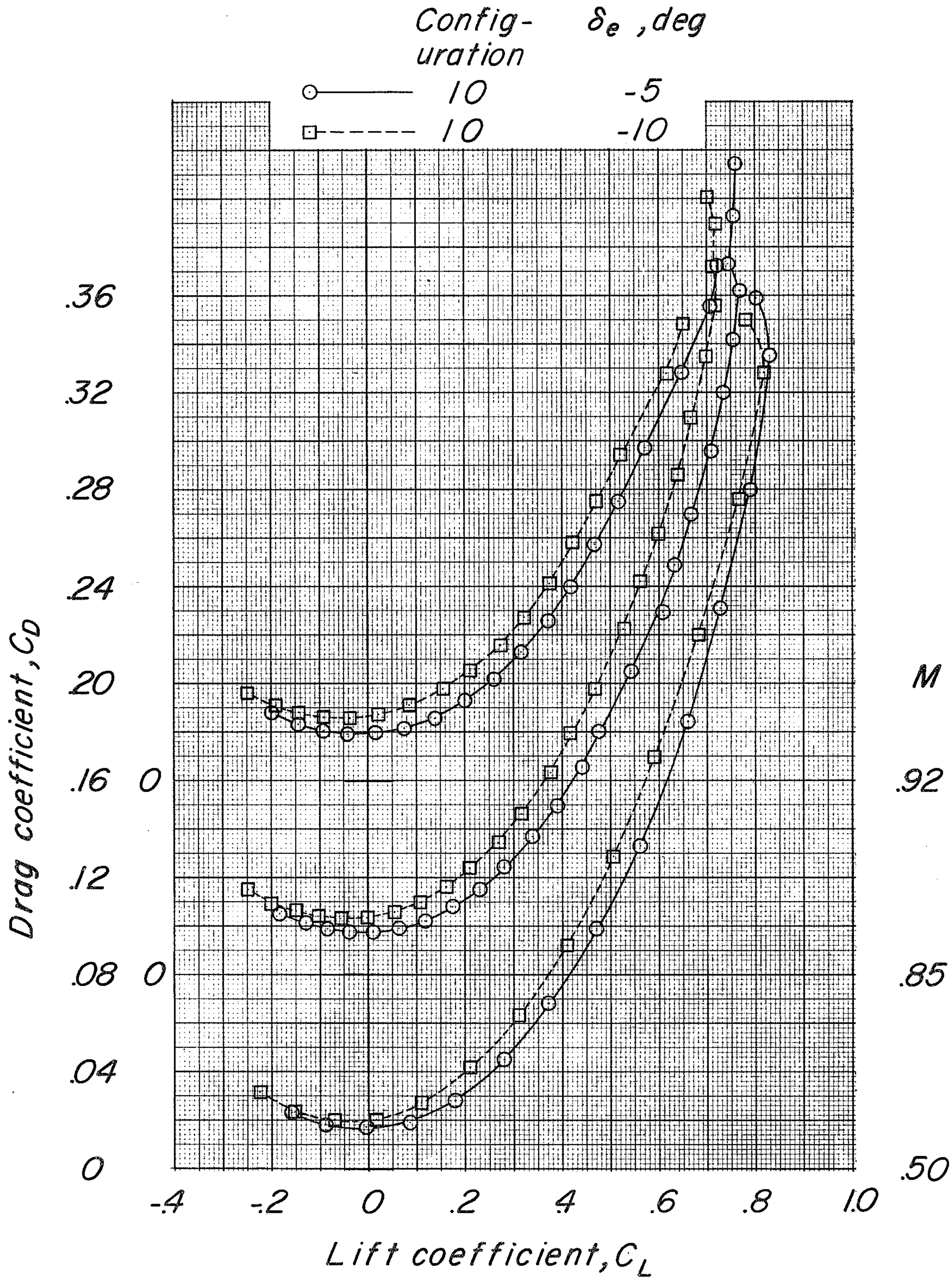

(b) Variation of C_D with C_L.

Figure 22.- Continued.

[redacted]

 [redacted]

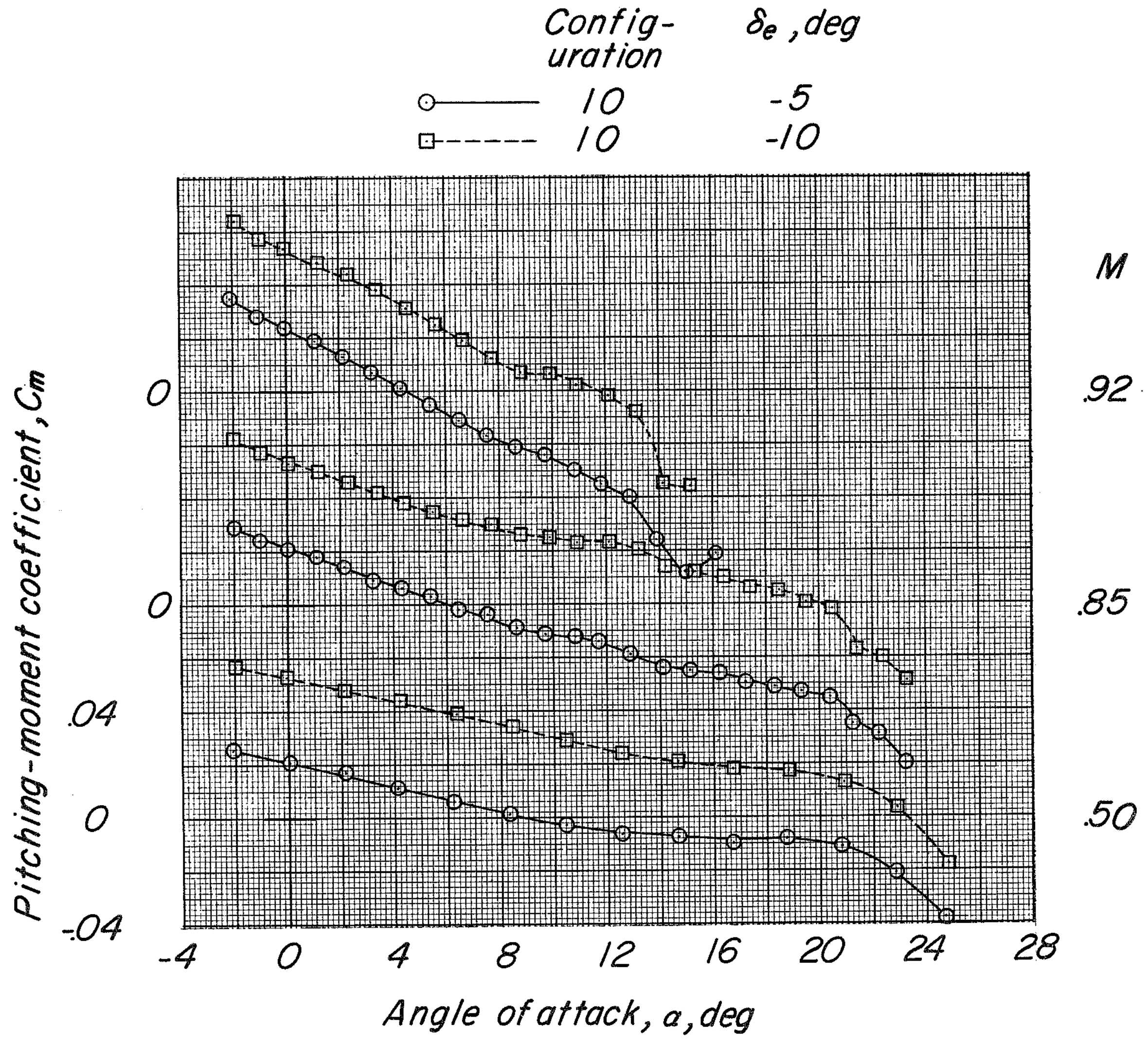

(c) Variation of C_m with α.

Figure 22.- Continued.

[redacted]

 [redacted]

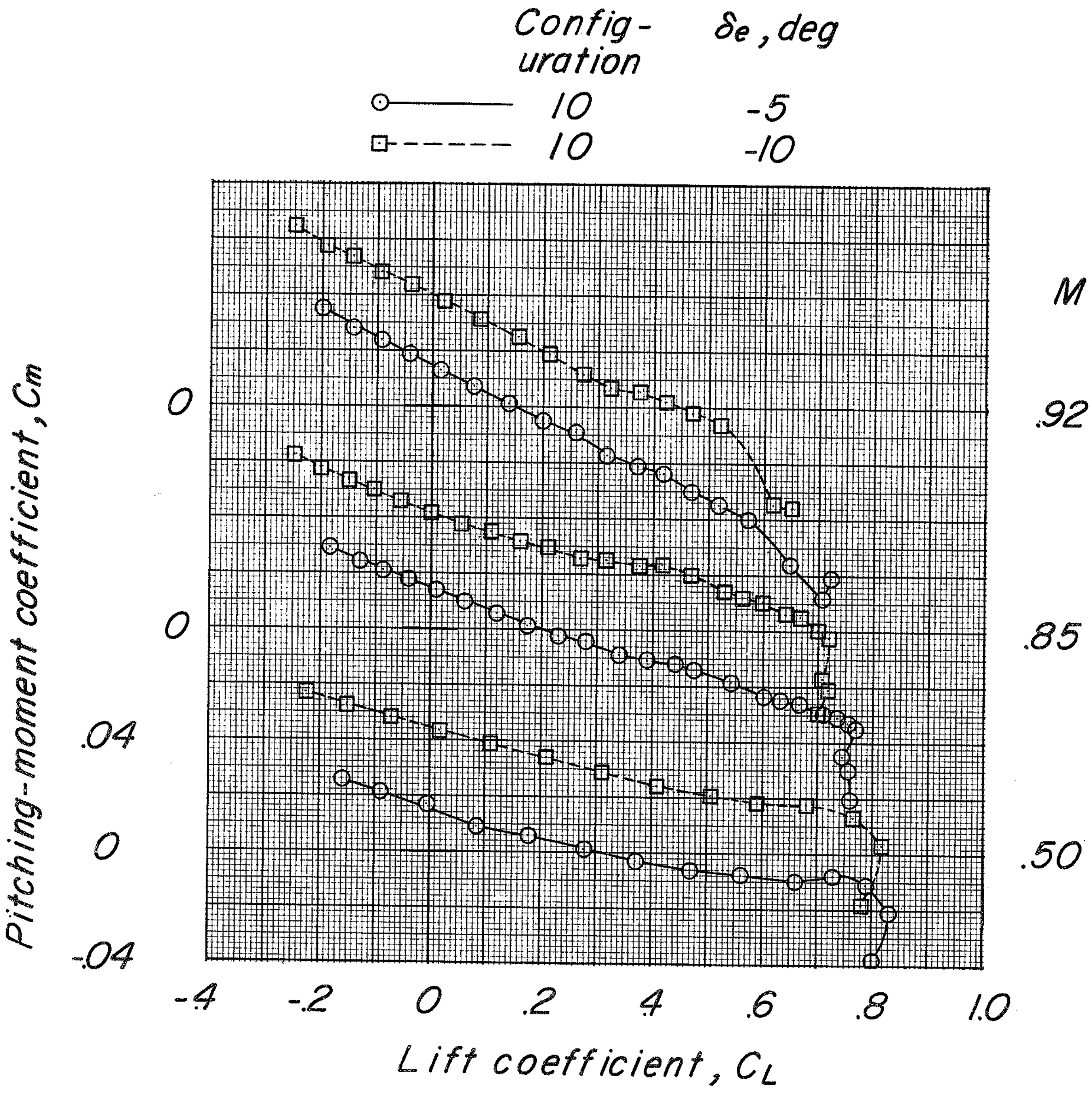

(d) Variation of C_m with C_L.

Figure 22.- Concluded.

[redacted]

[redacted]

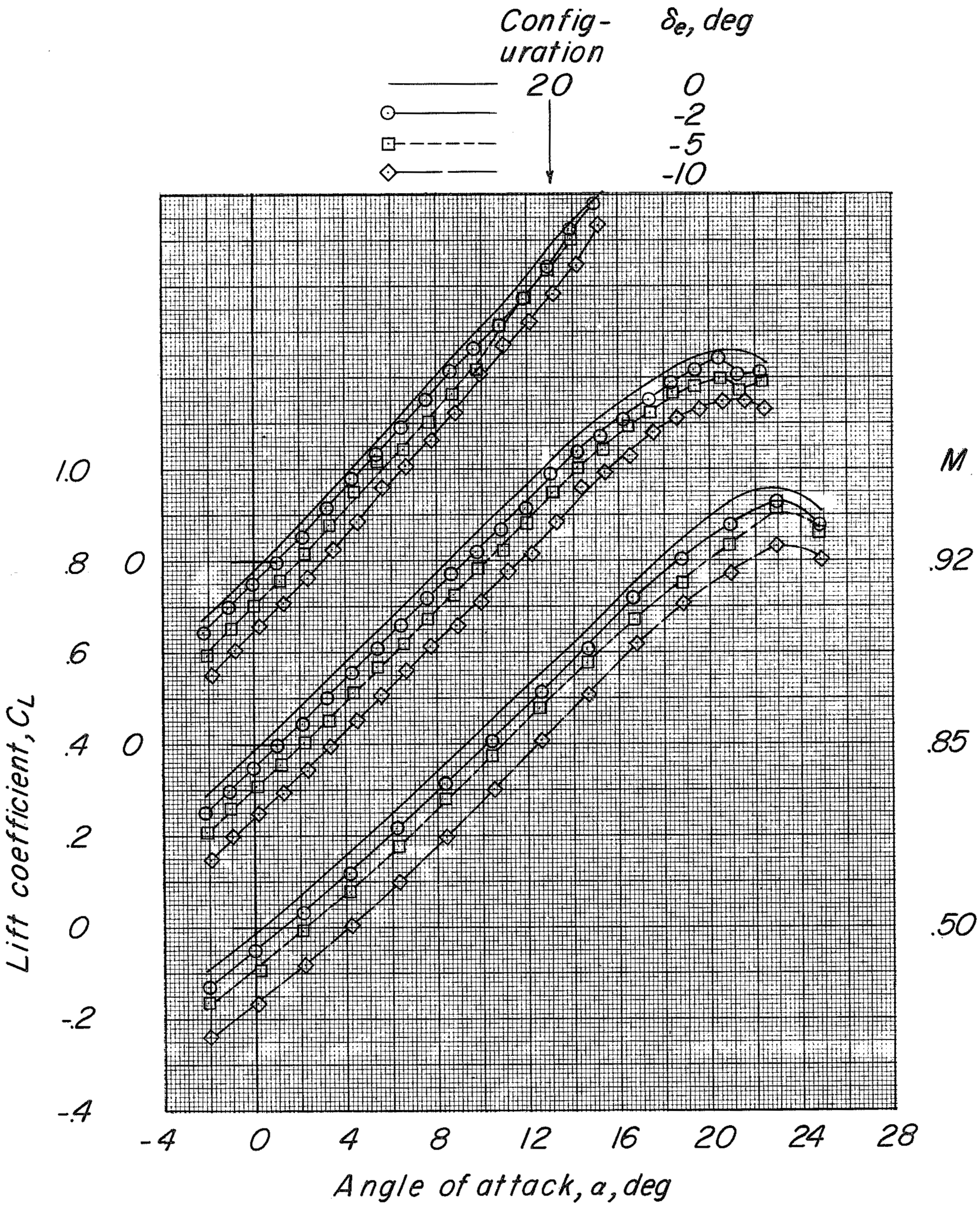

(a) Variation of C_L with α.

Figure 23.- Basic longitudinal characteristics of configuration $BCW_{N_1}V$, $\delta_r = 0^\circ$ with leading-edge chord-extension from 0.68b/2 to 0.85b/2 showing effects of the elevons.

[redacted]

[redacted]

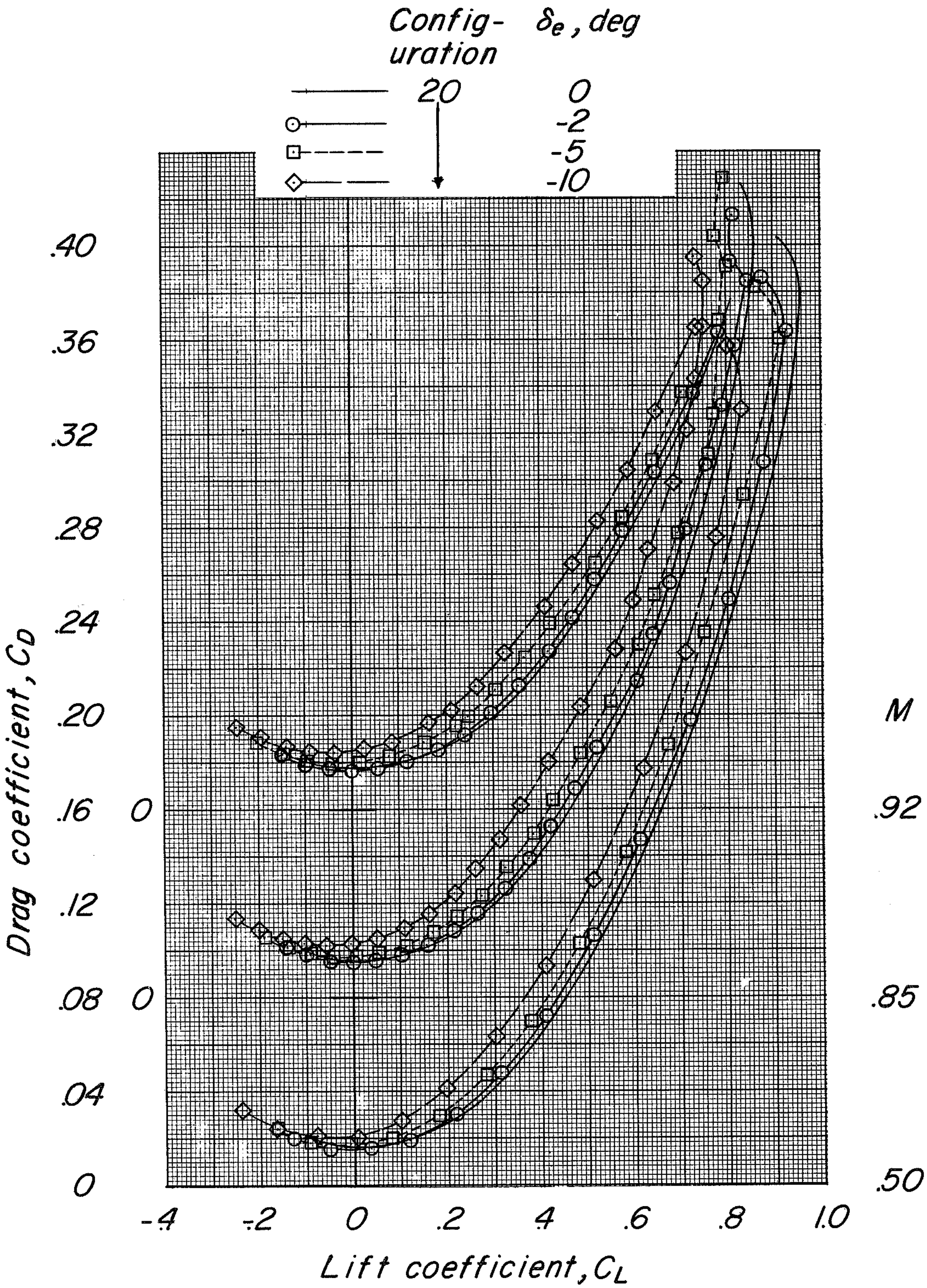

(b) Variation of C_D with C_L.

Figure 23.- Continued.

[redacted]

[redacted]

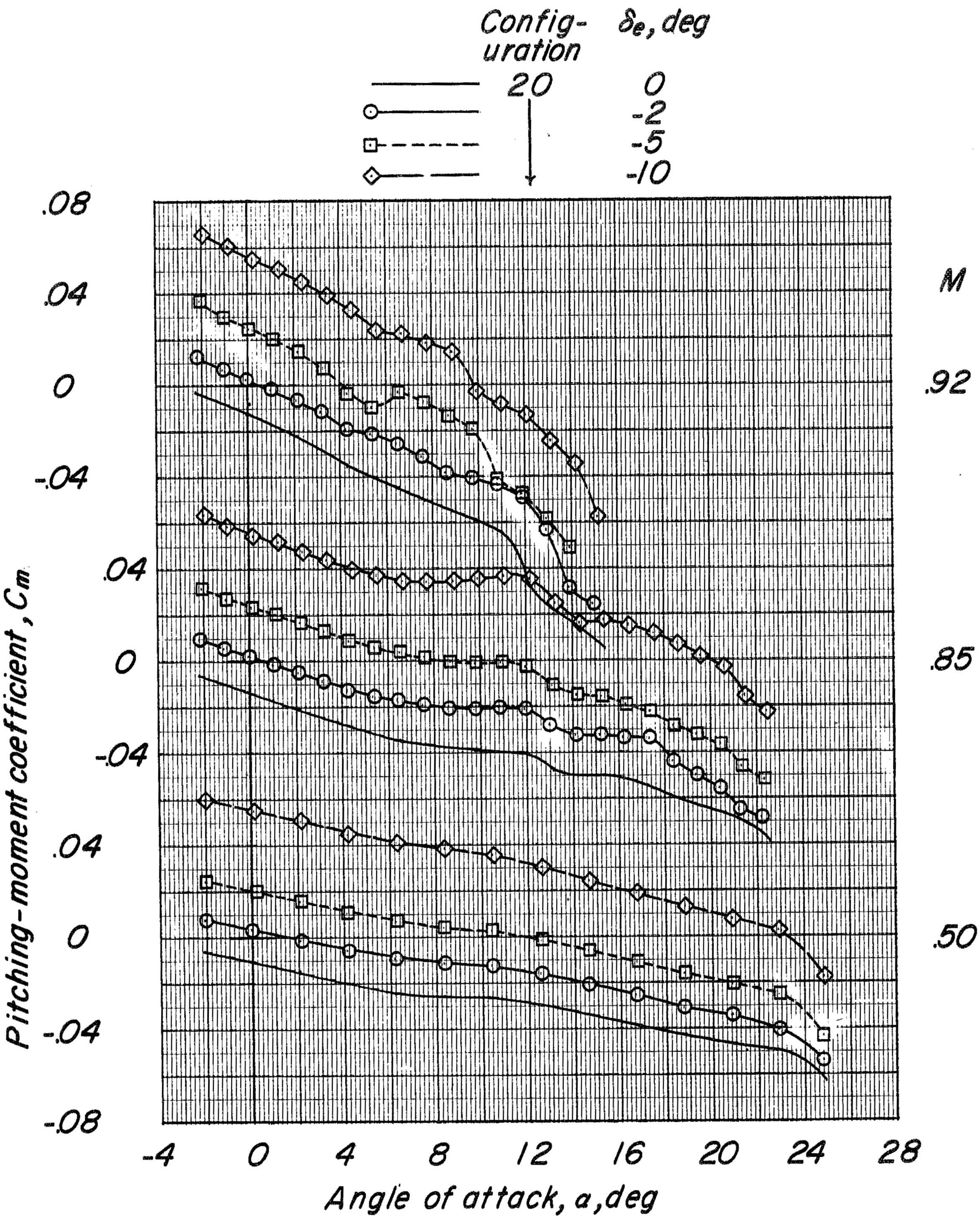

(c) Variation of C_m with α.

Figure 23.- Continued.

[redacted]

[redacted]

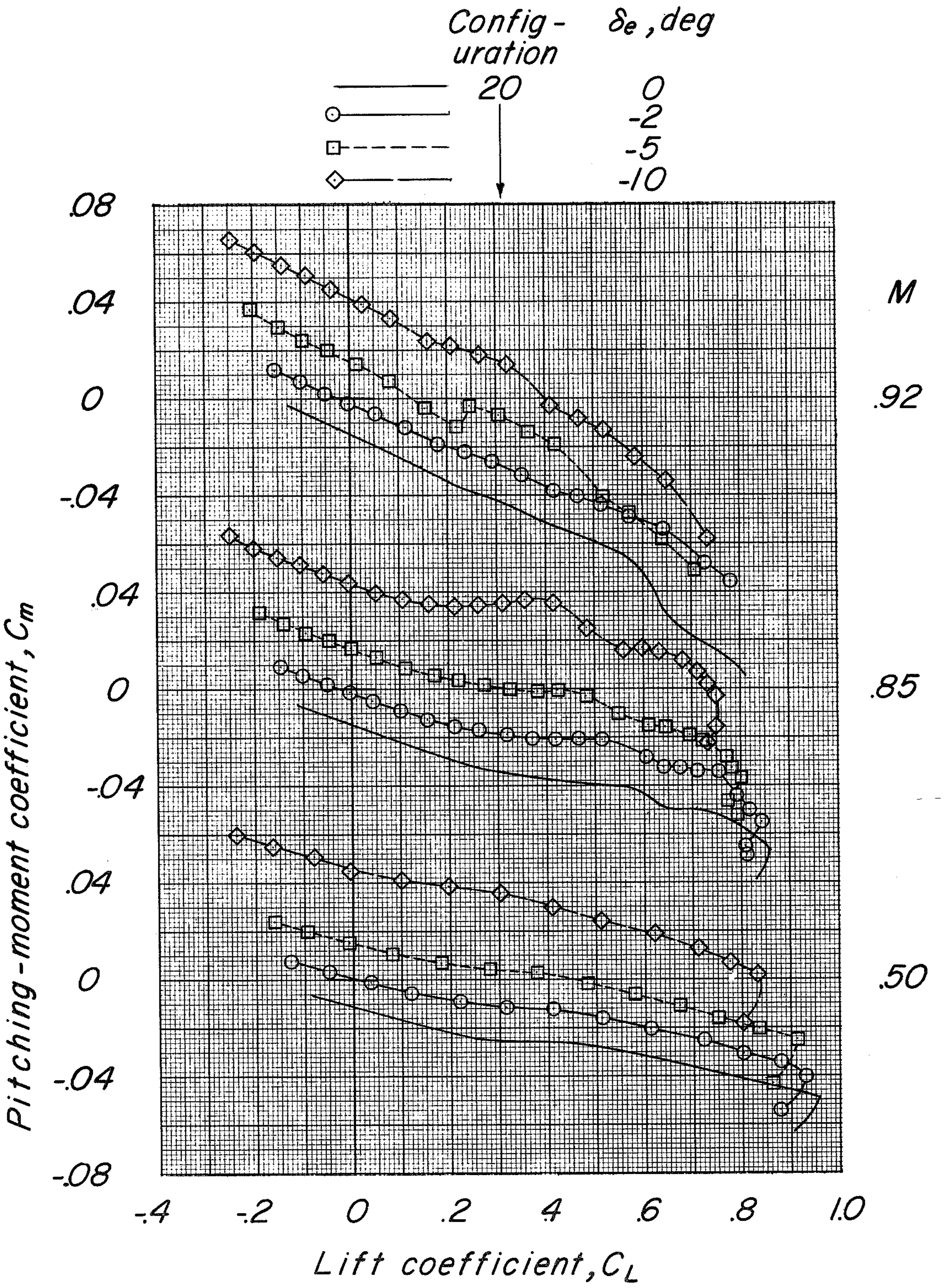

(d) Variation of C_m with C_L.

Figure 23.- Concluded.

[redacted]

[redacted]

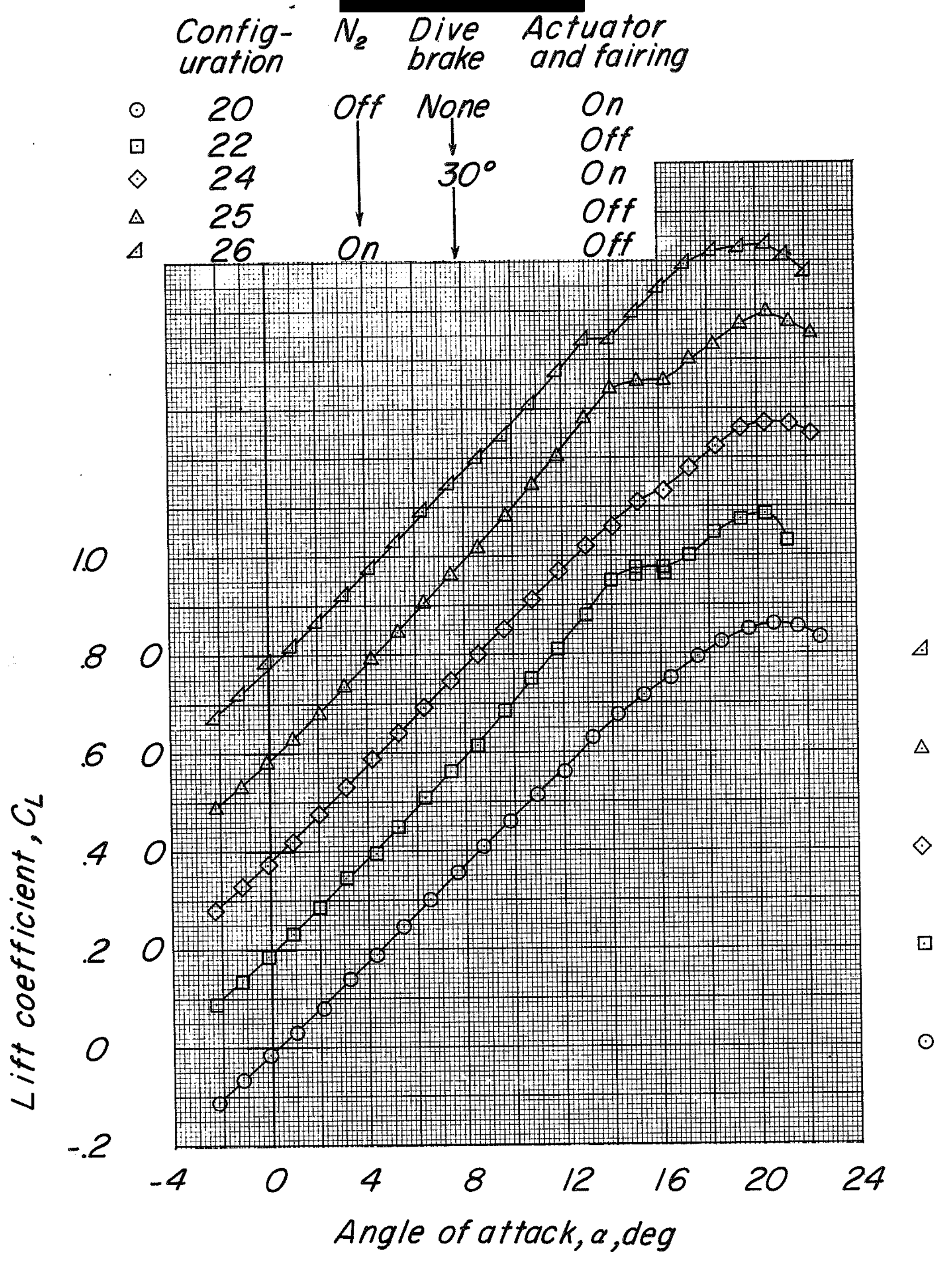

(a) Variation of C_L with α.

Figure 24.- Basic longitudinal characteristics of configuration $BCW_{N_1}V$, $\delta_e = 0^{\circ}$, $\delta_r = 0^{\circ}$ with leading-edge chord-extension from 0.68b/2 to 0.85b/2 showing effects of elevon actuator and fairing with and without 30° dive brake and notch 2 at a constant Mach number of 0.85.

[redacted]

[redacted]

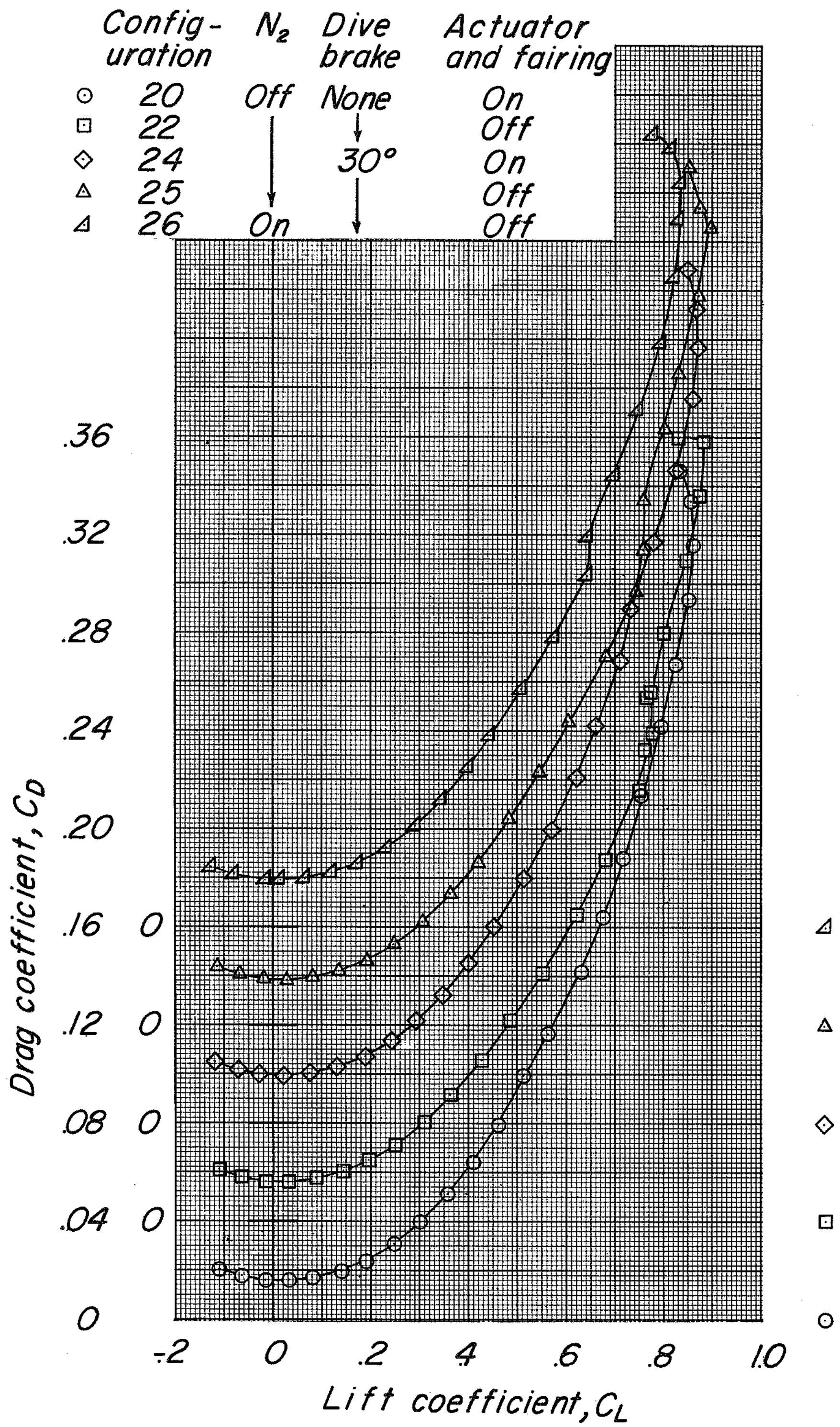

(b) Variation of C_D with C_L.

Figure 24.- Continued.

[redacted]

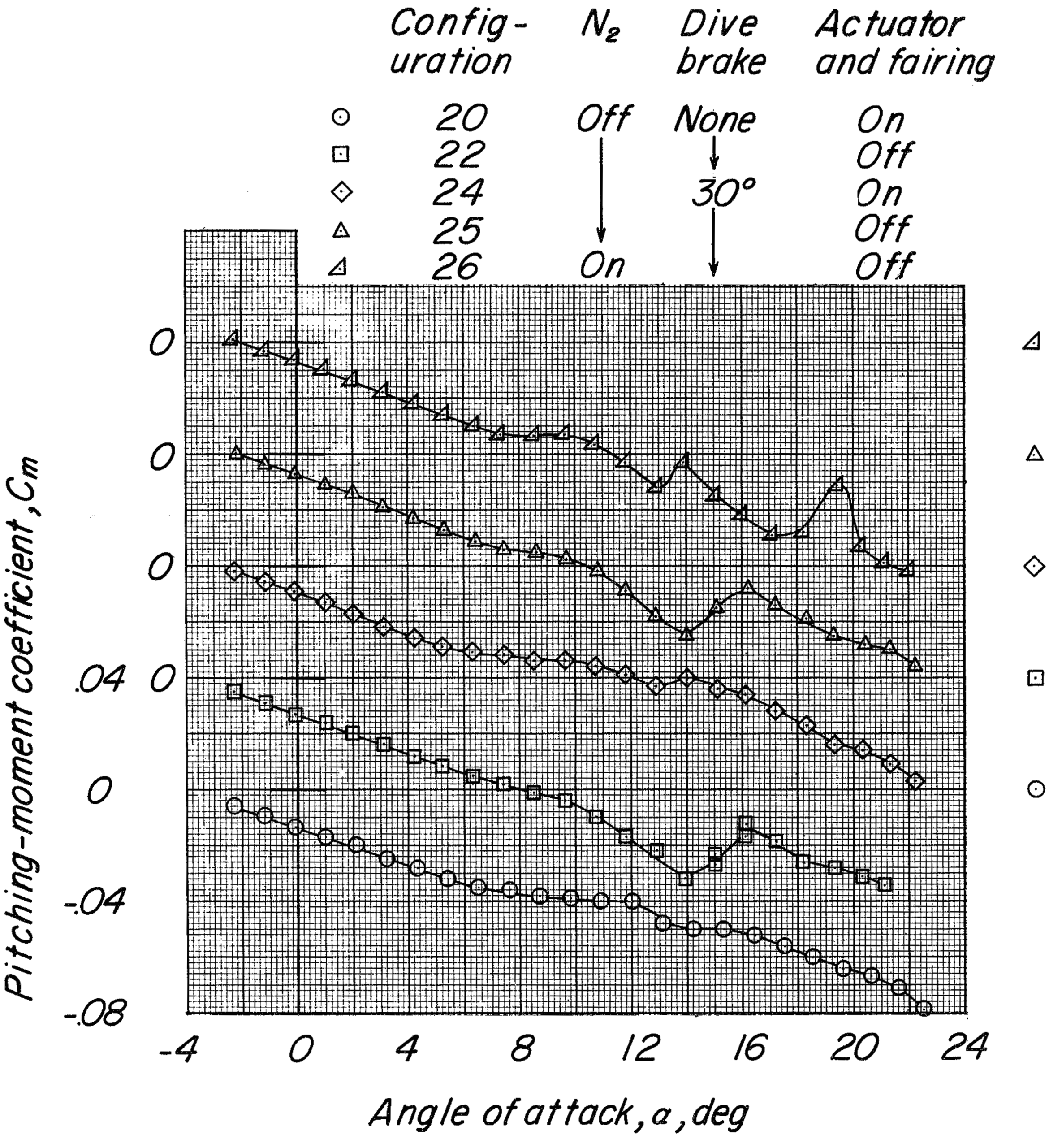

(c) Variation of C_m with α.

Figure 24.- Continued.

[redacted]

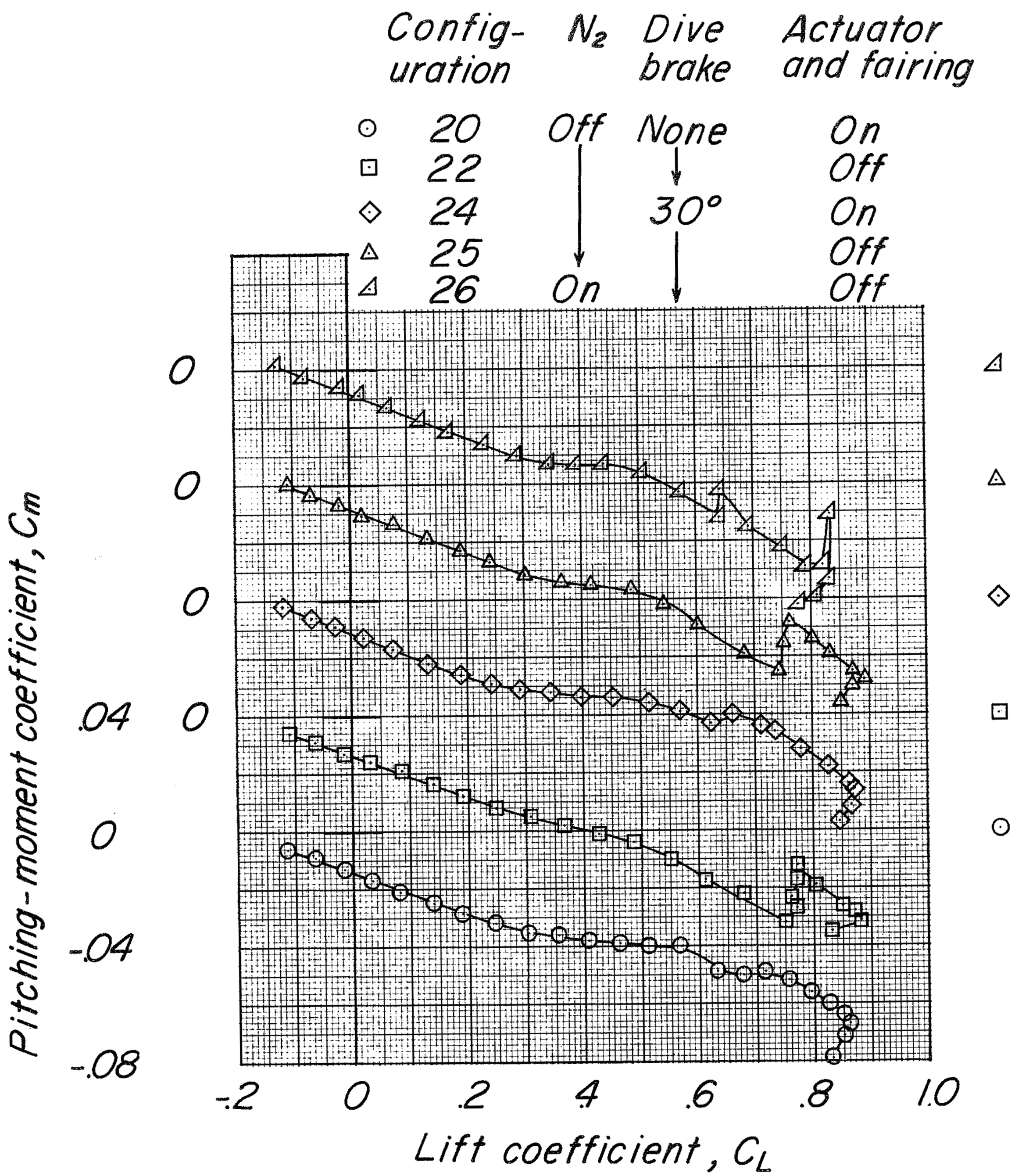

(d) Variation of C_m with C_L.

Figure 24.- Concluded.

[redacted]

[redacted]

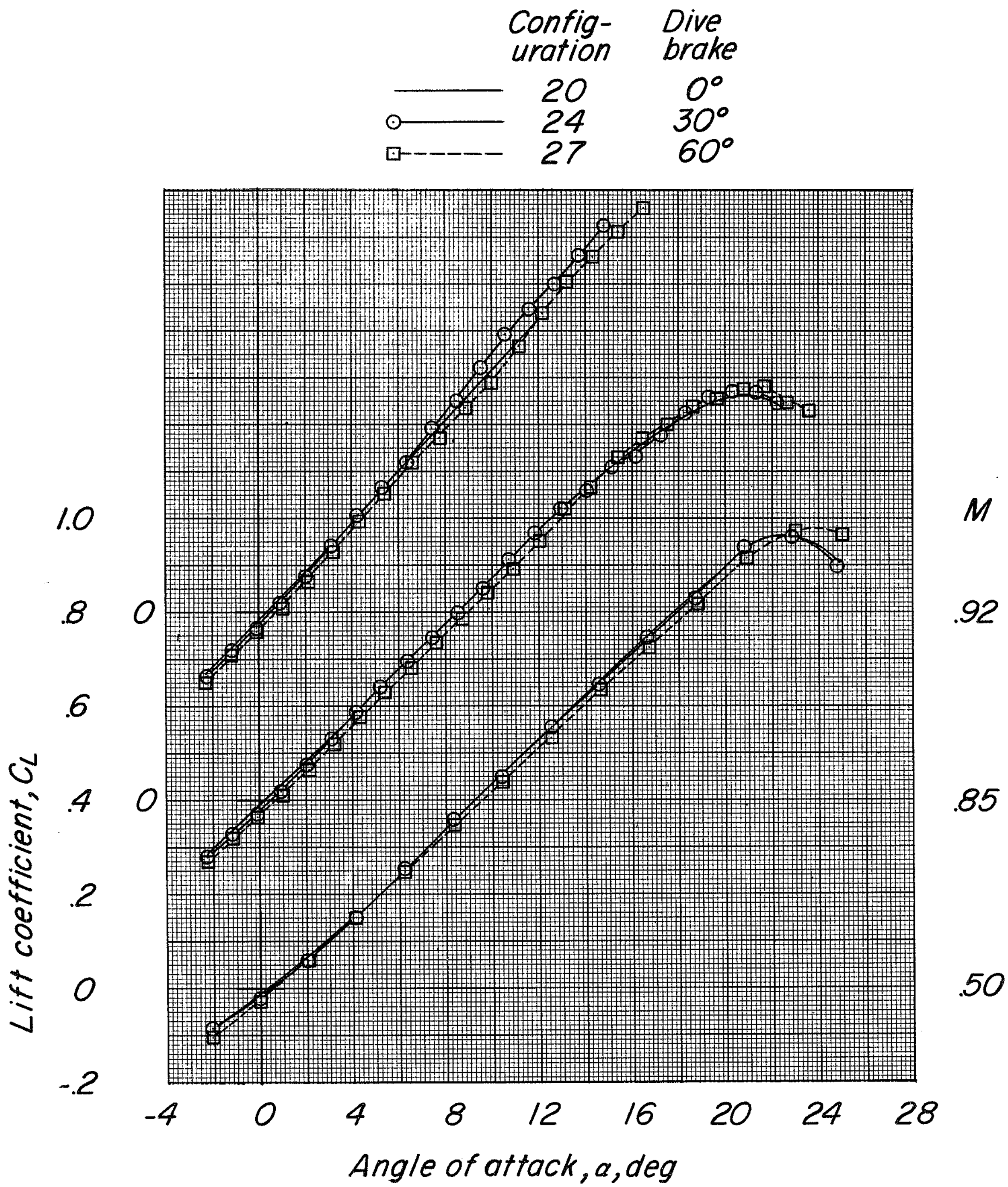

(a) Variation of C_L with α.

Figure 25.- Basic longitudinal characteristics of configuration $BCW_{N_1}V$, $\delta_e = 0^o$, $\delta_r = 0^o$ with a leading-edge chord-extension from 0.68b/2 to 0.85b/2 showing effects of a dive brake.

[redacted]

 [redacted]

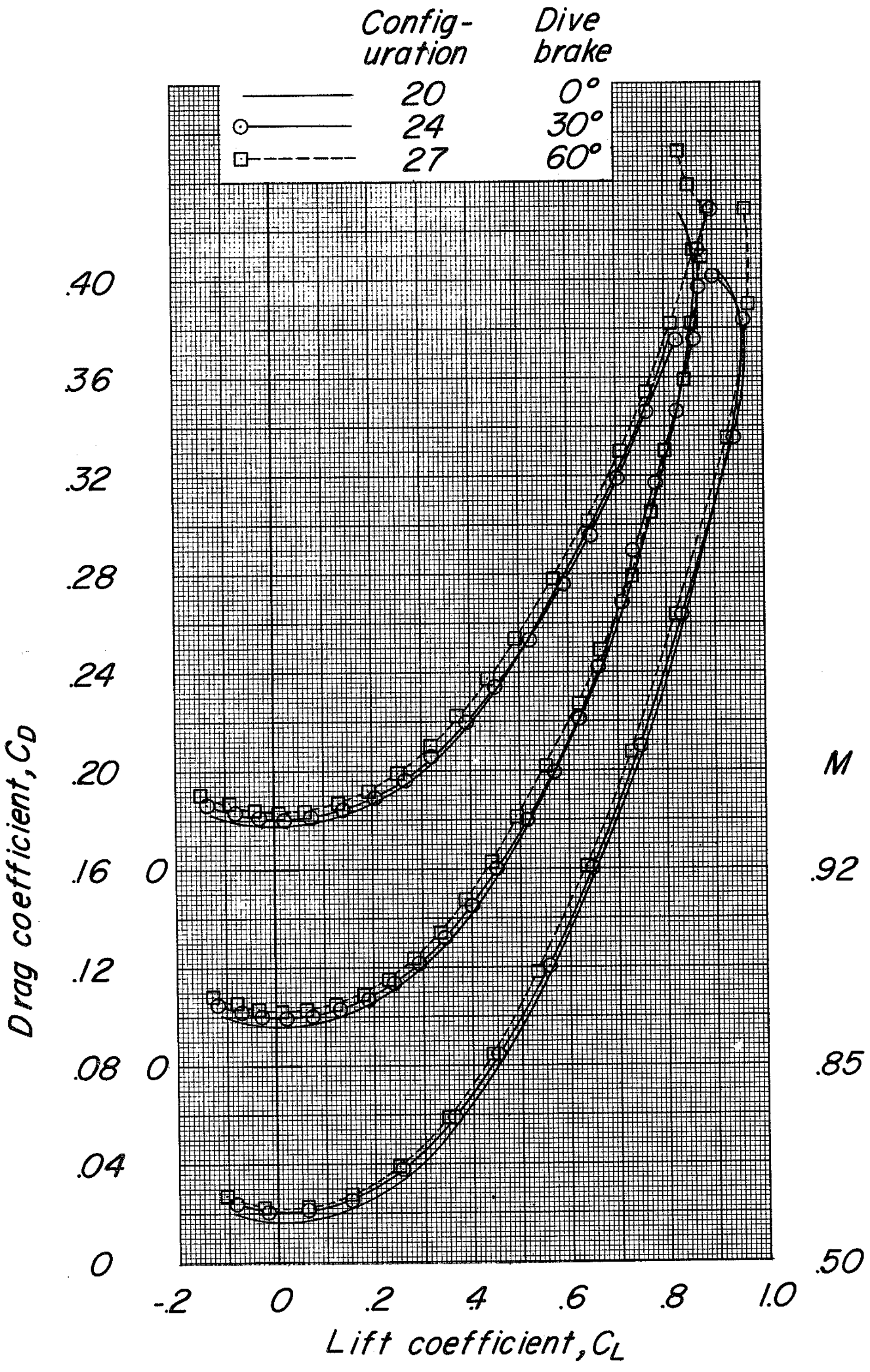

(b) Variation of C_D with C_L.

Figure 25.- Continued.

[redacted]

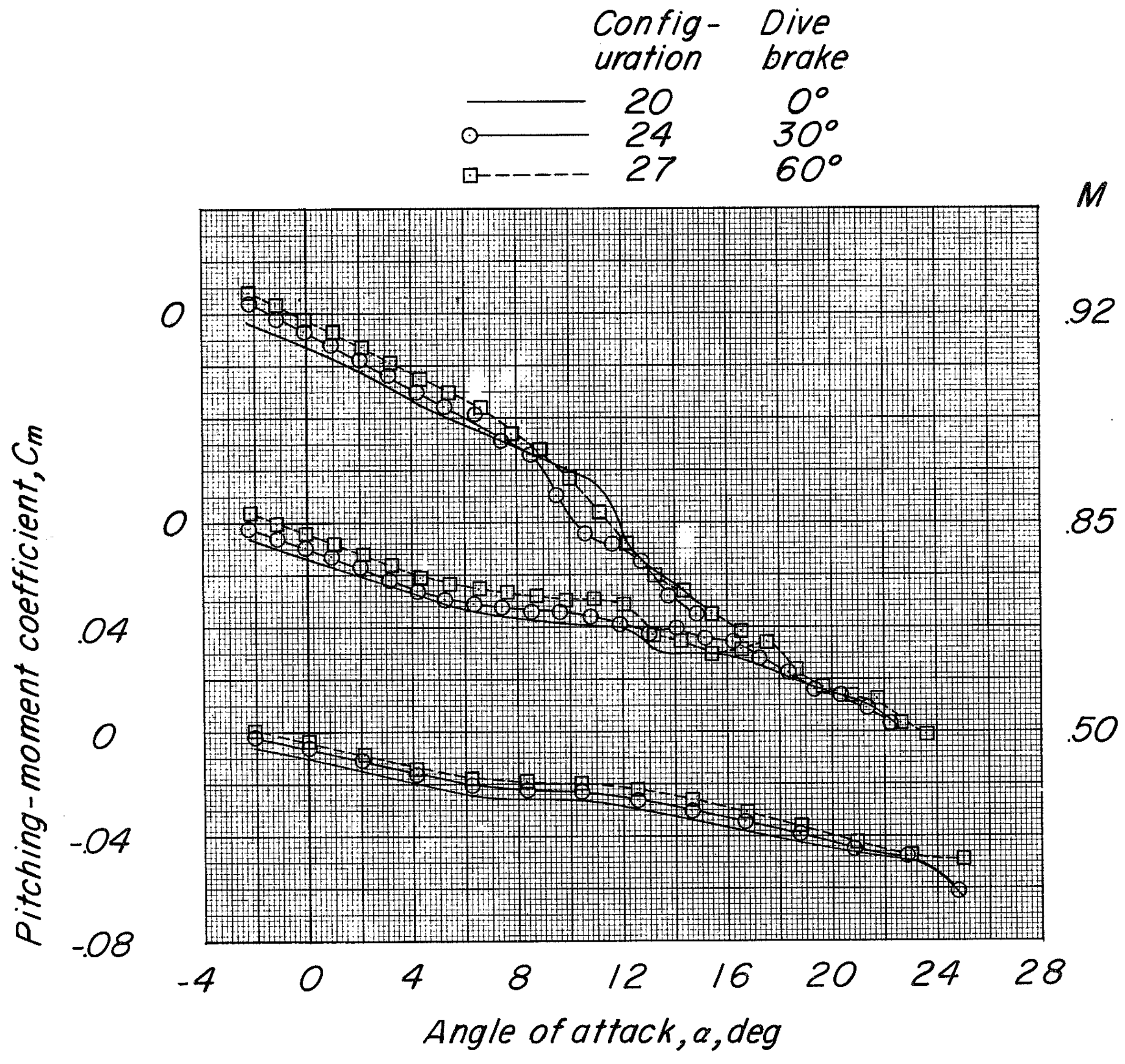

(c) Variation of C_m with α.

Figure 25.- Continued.

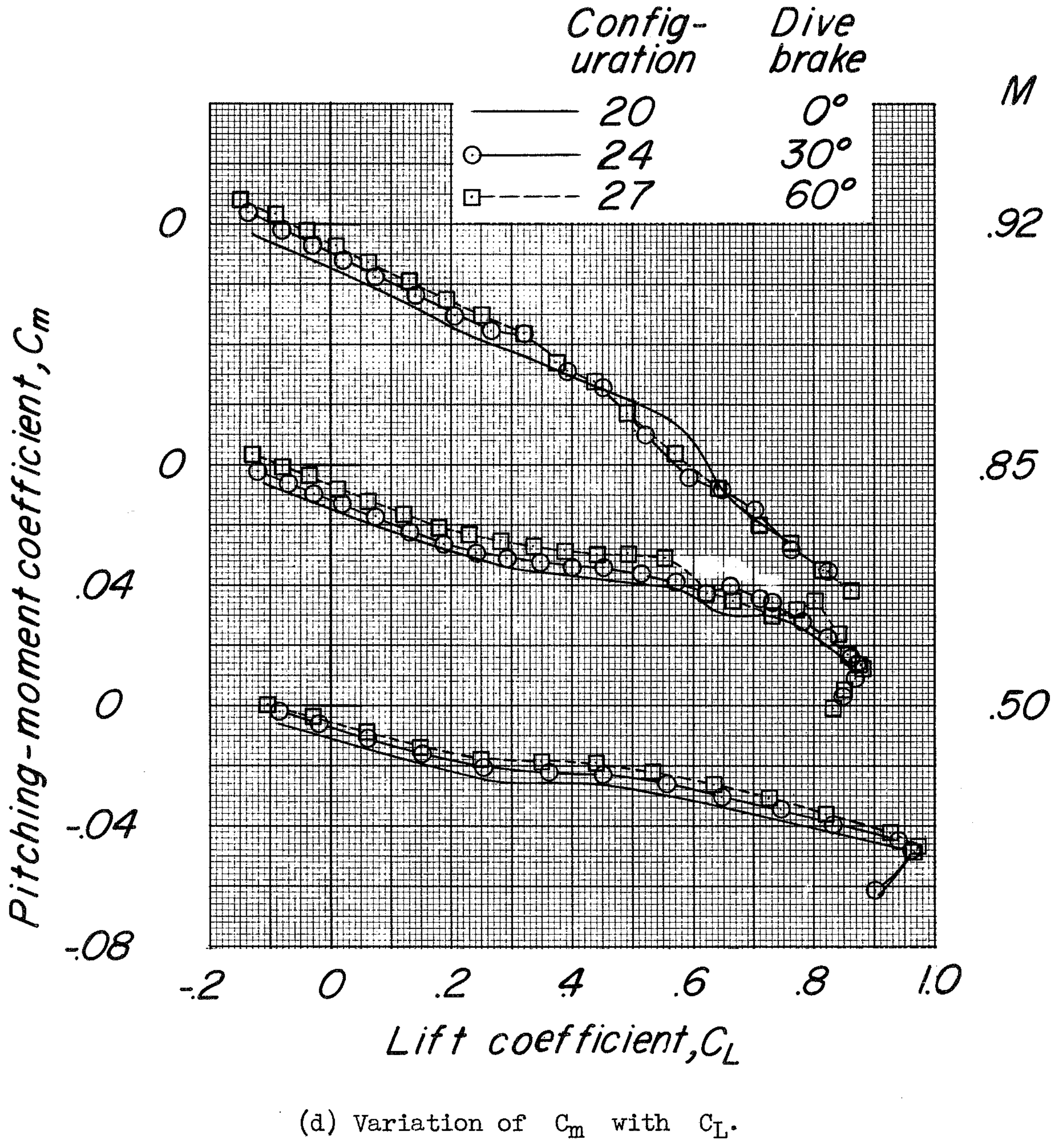

(d) Variation of C_m with C_L.

Figure 25.- Concluded.

 [redacted]

	Configuration	Fuselage spoiler	Fuselage fence	Height inches	Distance from duct exit, inches
⊙	20	None	None	—	—
⊡	28	Upper	↓	1/4	8.6
◇	29	↓	↓	↓	3.25
△	30	↓	↓	1/8	↓
◿	31	Lower	↓	↓	2.5
◺	32	(Fuselage faired at aft end to sting exit)			
◚	33	None	Upper	1/4	0
◈	34	↓	↓	↓	3.25

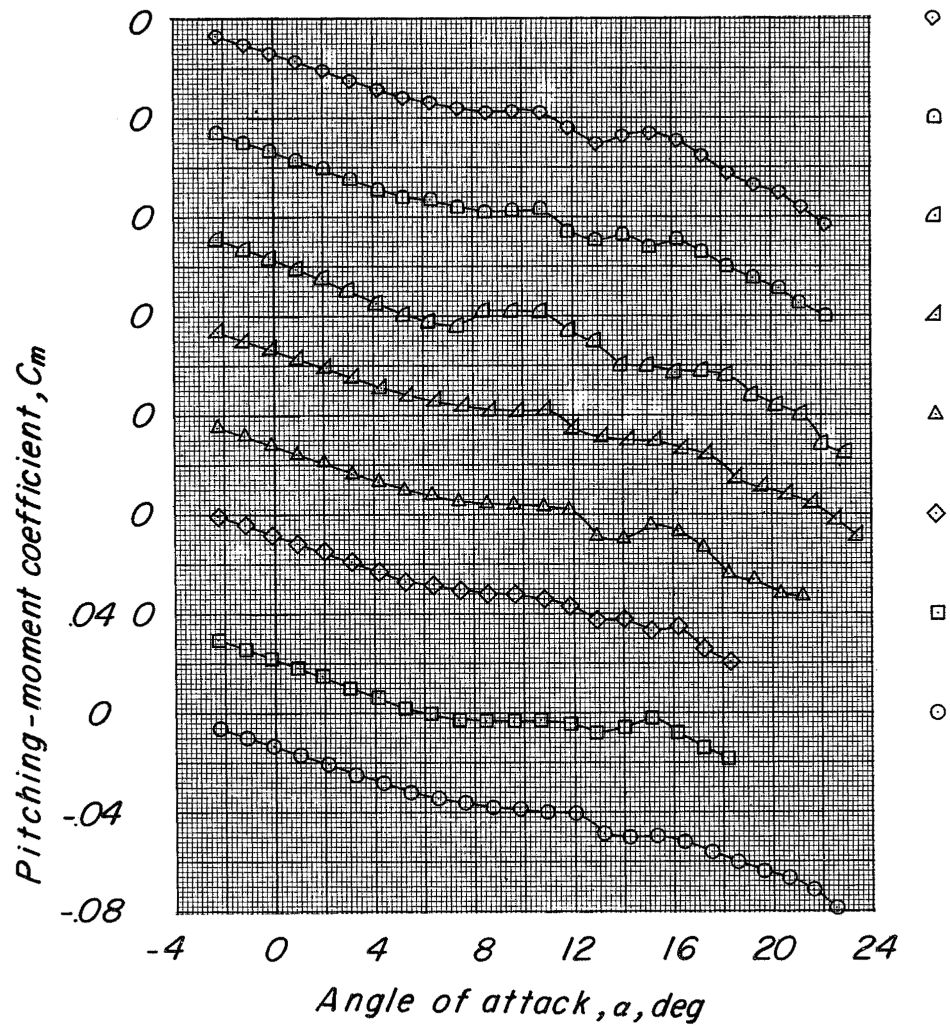

(a) Variation of C_m with α.

Figure 26.- Pitching-moment characteristics of configuration BCWV, $\delta_e = 0^{\circ}$, $\delta_r = 0^{\circ}$ showing effects of a number of fuselage spoilers and fences at a constant Mach number of 0.85. (Note that notch 1 and leading-edge chord-extension from 0.68b/2 to 0.85b/2 was a part of all configurations except number 32.)

[redacted]

 [redacted]

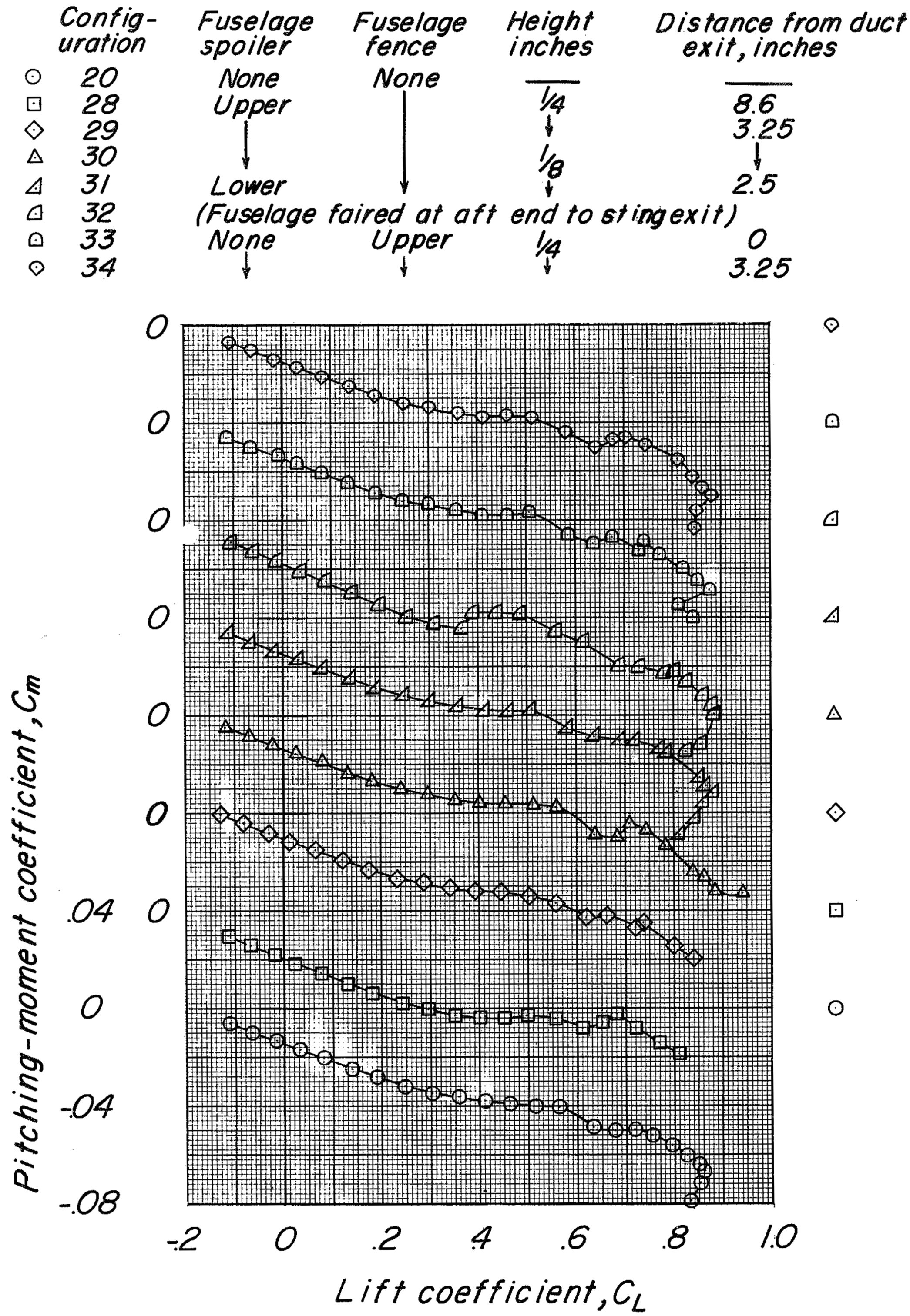

(b) Variation of C_m with C_L.

Figure 26.- Concluded.

 [redacted]

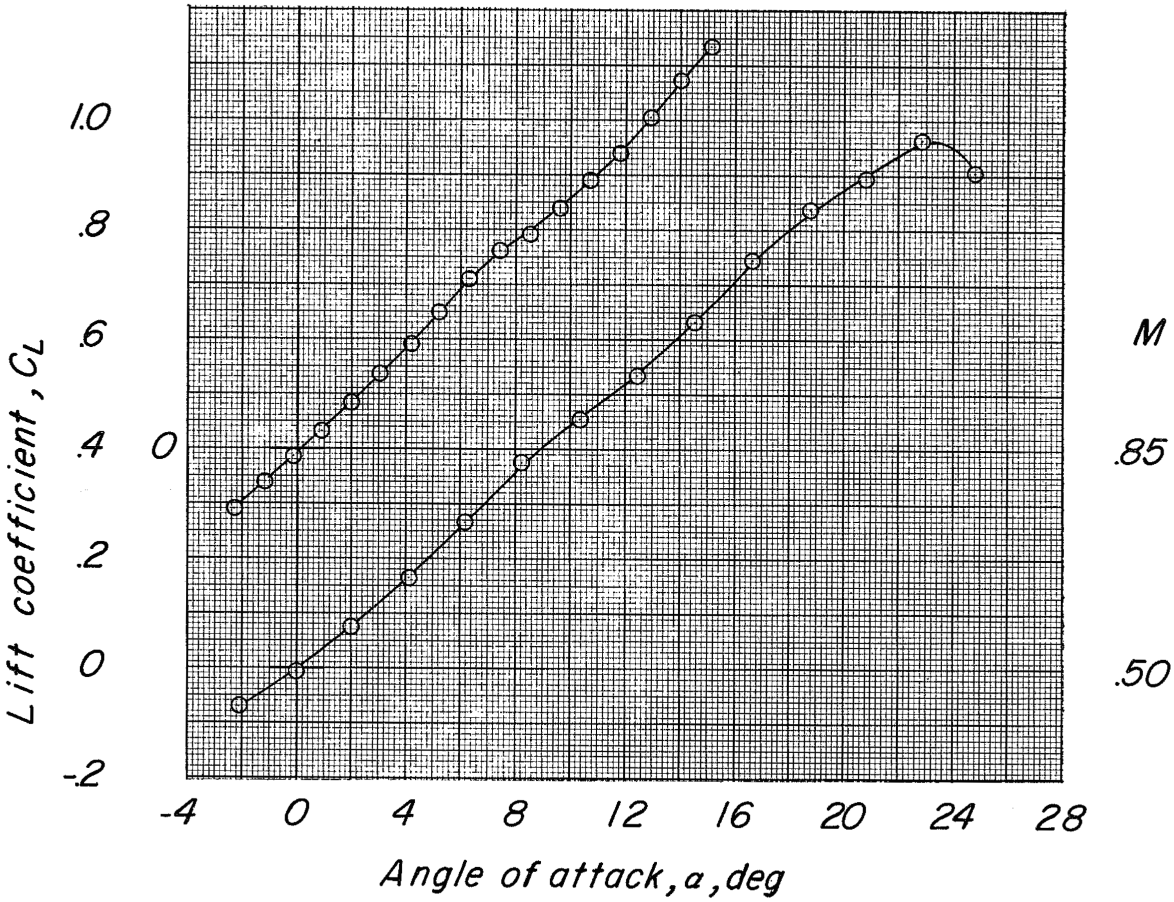

(a) Variation of C_L with α.

Figure 27.- Basic longitudinal characteristics of configuration BCWV, $\delta_e = 0^o$, $\delta_r = 0^o$ with transition strip at 0.05$\bar{c}$ along the wing leading edge (designated as configuration 35).

[redacted]

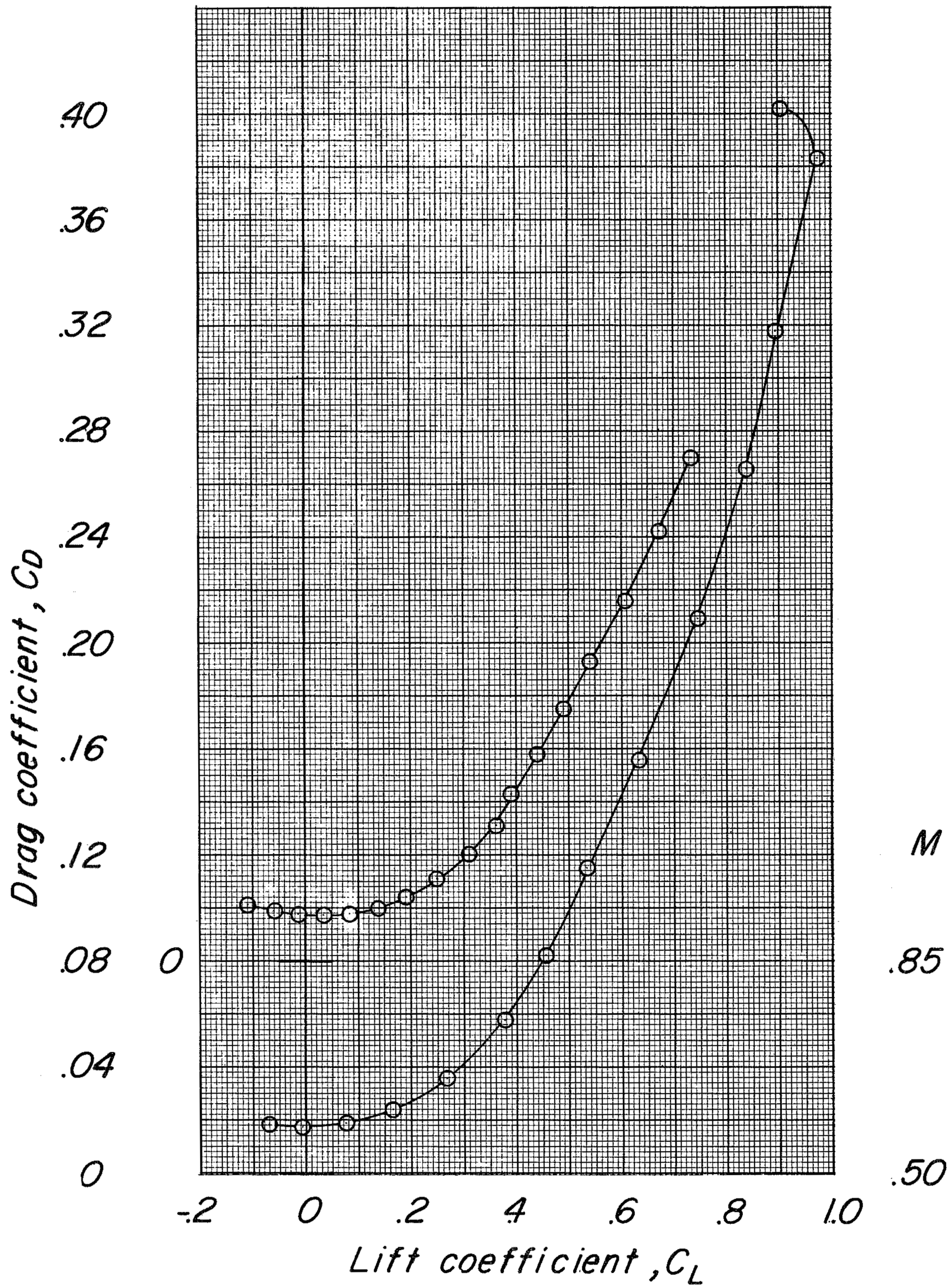

(b) Variation of C_D with C_L.

Figure 27.- Continued.

[redacted]

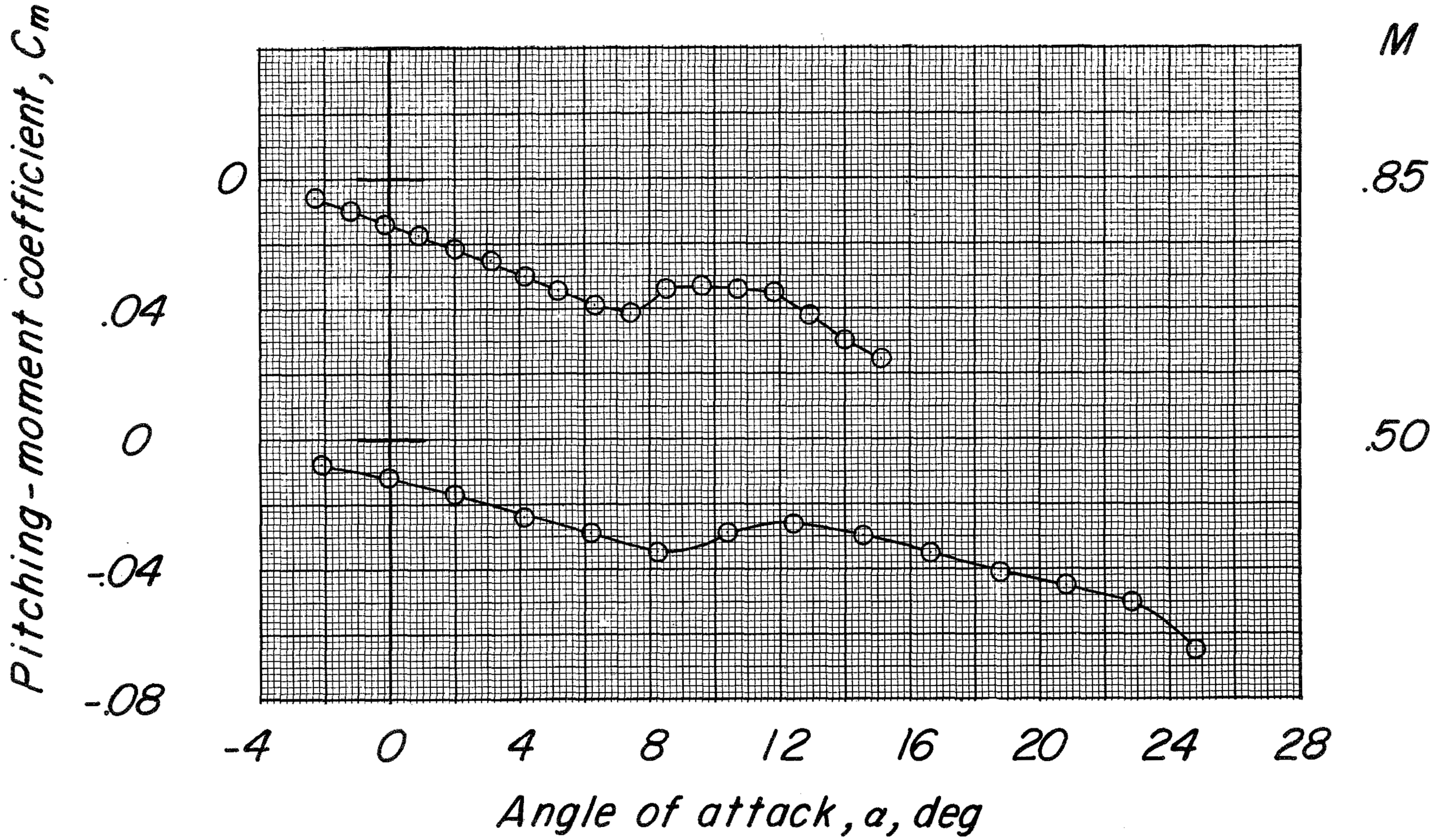

[redacted]

(c) Variation of C_m with α.

Figure 27.- Continued.

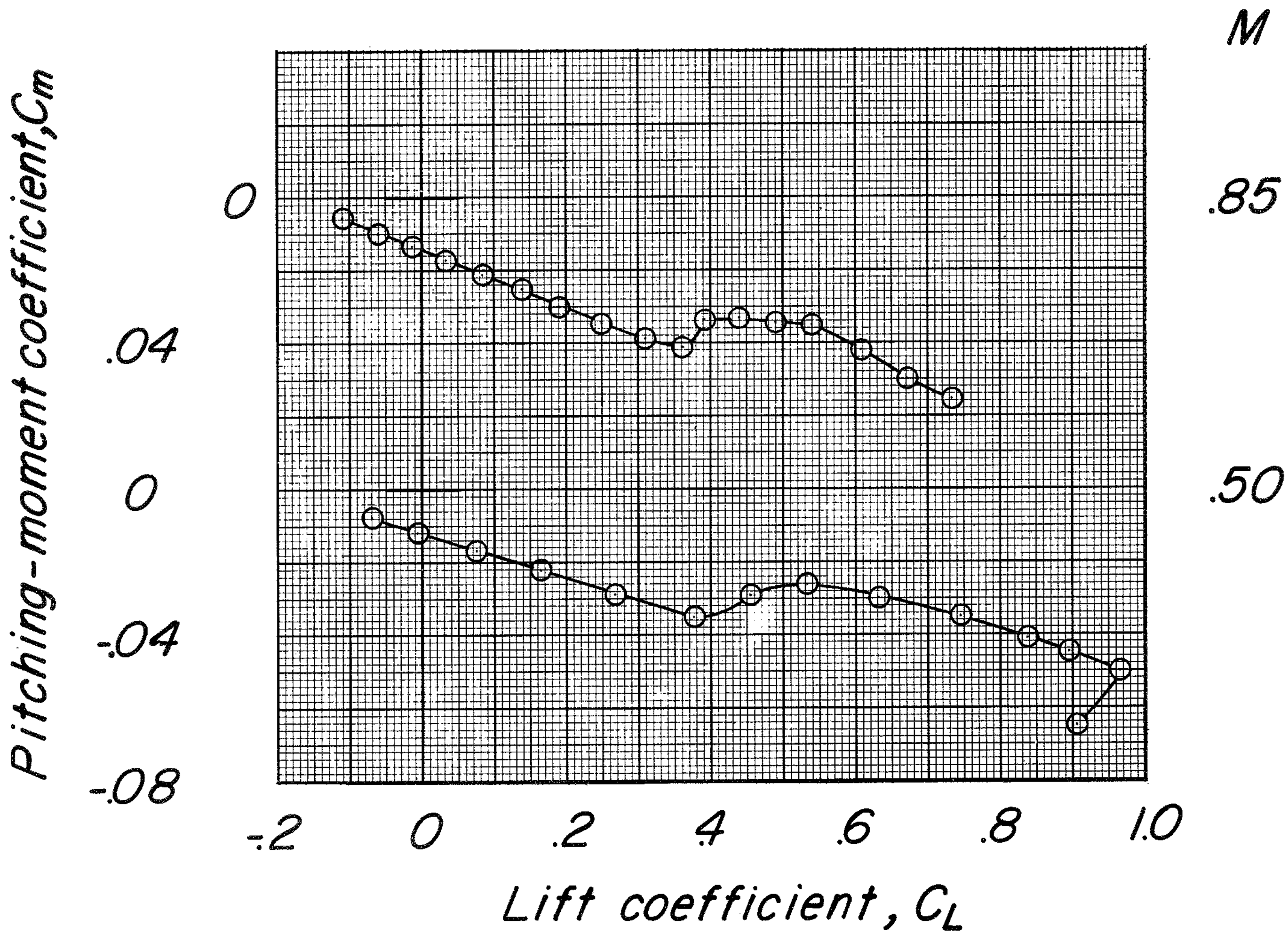

(d) Variation of C_m with C_L.

Figure 27.- Concluded.

[redacted]

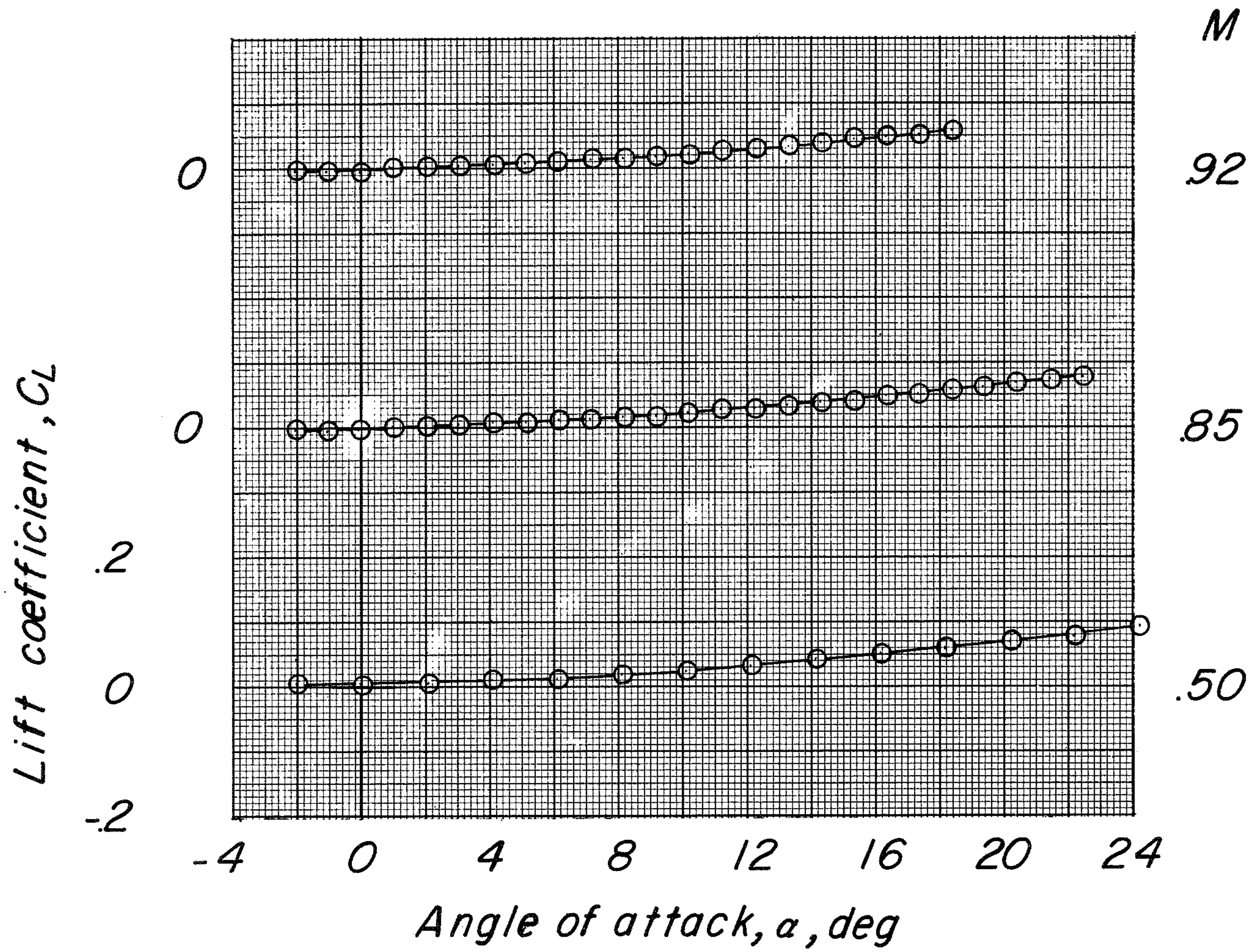

(a) Variation of C_L with α.

Figure 28.- Basic longitudinal characteristics of configuration BC (designated as configuration 36).

[redacted]

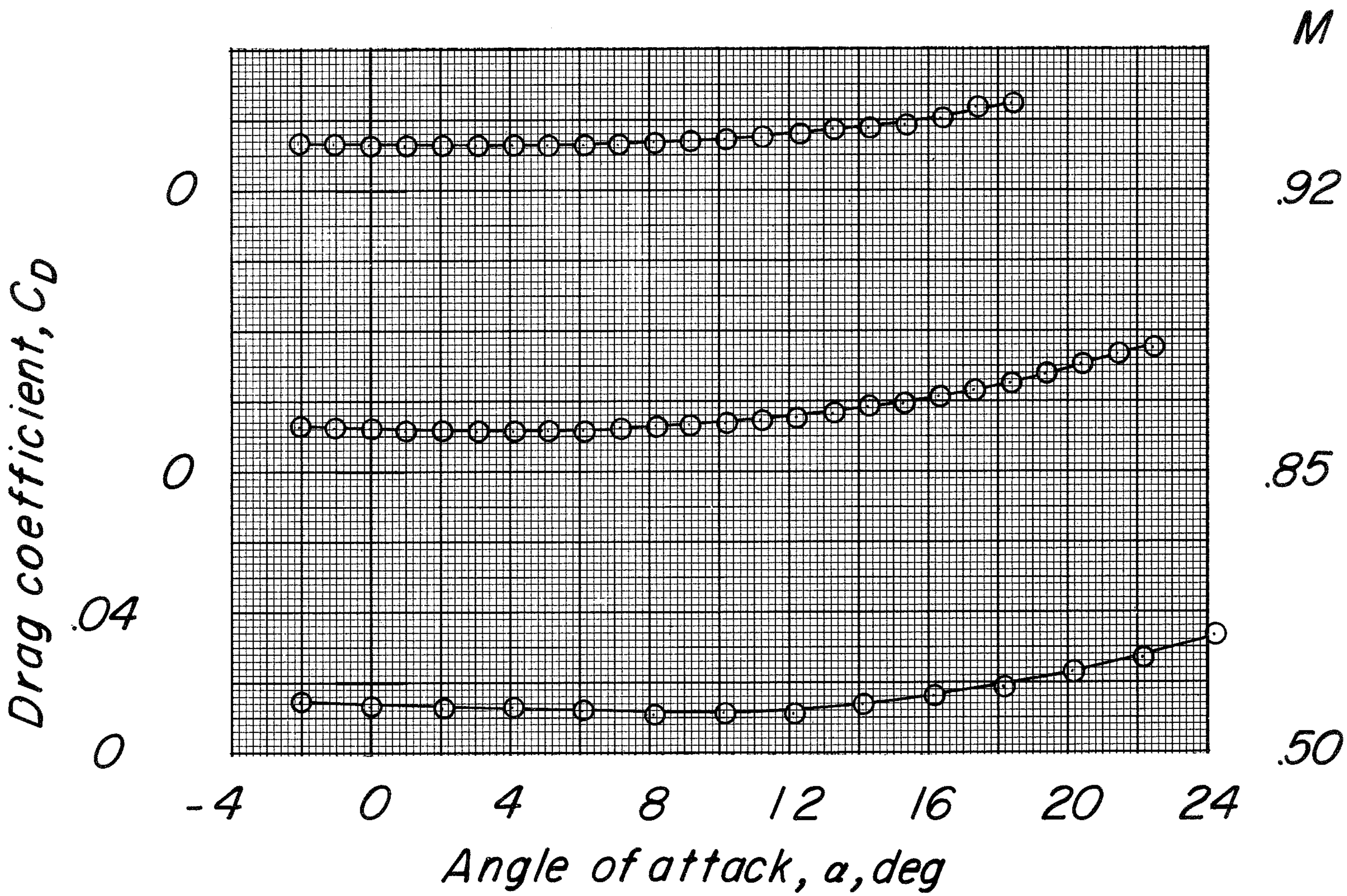

(b) Variation of C_D with α.

Figure 28.- Continued.

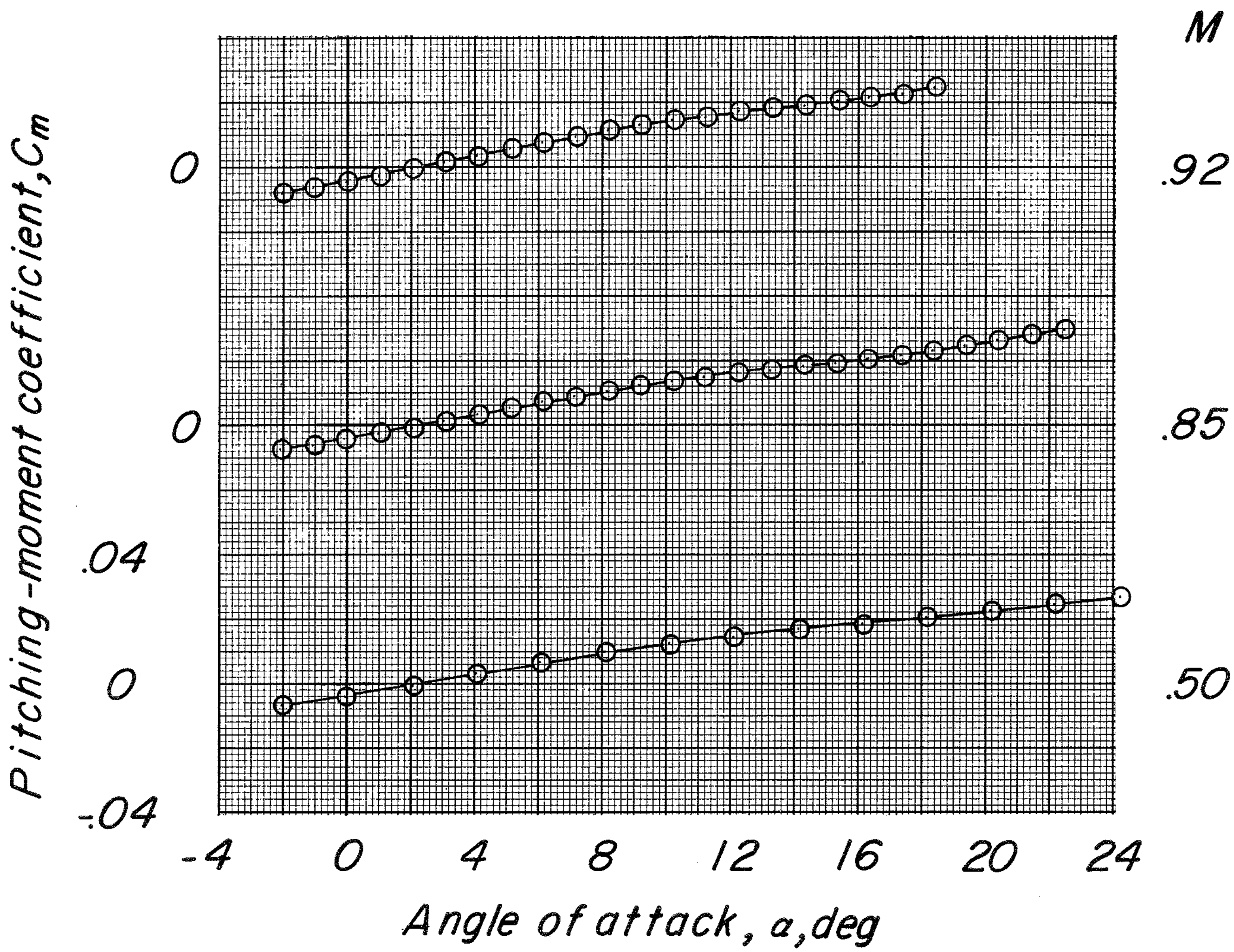

(c) Variation of C_m with α.

Figure 28.- Concluded.

[redacted]

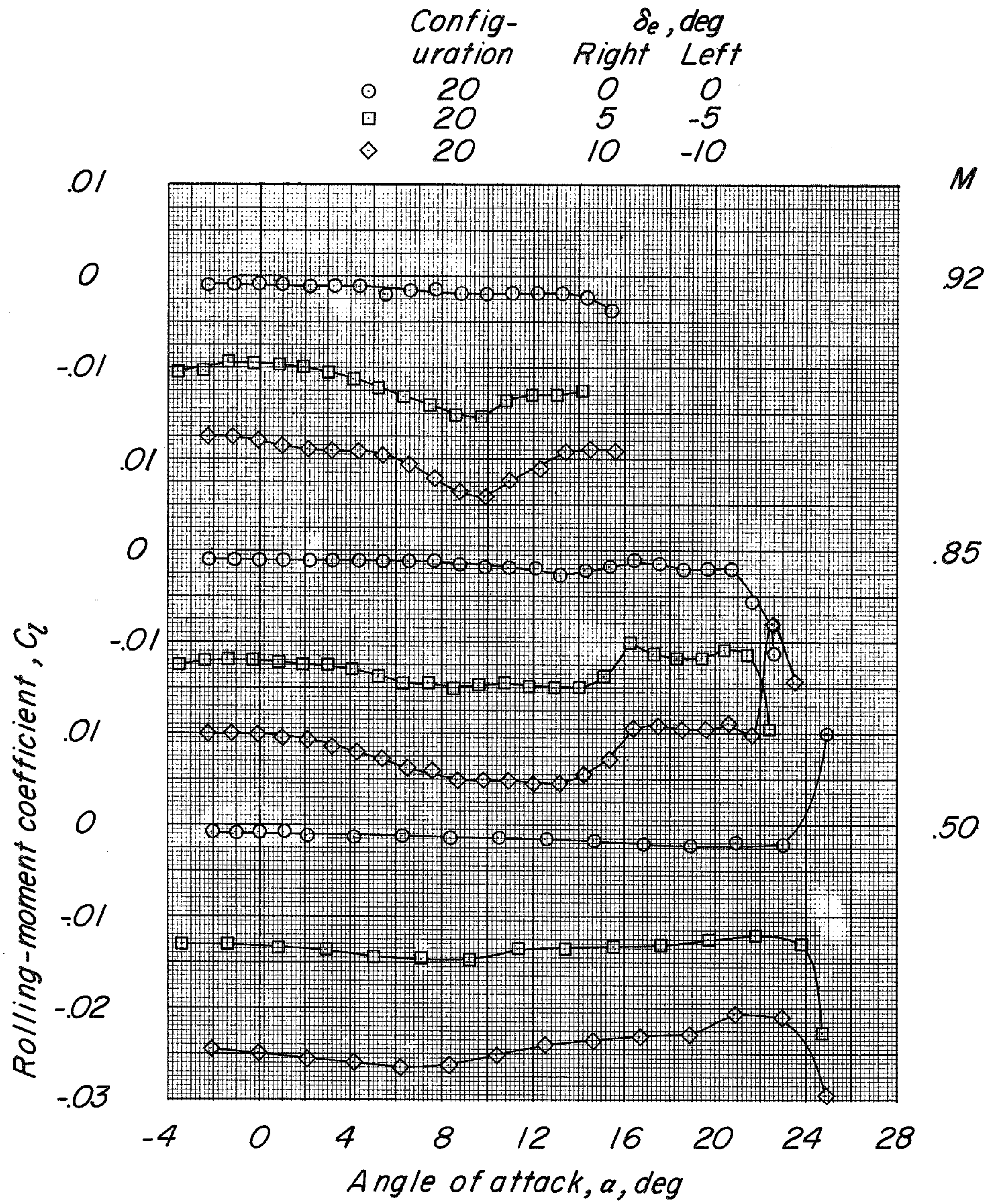

(a) Variation of C_l with α.

Figure 29.- Aerodynamic characteristics in pitch to determine lateral-control effectiveness of configuration $BCW_{N_1}V$, $\delta_r = 0^\circ$ with leading-edge chord-extension from 0.68b/2 to 0.85b/2.

[redacted]

[redacted]

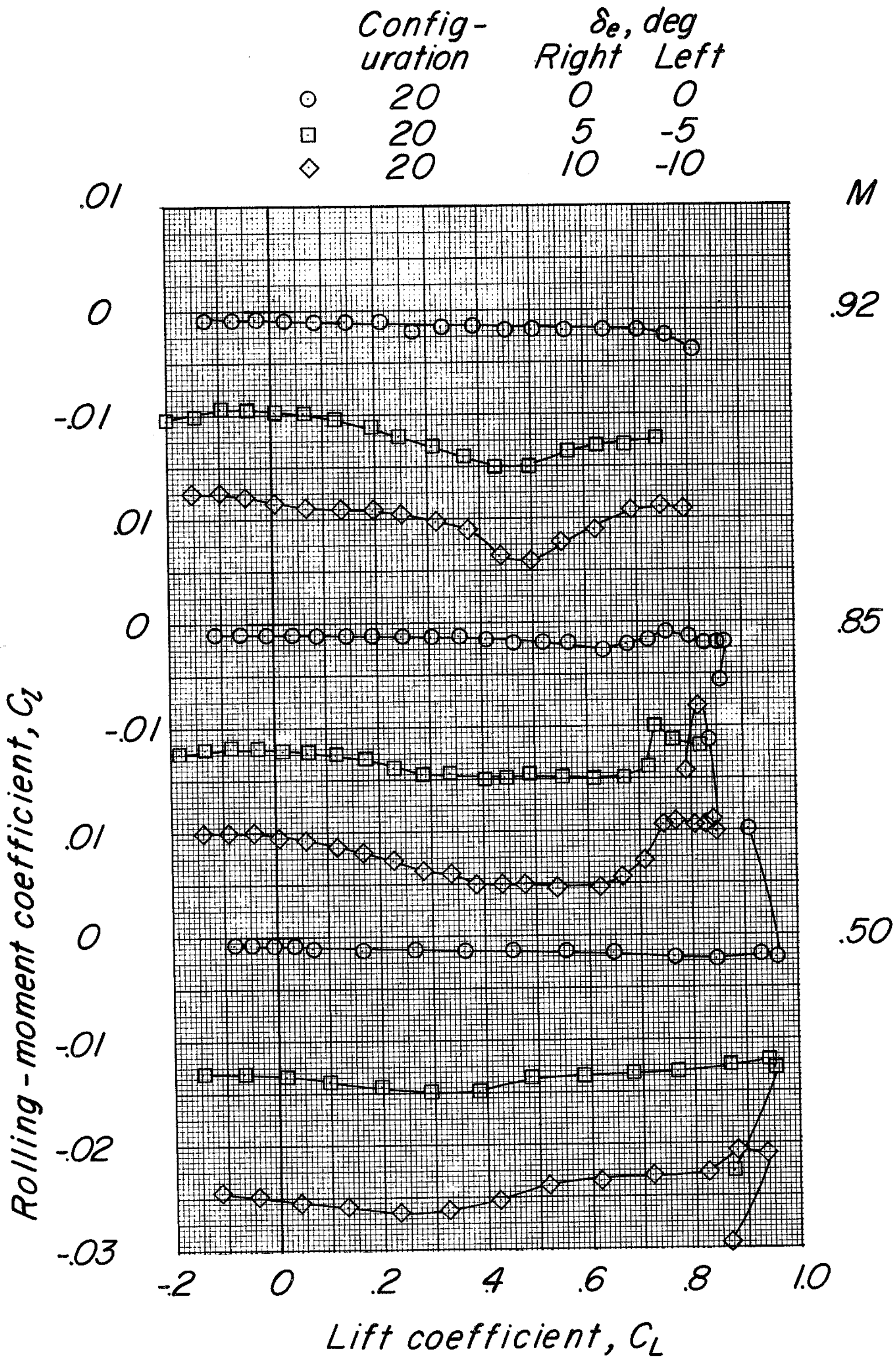

(b) Variation of C_l with C_L.

Figure 29.- Continued.

[redacted]

[redacted]

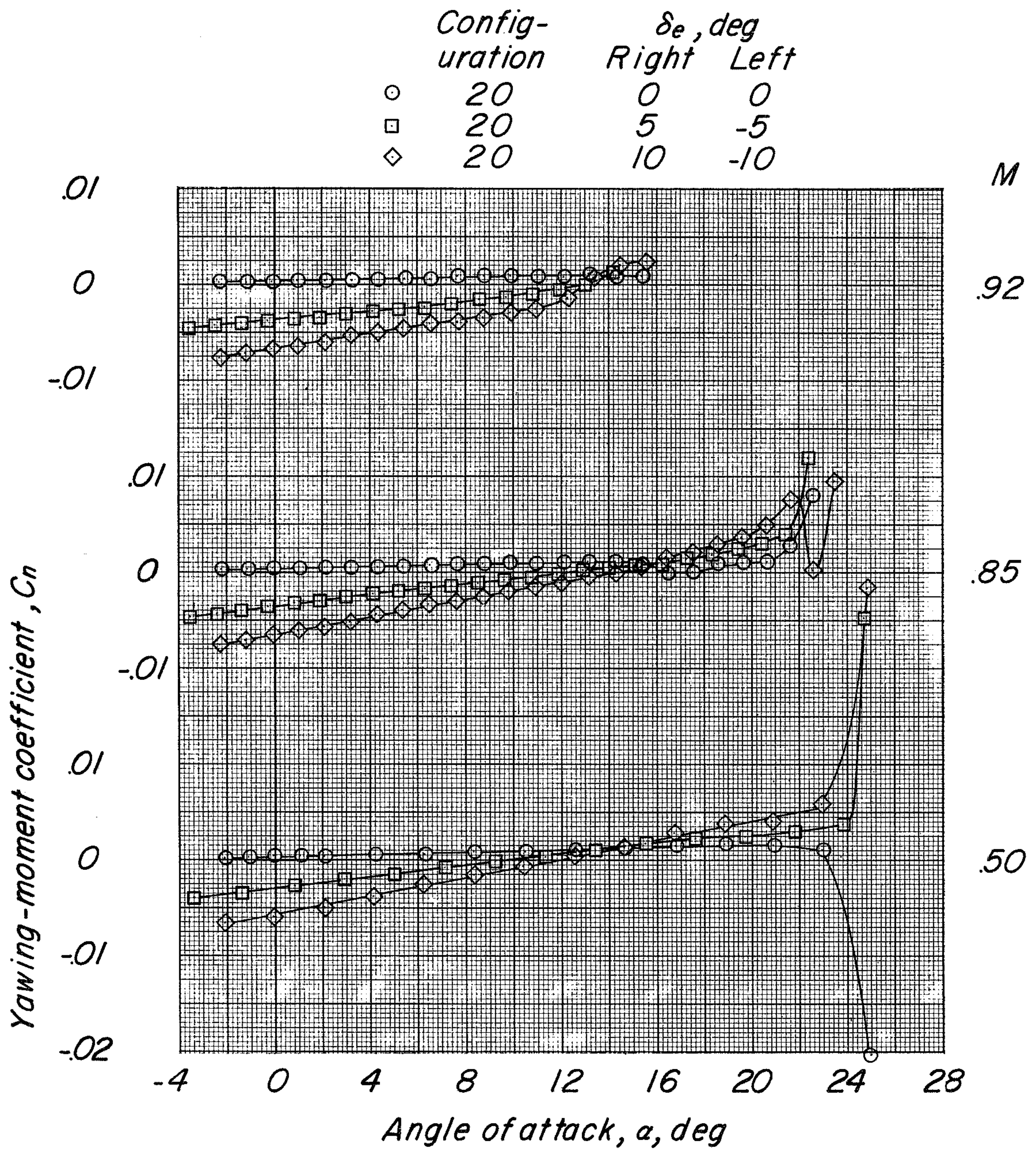

(c) Variation of C_n with α.

Figure 29.- Continued.

[redacted]

[redacted]

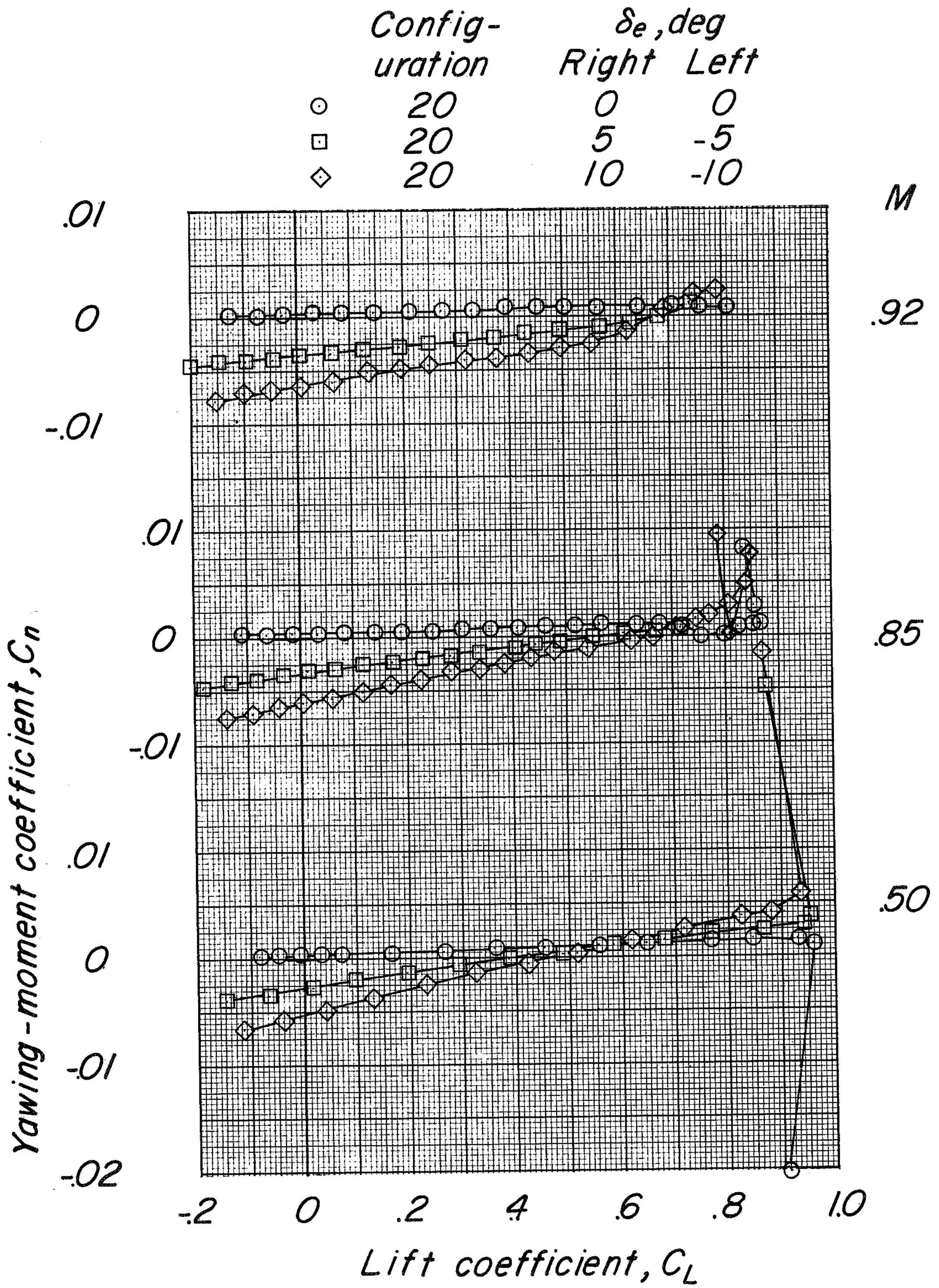

(d) Variation of C_n with C_L.

Figure 29.- Continued.

[redacted]

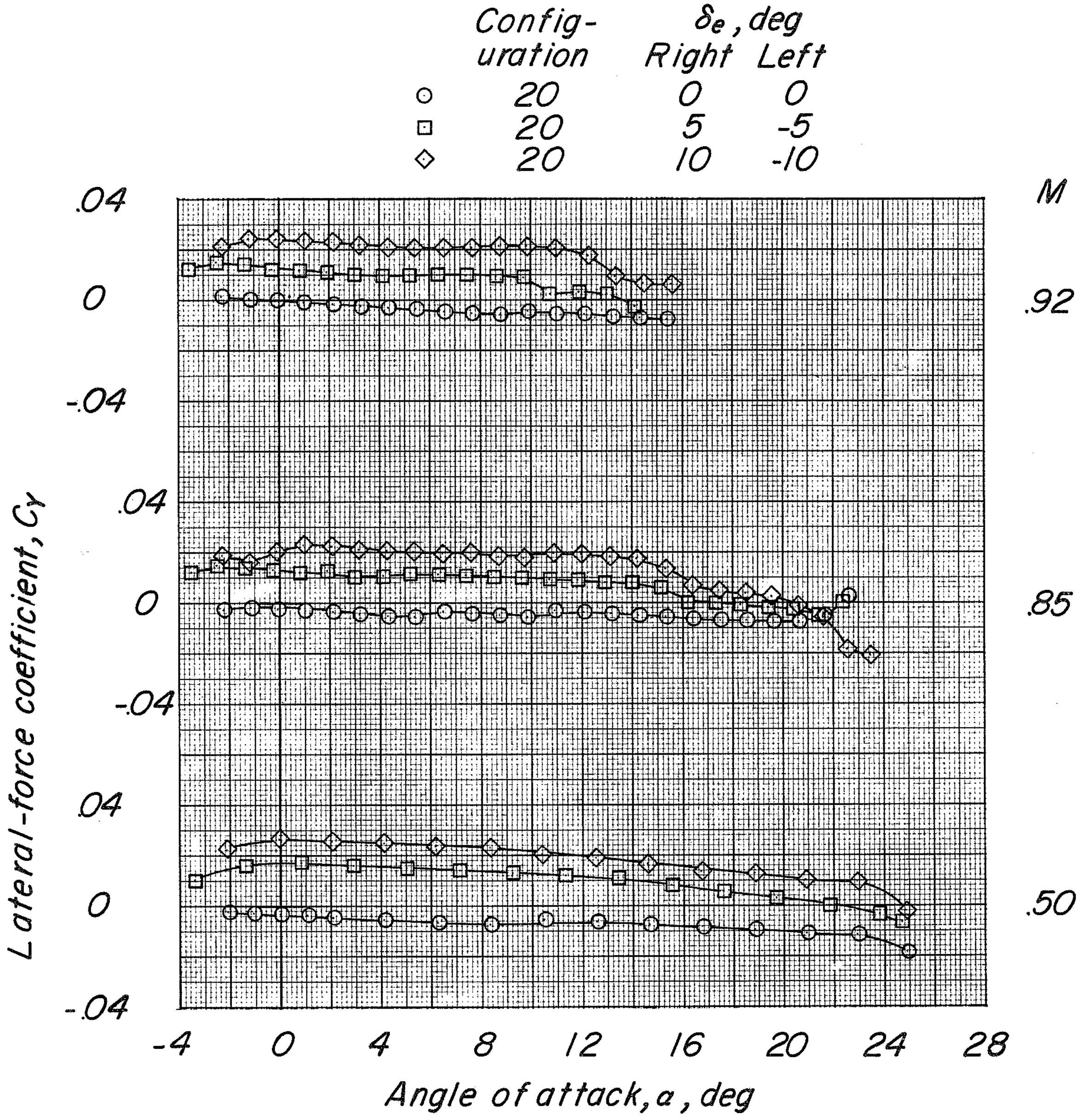

(e) Variation of C_Y with α.

Figure 29.- Continued.

 [redacted]

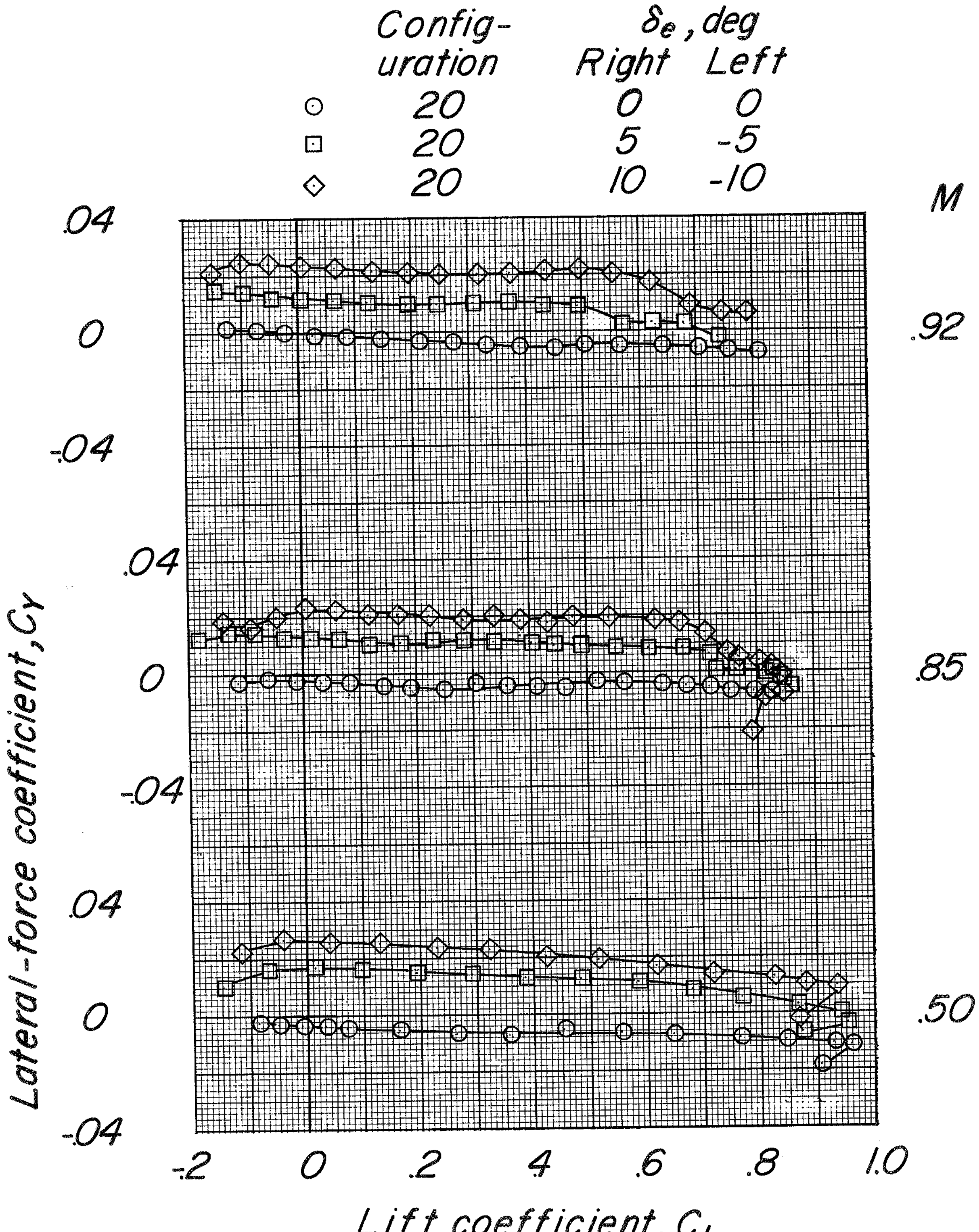

(f) Variation of C_Y with C_L.

Figure 29.- Concluded.

[redacted]

[redacted]

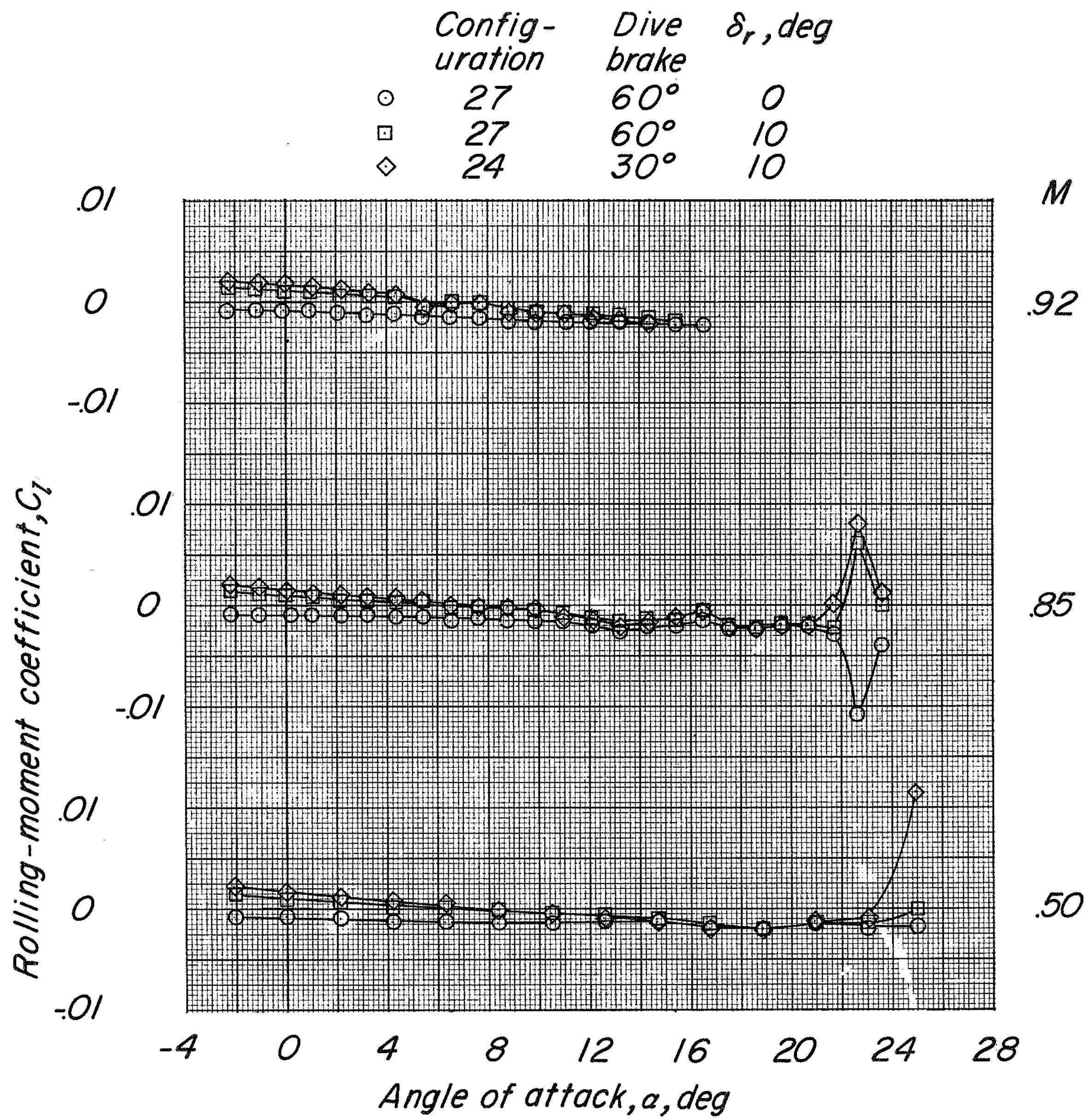

(a) Variation of C_l with α.

Figure 30.- Aerodynamic characteristics in pitch to determine directional-control effectiveness of configuration $BCW_{N_1}V$, $\delta_e = 0^o$ with leading-edge chord-extension from 0.68b/2 to 0.85b/2.

[redacted]

 [redacted]

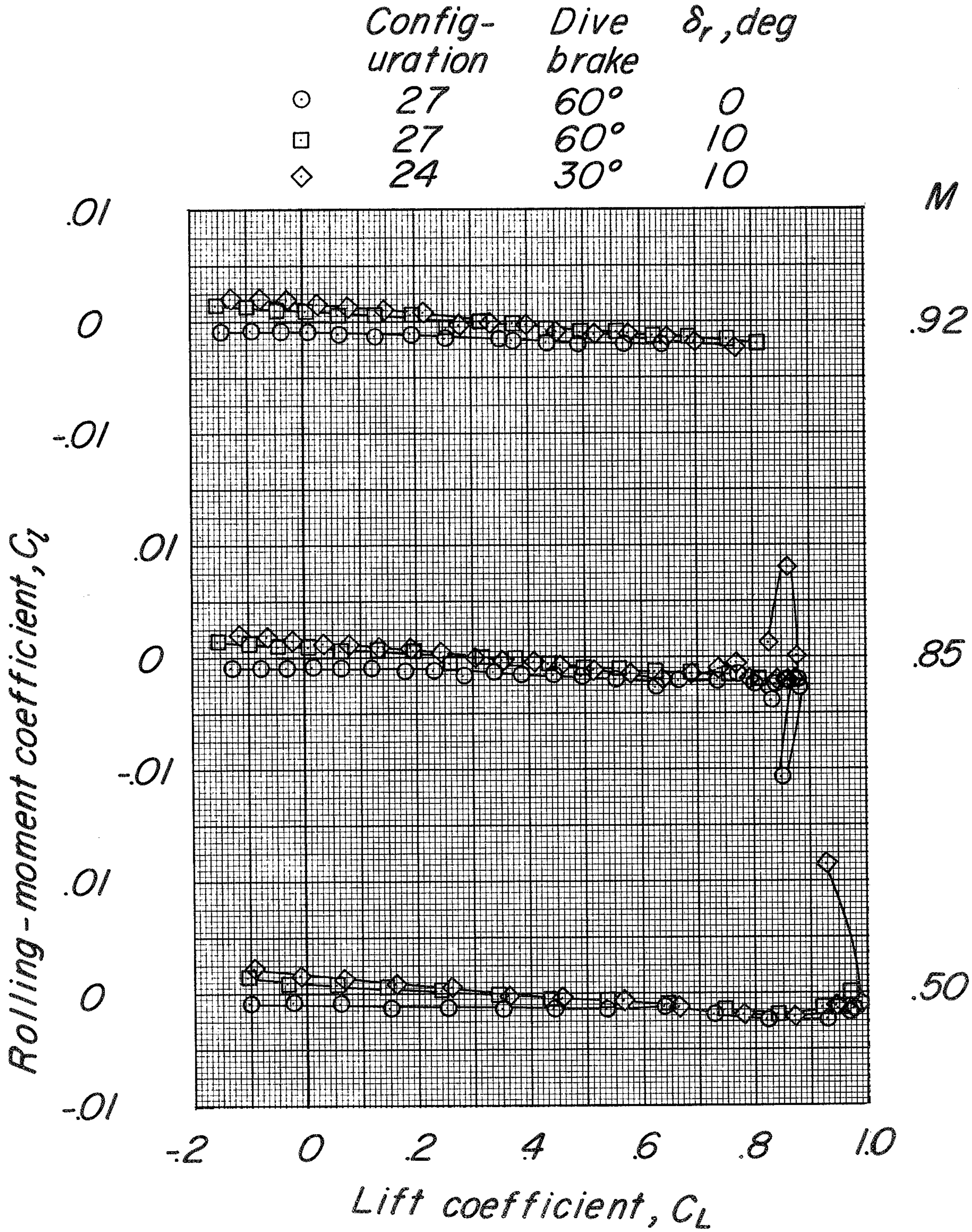

(b) Variation of C_l with C_L.

Figure 30.- Continued.

[redacted]

[redacted]

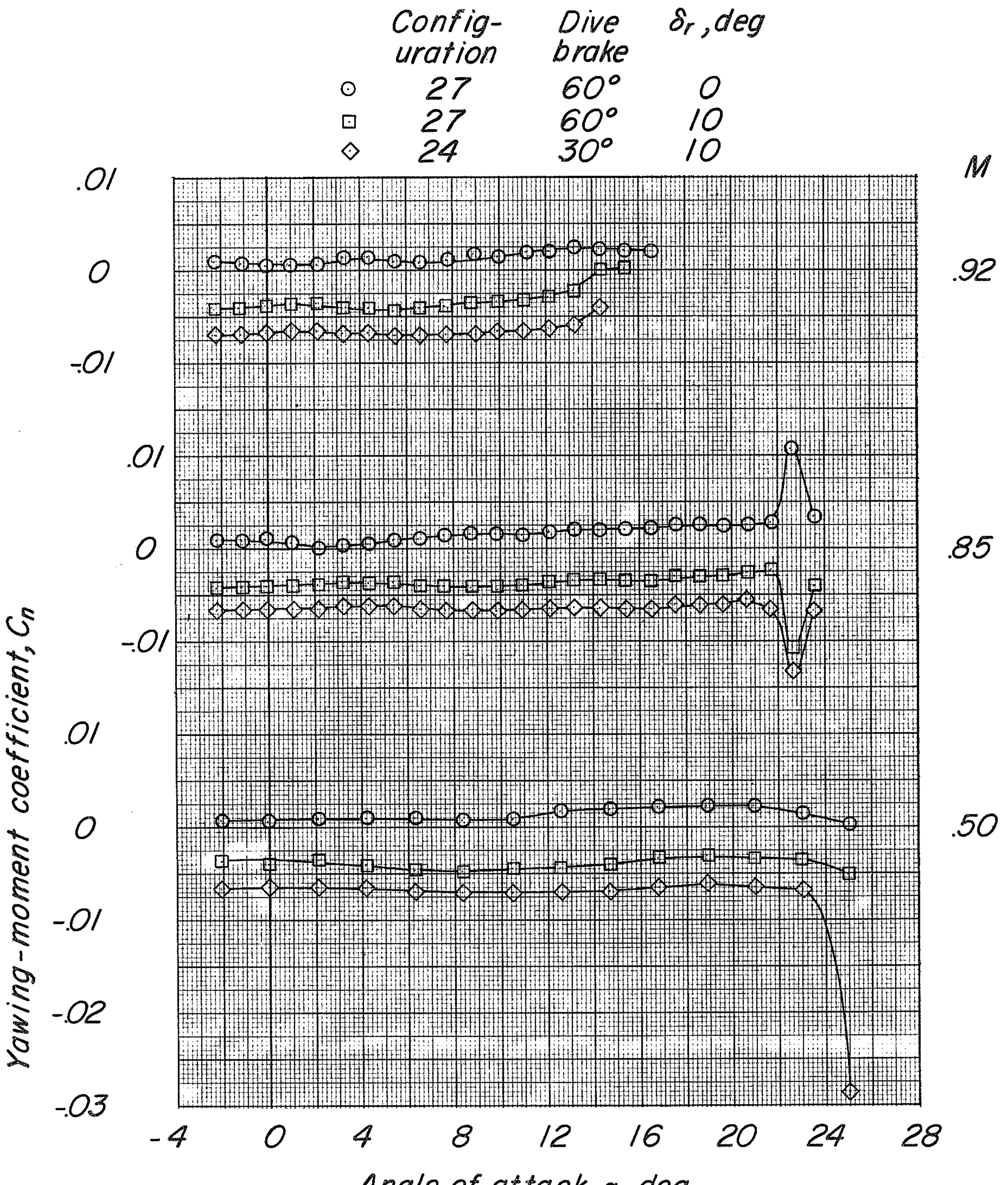

(c) Variation of C_n with α.

Figure 30.- Continued.

[redacted]

[redacted]

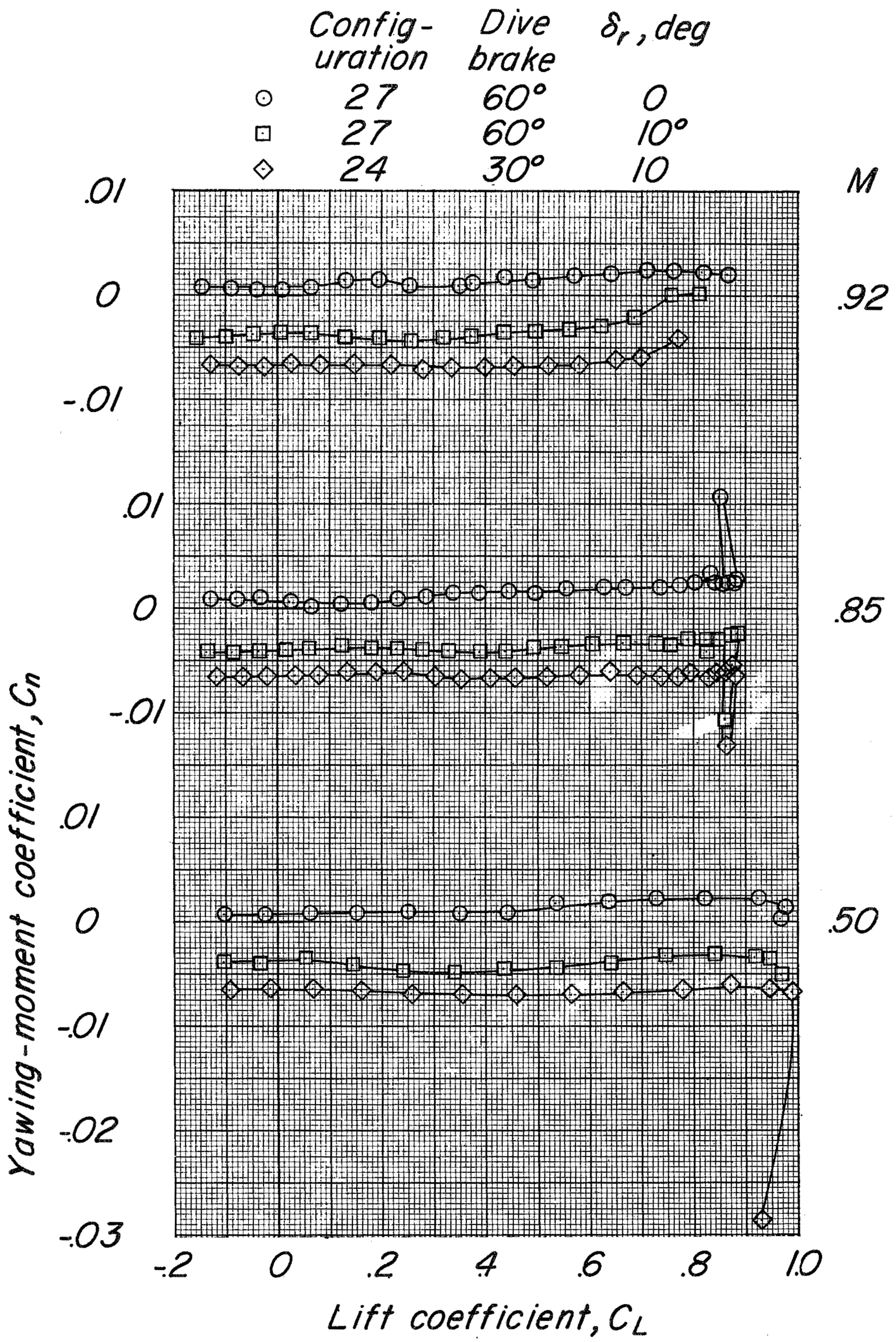

(d) Variation of C_n with C_L.

Figure 30.- Continued.

[redacted]

[redacted]

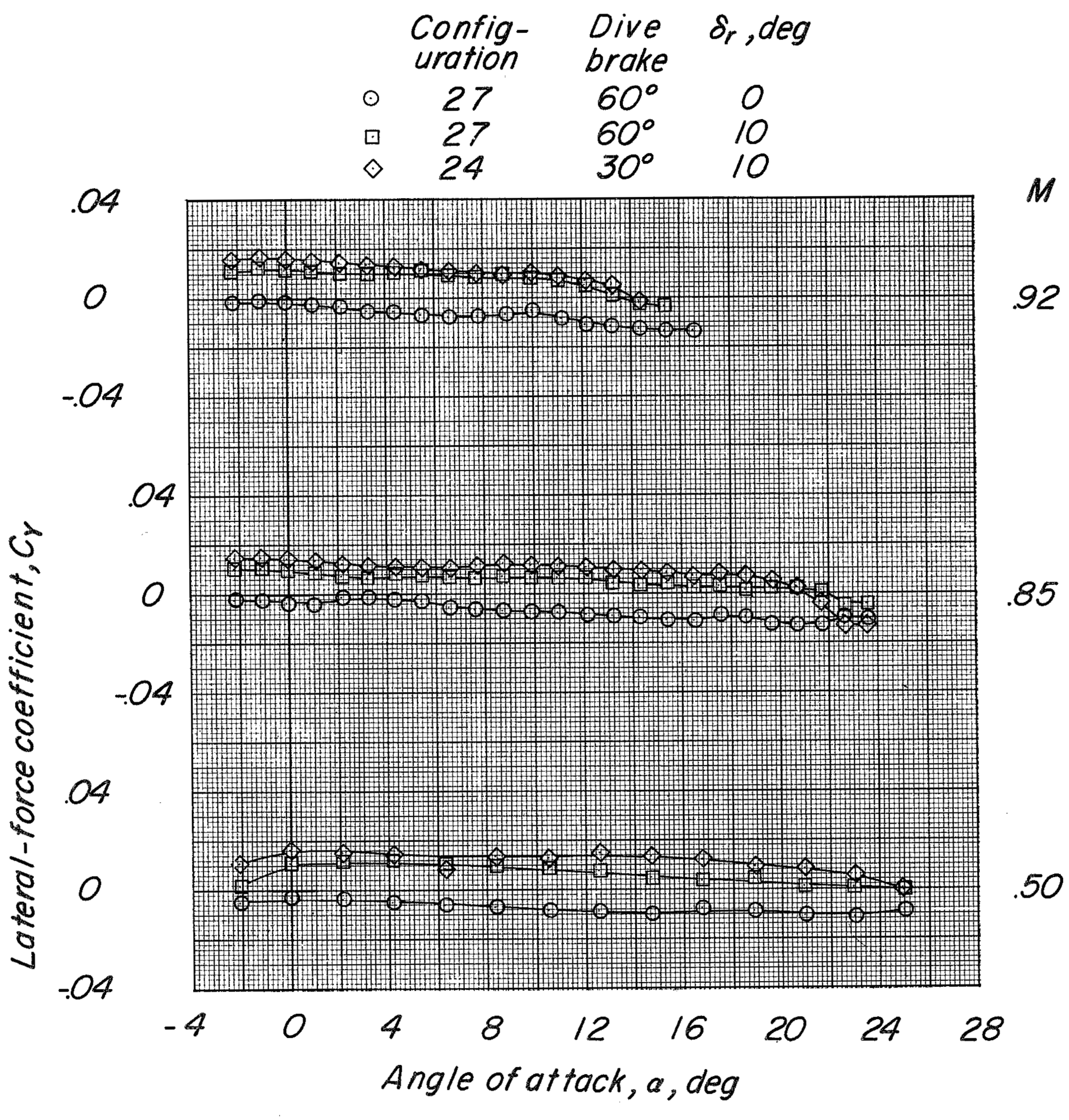

(e) Variation of C_Y with α.

Figure 30.- Continued.

[redacted]

 [redacted]

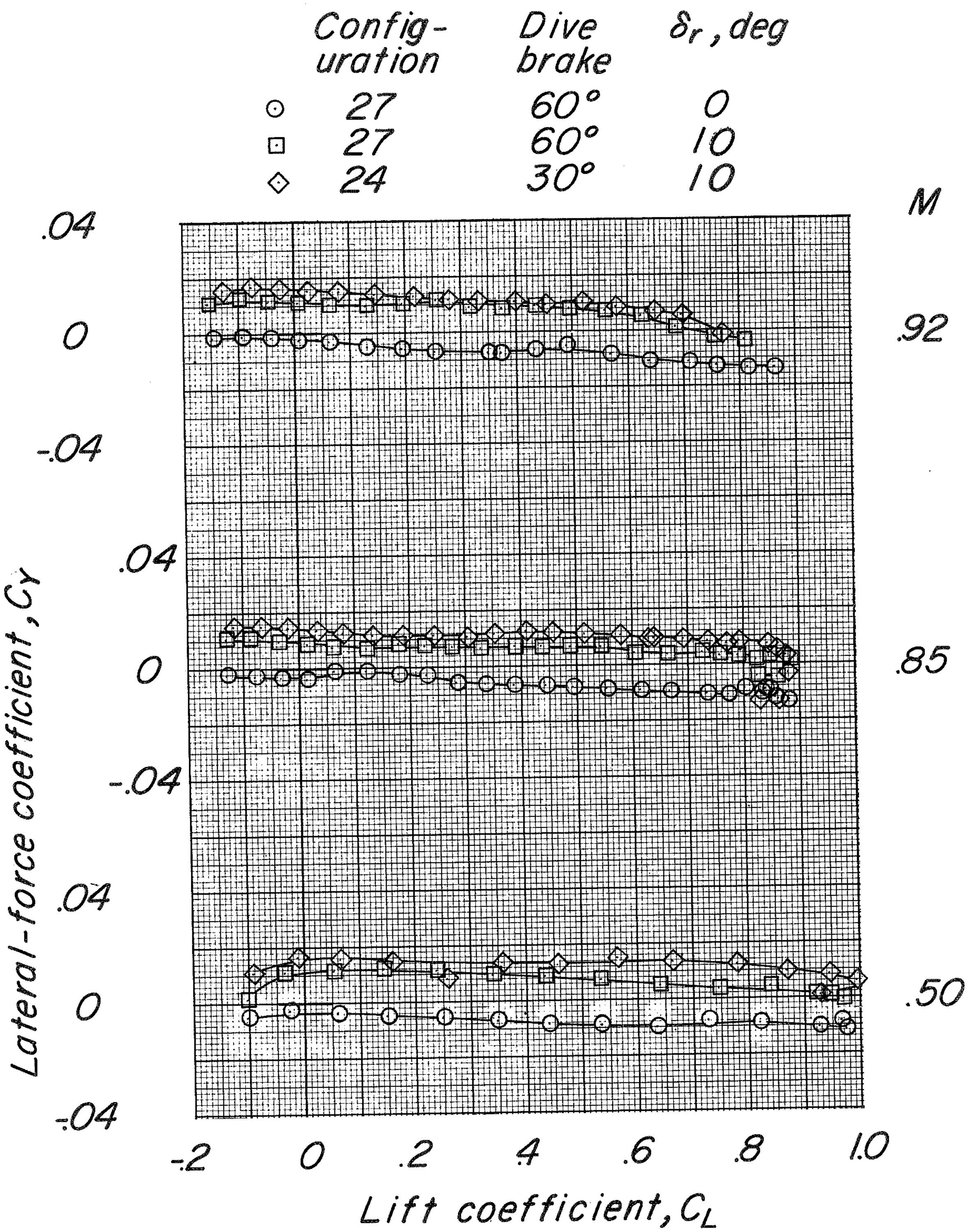

(f) Variation of C_Y with C_L.

Figure 30.- Concluded.

[redacted]

[redacted]

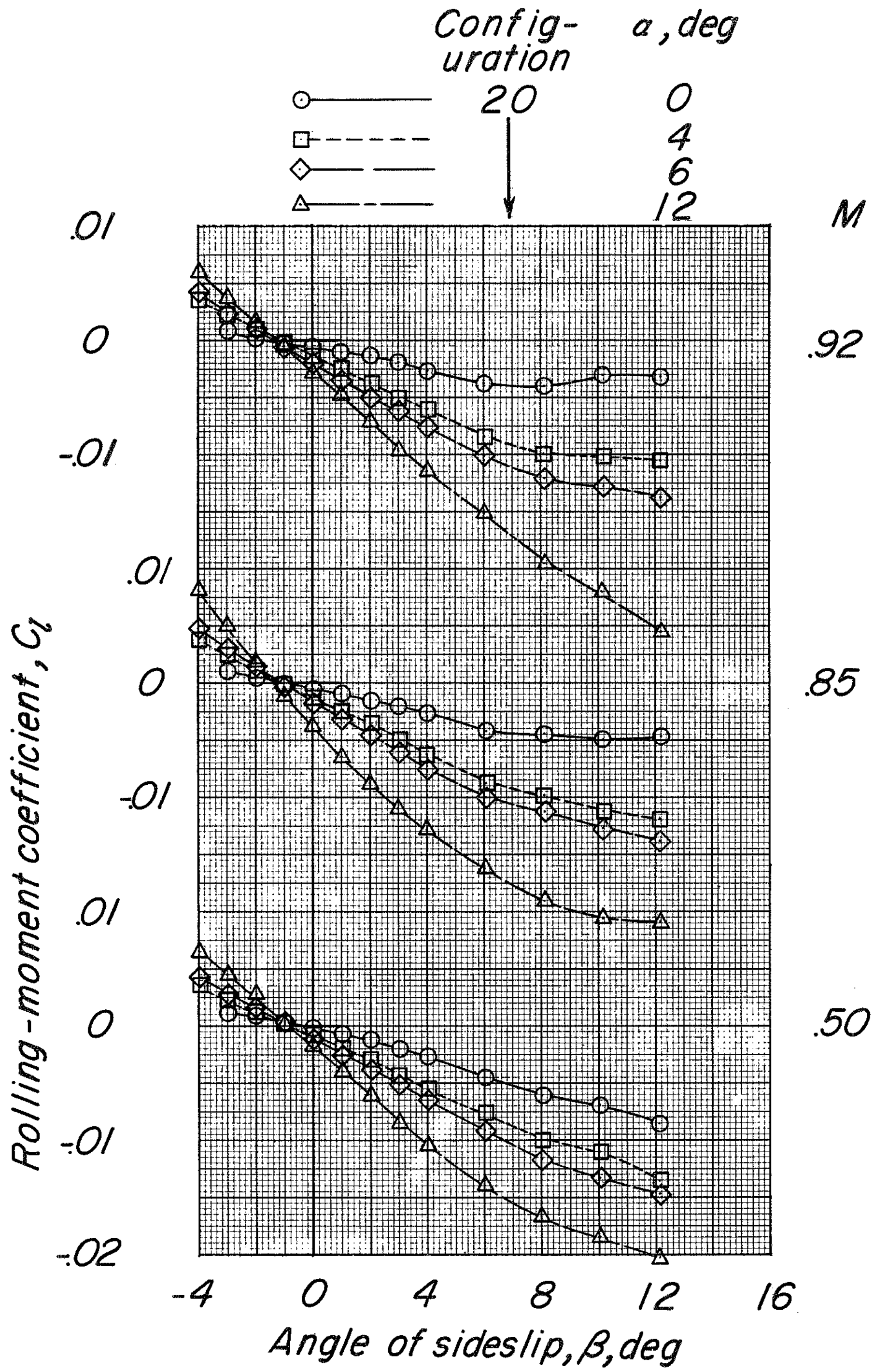

(a) Variation of C_l with β.

Figure 31.- Variation of lateral coefficients with angle of sideslip for configuration $BCW_{N_1}V$, $\delta_e = 0^{\circ}$, $\delta_r = 0^{\circ}$ with leading-edge chord-extension from 0.68b/2 to 0.85b/2.

[redacted]

[redacted]

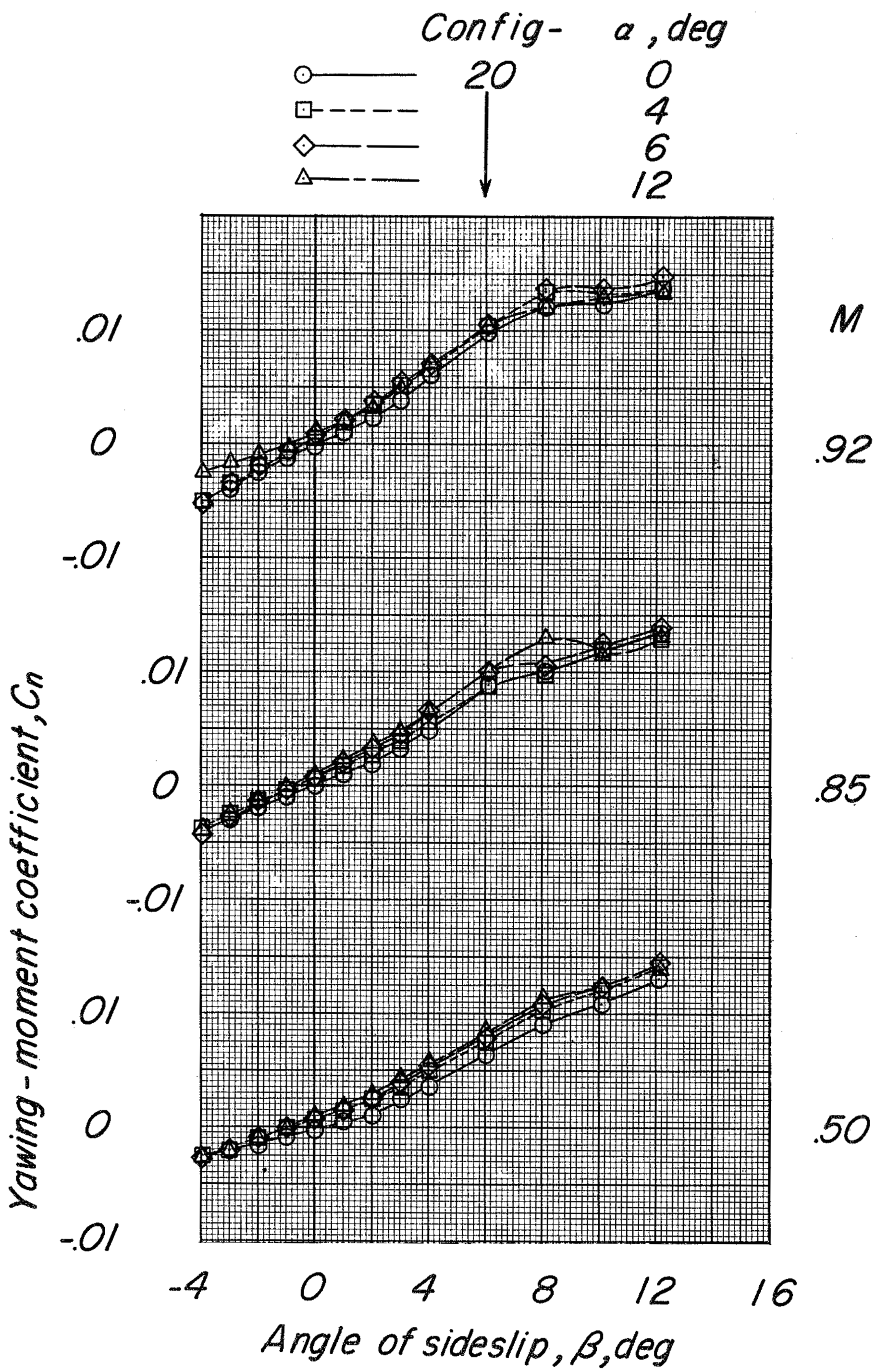

(b) Variation of C_n with β.

Figure 31.- Continued.

[redacted]

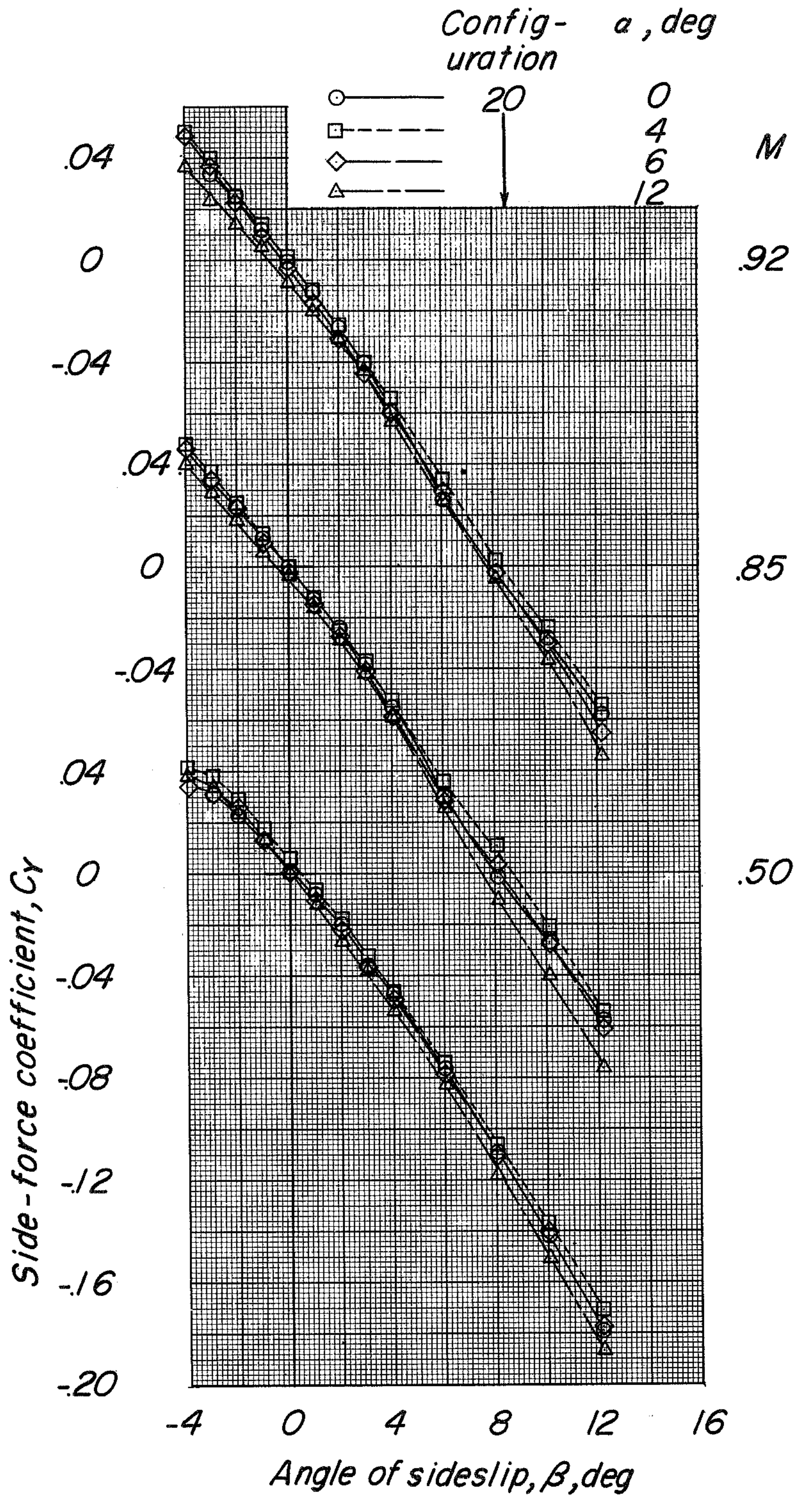

(c) Variation of C_Y with β.

Figure 31.- Concluded.

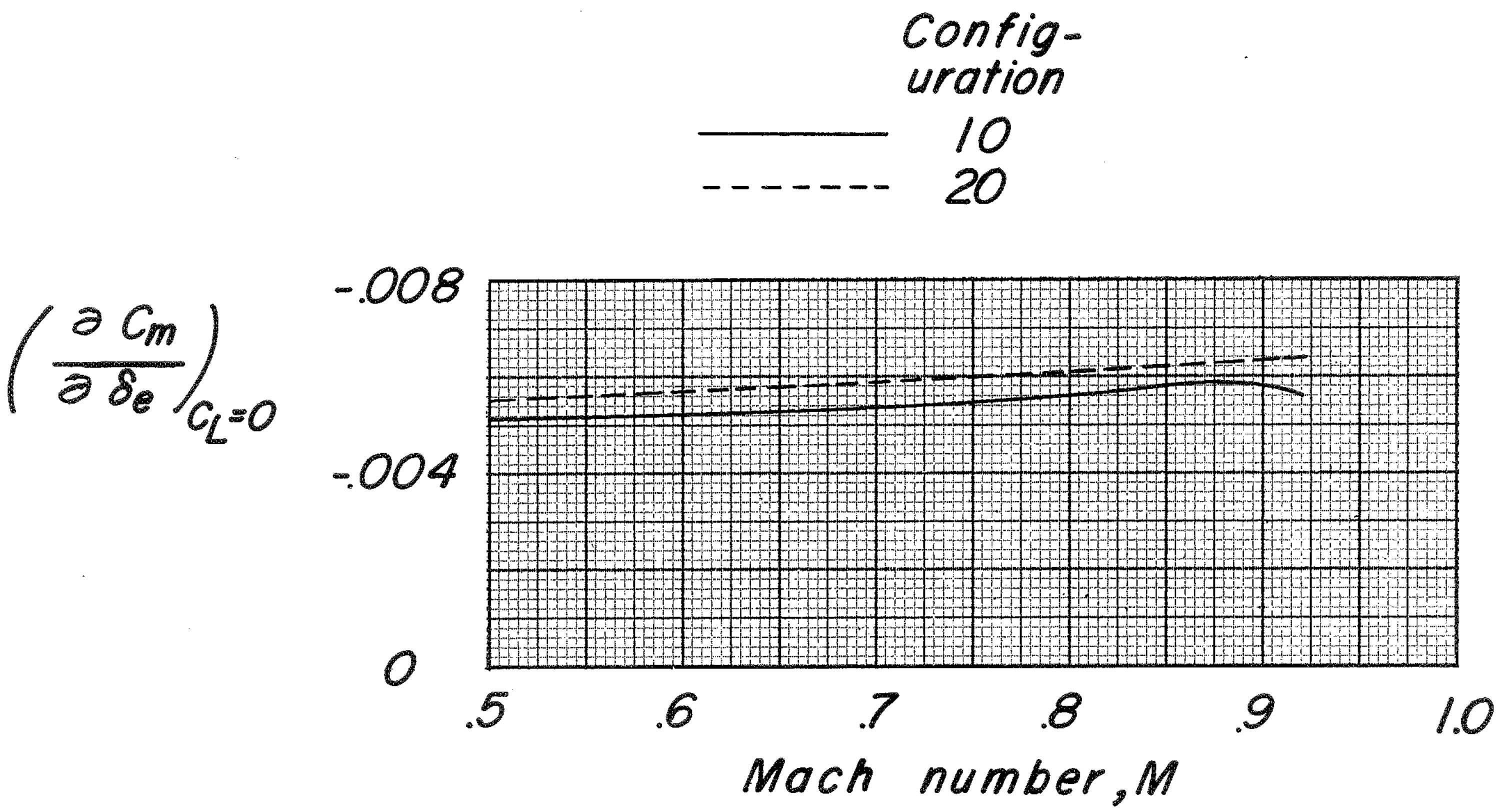

Figure 32.- Elevator effectiveness of configurations 10 (fences 1 and 3 at 0.63b/2 and 0.55b/2, respectively) and 20 (leading-edge chord-extension from 0.68b/2 to 0.85b/2 and notch at 0.68b/2), $\delta_r = 0^{\circ}$.

[redacted]

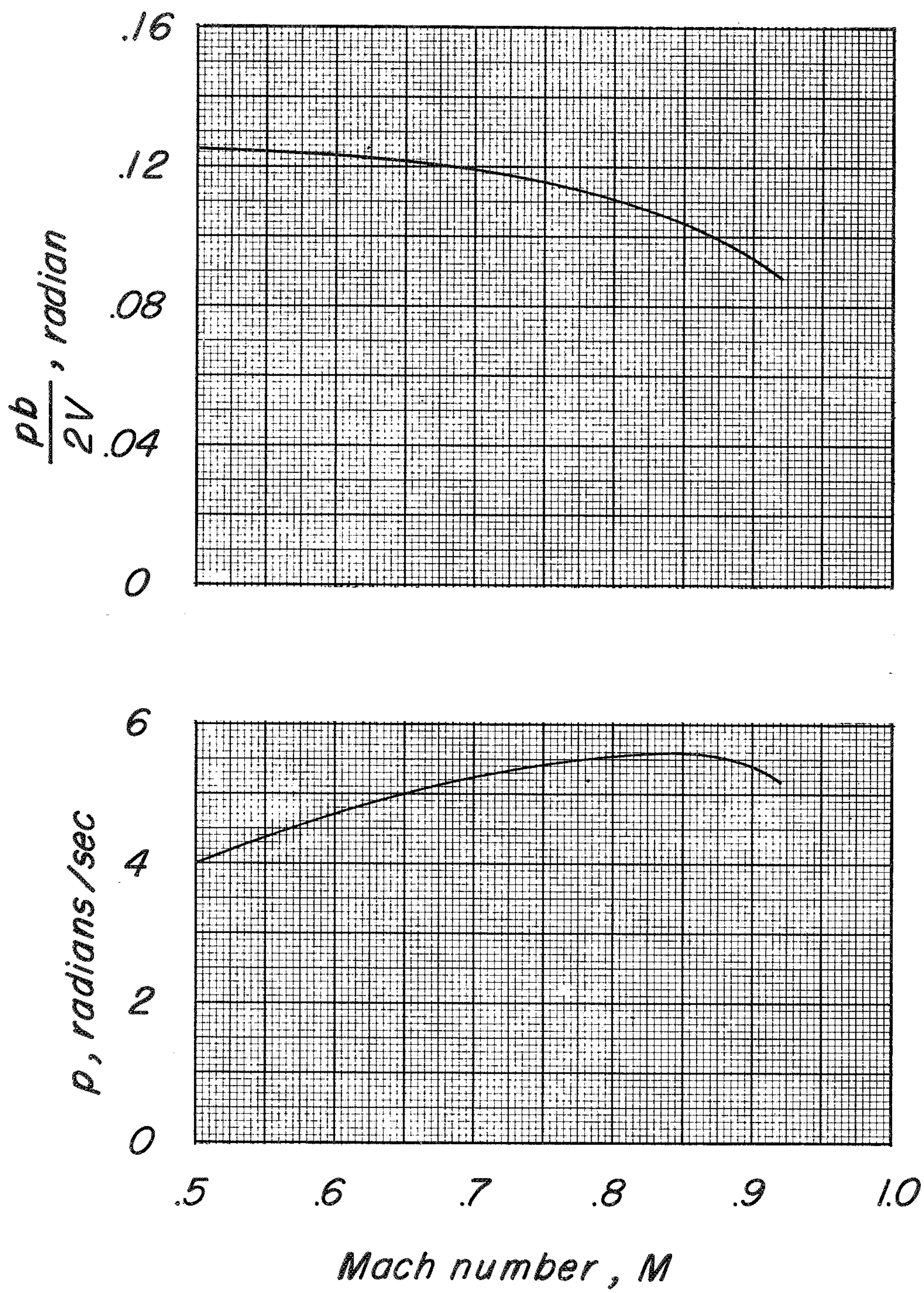

Figure 33.- Variation with Mach number of wing-tip helix angle pb/2V and rate of roll p with $\pm 10^{\circ}$ aileron of configuration 20 (leading-edge chord-extension from 0.68b/2 to 0.85b/2 and notch at 0.68b/2), $\delta_r = 0^{\circ}$. (Altitude of 10,000 feet and wing loading of 32 pounds per square foot.)

[redacted]

[redacted]

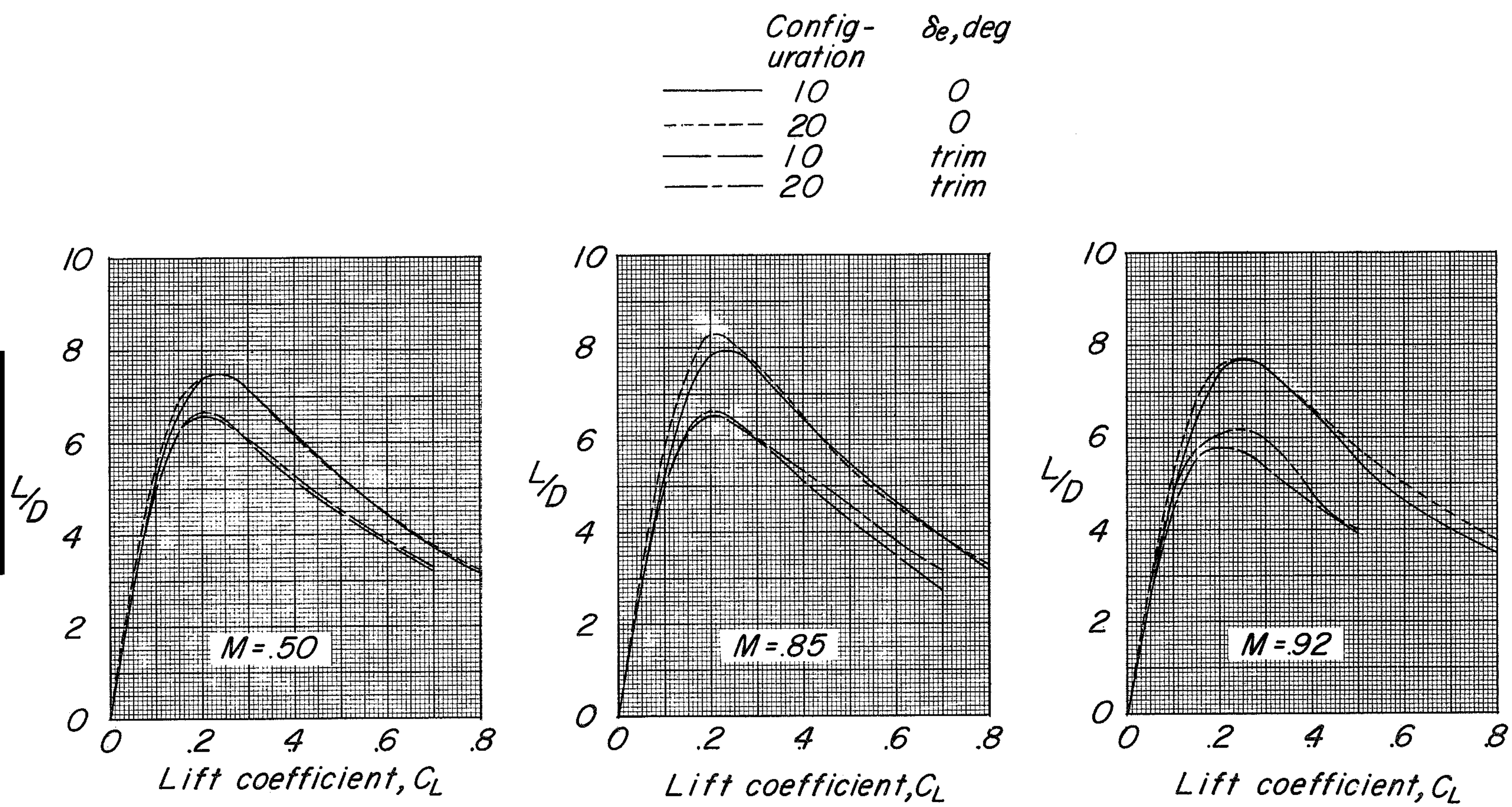

[redacted]

Figure 34.- Lift-drag ratios of configurations 10 (fences 1 and 3 at 0.63b/2 and 0.55b/2, respectively) and 20 (leading-edge chord-extension from 0.68b/2 to 0.85b/2 and notch at 0.68b/2), $\delta_r = 0^{\circ}$.

 [redacted]

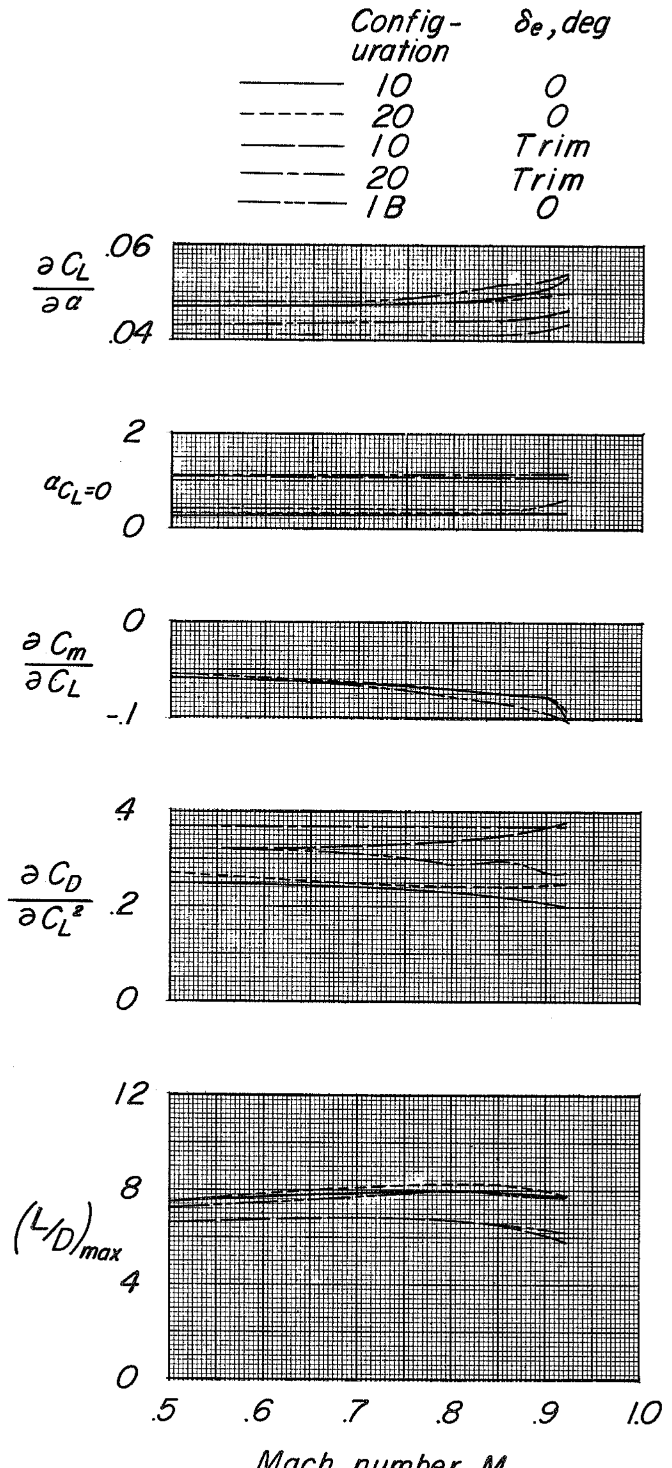

Figure 35.- Summary of aerodynamic characteristics in pitch of configurations 10, 20, and 1B, $\delta_r = 0^{\circ}$. (Slopes are averaged over lift-coefficient range of 0 to 0.4.)

[redacted]

[redacted]

[redacted]